Buried Alive: Analysis of Uncultured Microbes in Marine Sediments

A Dissertation Presented for the

Doctor of Philosophy

Degree

The University of Tennessee, Knoxville

Richard Kevorkian

August 2019

ABSTRACT

The vast majority of microbes in marine sediments have yet to be isolated in pure culture, this leaves many questions as to their ecological relevance and relationship with other taxa and their environment. We applied next generation sequencing techniques to high resolution depth profiles of marine sediments and geochemical analyses to investigate microbial population abundance and composition with depth in Chapter 2. This revealed a putative methanotroph, ANME-1, to be the sole microbe capable of producing methane in the methane producing zone and the area suspected of methane oxidation. This suggests that these OTU's of ANME-1 are capable of both methane production and oxidation, the mechanism used dependent upon geochemical conditions. In Chapter 3, RNA transcript abundance was combined with 16S rRNA gene composition analysis and long-term incubations of marine sediments to investigate microbial population succession in concert with the depletion of sulfate as a temporal analog for depth. This separated methane production from sulfate reduction, revealing an increase in abundance of ANME-3, a methanotroph, simultaneous to an increase in methane concentrations, indicating that this methanotroph is also capable of methane production. Additionally, methanotrophic archaea could not be stimulated to increase in abundance by the addition of methane to the sulfate reduction zone; again, ANME-3 only increased after sulfate was depleted and was observed alongside an increase in methane production, further supporting its role as a putative methane producer. Lastly, in Chapter 4 metabolomic profiles were combined with single cell amplified genomes to explore microbial life in serpentinization sourced mud volcanoes associated with the Mariana Forearc. These constitute the first single cell genomes isolated from marine sediments of this type and alkalinity. Overall, this work offers new insights into methanogenic metabolism flexibility, as well as an improved understanding of microbes associated with sediments influenced by serpentinization sourced fluids.

TABLE OF CONTENTS

LIST OF TABLES

LIST OF FIGURES

CHAPTER 1

INTRODUCTION

Approximately 70% of the Earth is covered by oceans, a majority of which's sediments can be considered as the "Deep Biosphere", defined as an environment that exists at least one meter beneath the seafloor and in permanent darkness (1). The marine subsurface is believed to contain 4.1 petagrams of microbial biomass and a total population of 2.9 $X10^{29}$ cells with a significant portion hitherto yet isolated in pure culture (2, 3). Much of the microbial biomass in the marine deep biosphere is one or more steps removed from the photosynthetic world (4). Microbial populations in the deep biosphere depend upon either organic matter that originated from the photosynthetic zone as a source of energy and nutrients, or that which is derived from chemolithoautotrophy, utilizing reduced chemicals from geothermal sites (5, 6). As oxygen in many marine sediments can become limiting, other terminal electron acceptors, such as nitrate, sulfate, metal species, and carbon dioxide, must be used (7). While the body of work attempting to characterize the geological and chemical parameters surrounding conditions in the deep biosphere is vast, the attempt to elucidate how microbes adapt, respond, and alter those conditions is relatively nascent (5, 8–10). The work presented here sheds light on the role of microbes' ability to produce and oxidize methane in marine sediments, as well as survive extreme conditions in a mud volcano similar to that found on an early Earth or an exoplanet.

Marine sediments, in addition to being a giant biome, are amazingly diverse and host unique populations of microorganisms that thrive, often without input from photosynthetic derived organic matter or oxygen (11–13). Much of marine sediments are influenced by the world above and utilize photosynthetically derived organic matter that finds its way from terrestrial and marine photic zones to the deep biosphere. This results in a vertical zonation or a succession of redox reactions utilized by microbes; the composition of which is determined by the abundance, availability, and energetic yield of terminal electron acceptors (7). The upper layer of sediment associated with the seawater contains dissolved oxygen sourced from the seawater. This however is rapidly depleted resulting in anoxic conditions in the sediment beneath (14). Zonation is determined by the amount of energy production of a terminal electron acceptor per mole of organic matter (7). This results in oxygen being depleted first, followed by nitrate and metal oxides of iron and manganese (Fig. 1-1) (15). Sulfate reduction is utilized next, which is abundant in seawater at a concentration of 29mM (15). Finally, carbon dioxide is utilized by microbes as a terminal electron acceptor resulting in the production of methane.

The exclusion of lower energy yielding processes from each soil horizon is not fully understood and could occur through two mechanisms. First, common substrates used equilibrate

at a concentration as determined by the thermodynamic threshold of the higher energy metabolism, and therefore rendering the lower yield metabolism unfavorable (16). Second, the potentially slower growth rate of the lower energy yielding metabolism against the more energetic competitor results in an exclusion from that zone (17). The role of molecular hydrogen in driving zonation is not clearly understood and has been the subject of a recent study (18). Molecular hydrogen is a stoichiometrically important substrate in many anoxic redox reactions as the electron donor. The fermentation of complex organic matter creates a steady supply of molecular hydrogen in anoxic marine sediments; however, the buildup of this product would make the process unfavorable. This results in a balance of hydrogen consuming microbes and hydrogen producing microbes.

Methanogenesis

Methane is an important greenhouse gas that traps many times more energy per molecule in the atmosphere than CO_2. Nearly 2% of photosynthetically derived carbon ends up as methane (19). Globally, biological production of methane, methanogenesis, of which 80% (45-61 Tg) is oxidized back to CO_2 before it reaches the atmosphere by microbial action (10, 20, 21). There are three major types of methanogenesis; the first is hydrogenotrophic methanogenesis. This results in the reduction of carbon dioxide with molecular hydrogen serving as the electron donor. The second type, acetoclastic methanogenesis, utilizes the breakdown of acetate, which is an important microbial metabolic intermediate, resulting in a molecule of carbon dioxide and methane per molecule of acetate (20, 22). The third type, methylotrophic methanogenesis, removes a methyl group from C1 carbon compound such as methylamines or methanol (23). The majority of methanogen groups are hydrogenotrophs that reduce CO_2 with H_2 serving as the electron donor (20). Hydrogenotrophic methanogenesis is autotrophic and only requires salts, H_2, CO_2, and trace metals to produce energy and biomass (5). A critical final step is mediated by a nickel-containing enzyme, methyl coenzyme M reductase (*mcrA*), which serves as an indicator of methane production (24). This enzyme also catalyzes the reverse pathway of methanotrophy in consortia with sulfate reducing bacteria (25), and possibly also catalyzes butane oxidation (26). Recent evidence suggests that methane production is more widespread in archaea and not only specific to the clade *Euryarchaeota* (27).

The sulfate/ methane transition zone: understanding syntrophic interactions and identifying novel methanogens

The release of methane that is produced in marine sediments is strongly controlled by the anaerobic oxidation of methane (AOM), which is effectively coupled to the reduction of sulfate. This results in methane inputs from oceanic sources accounting for only about ~2% of current global atmospheric budgets (10, 28). The mechanism for AOM has seen recent advances on additional electron acceptors and geographic distribution (29–31). While numerous sulfate reducing partners of AOM have been studied, a complete list is lacking, as is clarity on what initiates this partnership (32–35). AOM occurs in a region of the sediment where methane, produced deeper, diffuses up into where sulfate reduction actively occurs forming a sulfate/ methane transition zone (SMTZ). This appears to create the conditions that allow AOM to occur. They do this by forming syntrophies with sulfate reducing bacteria (SRB), with whom they share electrons or some other reducing equivalent to perform AOM (25, 32, 36).

In the SMTZ, sulfate reducers keep hydrogen concentrations low enough to make reverse methanogenesis exergonic (10, 37). This is possible because methanogenesis, unlike almost all other respiratory mechanisms can be made to be exergonic in the reverse direction. This is due to two important features of methanogenesis: (1) hydrogenotrophic methanogenesis has a Gibbs Free Energy (ΔG) close to equilibrium in the standard state (ΔG° = -137 kJ/mol, compared to about -3000 kJ/mol for aerobic heterotrophy), and 2) has a stoichiometry of 4 molecules of hydrogen per reaction (38). This means that the direction of exergonicity (designated by a negative ΔG value) is reversed when H_2 concentrations are very low. In situ measurements of porewater chemistry have shown that the ΔG of methanogenesis reverses between the SMTZ and the methanogenic zone, as predicted by thermodynamic theory (39).

The microbes that perform AOM in partnership with SRB's are called anaerobic methanotrophs (ANME). ANME's comprise multiple non-monophyletic groups, encompassed within Methanomicrobia (Fig. 1-2). The class Methanomicrobia has many cultured representatives; all of which are obligate methanogens (40). ANME-1 is its own order in Methanomicrobia, ANME-2a/b and ANME-2c are families within the order Methanosarcinales, and ANME-3 is a species within the *Methanococcoides* genus of the order Methanosarcinales. However, despite the presence and activity of ANME's in methanogenic sediments, direct evidence that ANME archaea either are capable of methanogenesis or shift between methanogenesis and AOM in marine sediments is lacking (36).

ANME-1 are phylogenetically related to cultured methanogens, falling in Methanomicrobia, a group for which all cultured strains are methanogens. Initial incomplete genomes from ANME-1 contained all of the genes required for methane production except for N5, N10-methylene-tetrahydromethanopterin reductase (Mer) (41–43). More recently, Mer has been found in ANME-1 genomes (43). However, solid evidence that ANME-1 reverses between methanogenesis and AOM in marine sediments is lacking. There is evidence that ANME-1, while previously associated with AOM, may also be responsible for methane production based on the mRNA analysis of key genes (44). Furthermore, the *mcrA* gene analog identified from a Bathyarchaeotoa genome indicates that methane production is more widespread than previously believed; although, this gene was not detected in the White Oak River Estuary, one of the environments studied here (45). The White Oak River estuary is a shallow brackish estuary in North Carolina (Fig. 1-3) that has been the focus of marine biogeochemistry studies for decades. The geochemical influences of this site are well understood, with a SMTZ less than one meter from the sediment seawater interface (14, 16, 44, 46–48). Additionally, it is easily accessed with a depth between 3-6 feet without additional equipment and has a known sedimentation rate of 0.25 cm per year (49).

Characterizing microbes related to subduction zones along the Mariana Forearc

In addition to microbes in marine sediments that are supported by photosynthetically derived organic matter from above it is also possible for populations to be supported by nutrients and energy derived from below due to geological action. One such source is via serpentinization reactions found at the convergent margin, which is formed by the Pacific plate subducting beneath the eastern edge of the Philippine plate (Fig. 1-4.). This produces a region of serpentinite mud volcanoes in the Mariana Forearc between the Mariana Trench and the volcanic arc that creates the Mariana Island Chain (50), which was the subject of a drilling expedition by the International Ocean Discovery Project (IODP) expedition 366 in late 2016/ early 2017 (Fig. 1-5). The increasing pressure and temperature of the downgoing slab leads to dehydration reactions (50–52). This transformation results in a hydrated serpentinite mud that is pushed upwards through fault conduits resulting in mud volcanoes 2 km in height (Fig. 1-6) (50, 51). The process of serpentinization is a geological transformation by which iron and manganese react with water to form serpentinite rock (53). The fluid that is released from the formation of serpentinite is very alkaline, at a pH of up to 12.5, and is rich in molecular hydrogen and light hydrocarbons (52, 54),

which classifies these locations as harboring extreme conditions for life on Earth. In environments influenced by serpentinization the formation of methane is thermodynamically favored (55). Hydrocarbons and amino acids have been shown to be produced abiotically under conditions similar to serpentinization in a laboratory setting (56). The rich reduced chemicals and the abundance of molecular hydrogen makes this environment similar to possible analogs of early Earth, at the origin of life (53, 55, 57).

Previous work at the Mariana forearc mud volcanoes have shown a predominance of archaea, including groups commonly associated with marine sediments such as Marine Group I (*Thaumarchaeota*), Marine Benthic Group B (*Lokiarchaeota*), *Methanosarcinales*, and *Methanobacteriales* (51, 58). The unique geochemistry and high pH likely hosts divergent microbial clades adapted to the conditions as seen in the Lost City Hydrothermal Field (LCHF), another serpentinite hosted ecosystem (59). The LCHF is different, however, in terms of a higher temperature (40-74°C instead of 2-4°C) and is not a subduction zone, but a hydrothermal vent field near the Mid-Atlantic Ridge (52, 54, 60). With previous community analyses identifying different clades of microbes at these two serpentinizing systems, we anticipate that the Mariana convergent margin communities will yield unique clades as well.

In the environment at the Mariana forearc, the rising fluid provides the electron donors and acceptors for the microbial metabolic pathways (5). Abundant molecular hydrogen in the fluid readily serves as an electron donor (61). Studies of nearby South Chamorro Seamount, Ocean Drilling Program (ODP) site 1200, and at LCHF discovered uncultured and unique clades, including an abundance of methanogens, at shallow sediment depth (8, 58, 59, 62). The methane that was sampled at South Chamorro Seamount, from the Mariana forearc suggested that it was thermogenic in origin and not from a microbial source (51). However, 16S rRNA genes were isolated indicating that several putative methanogen members of the *Euryarchaeota,* including *Methanosarcinales,* were present at this serpentinization site, suggesting that methanogenesis is occurring at a low enough rate that it does not greatly shift the isotopic composition of the total pool of stable carbon isotopes. At LCHF the available carbon pool was unusually depleted in C^{12} resulting in obfuscated isotopic signatures which could also be occurring at the Mariana forearc (63). Another possibility is that these methanogens are utilizing some non-methane-related metabolism (58).

The porewater geochemistry at South Chamorro Seamount and the Mariana forearc have elevated concentrations of short chain hydrocarbons, as well as low organic matter (51). The fluid

carried up from the subduction zone is rich in methane (51). Alkaline conditions present unique obstacles for microbial life such as damage to DNA, enzymes, and the plasma membrane. Additionally, a lack of protons relative to the cytoplasm detrimentally effects the proton motive force hindering ATP synthase (64). A potential alternative, which has been observed in alkaline conditions, is use of a sodium motive force in the production of ATP (65). Elevated pH also reduces the amount of bioavailable dissolved inorganic carbon (DIC) due to its conversion to carbonate species. While microbial life can survive environments at pH's 11-12 such as soda lakes, they do so with specialized cellular machinery to maintain a proton motive force and nucleic acid viability (38). This creates conditions favorable for the formation of biotic and abiotic biomolecules and light hydrocarbons (e.g., methane) (55, 66, 67). Shipboard results suggest that the upwelling fluid at Yinazao is sourced from non-sterilizing temperatures (~80°C) while temperatures at Asùt Tesoro are much greater (~250°C).

The effect of serpentinization on microbial populations remains unclear and may have broader impacts related to the origins of life and exobiology. Geological processes such as serpentinization are as old as the Earth and provide sources of energy and nutrients for microbes at the ocean floor that could have fueled life before the energy of the sun was harnessed through photosynthesis (53, 55, 68). It is important to understand microbial life in extreme and novel places such as seamounts associated with the Mariana convergent margin. First, it serves as an analog for an early Earth, since the geological processes that provide reduced chemicals and nutrients to microbes in the marine sediments do so, separated from direct influences of photosynthetically-derived biomass (8, 53). Second, it is theorized that the same serpentinization reactions occurring at this site could be occurring on Enceladus, a moon of Saturn, resulting in liquid water rich in molecular hydrogen (69). Thus, by examining how microbes are adapted to this extreme environment on Earth, we will gain insights into exobiology and the origins of life on our own planet.

Organization

The first study presented here attempts to provide evidence that the microbes responsible for the oxidation of methane in the White Oak River estuary are also responsible for its production. While the presence of ANME's is well documented the source of methane produced remains unclear (44). Additionally, the White Oak River estuary is a common source of sequencing based studies as an analog for the deep biosphere despite the majority of taxa not

isolated in pure culture (45, 70–74). We utilized a novel technique, FRAxC, in the attempt to elucidate the turnover time of individual microbial OTU's, which lent credence to the belief that there are microbial populations that growth on the order of weeks or months (75). This begs the question of if these microbes are buried alive in marine sediments and potentially grow at an extraordinarily slow rate, is it possible that they are doing so in the possibility of being revived though some sort of geological action.

The second study presented here attempts to simulate a diagenic profile one using long term incubations of sediment take from the White Oak River estuary. Using two incubations, over 1500 days combined, we removed the SMTZ in one and simulated it in the other allowing for the removal of the diffusion and potential microbial motility seen in depth profiles. This research provides evidence for the production of methane by ANME-3 which was believed to be responsible for its anaerobic oxidation. Furthermore, we provide evidence that anaerobic oxidation of methane could not be stimulated in sulfate reducing sediments in microbial taxa that are believed to utilize this metabolism as their sole energy source. We were also able to characterize the microbial community responsible for methane production without being primed by methane oxidation, as they are in natural sediments.

Finally, the third study described here attempts to illuminate microbial life from serpentinization sourced mud volcanoes at the Mariana Forearc. We utilized numerous techniques, described below, to examine the genomic material of individual members of this community. Fluorescence activated cell sorting (FACS) is a technique by which cells are fluorescently tagged and individually separated then be sequenced and analyzed using Next Generation Sequencing techniques, and the genome and pathways reconstructed in order to elucidate the survival strategies and diversity of individual microbes. This technique is particularly important in marine sediments due to the lack of cultivability and the bias associated with other methods such as metagenomics that do not provide a clear picture of the microbial diversity and function. Every genome produced from uncharacterized environments pushes back the curtain and adds to the genomic databases providing a better picture of global microbial diversity. This allows for the precise observation of metabolic potential, via gene presence, at a particular location in the environment (76, 77). This approach also makes it possible to visualize the *in situ* functions of individual microbes associated with sediments at the Mariana Forearc fueled by deep subsurface serpentinization reactions.

Appendix

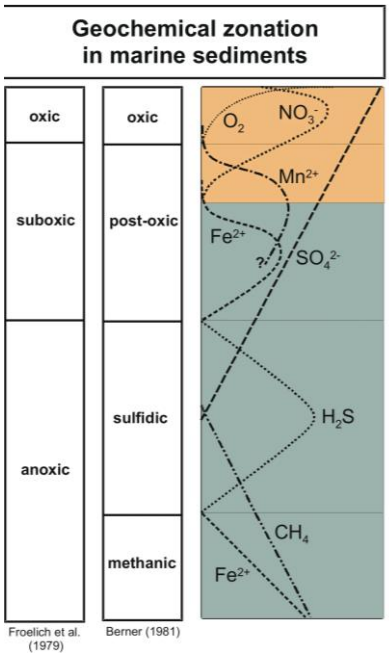

Figure 1-1. Terminal electron acceptor usage in marine sediments form distinct zones.

Redox zonation with depth in marine sediments (reprinted from Jorgenson Kasten et al. 2003)

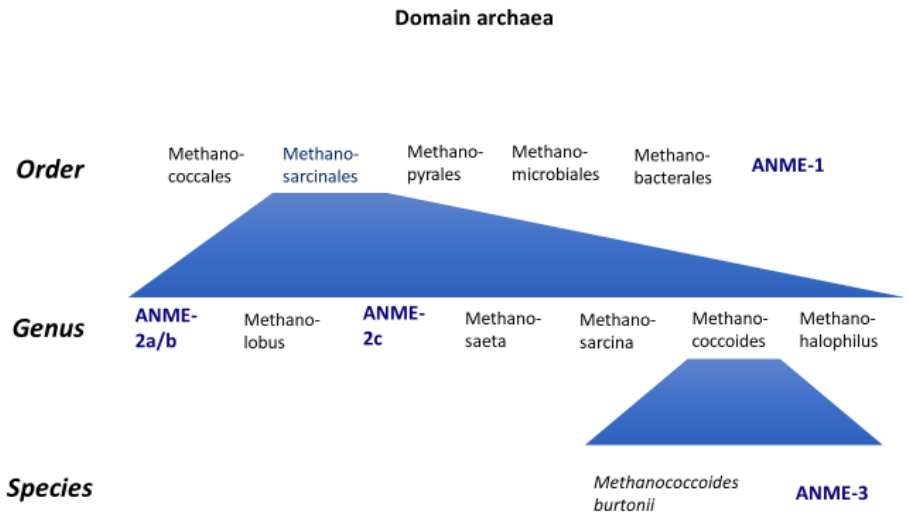

Figure 1-2. ANME's are a non-monophylatetic group of archaea related to cultured methanogens.

16s rRNA gene taxonomic classification of ANME's within the class Methanomicrobia.

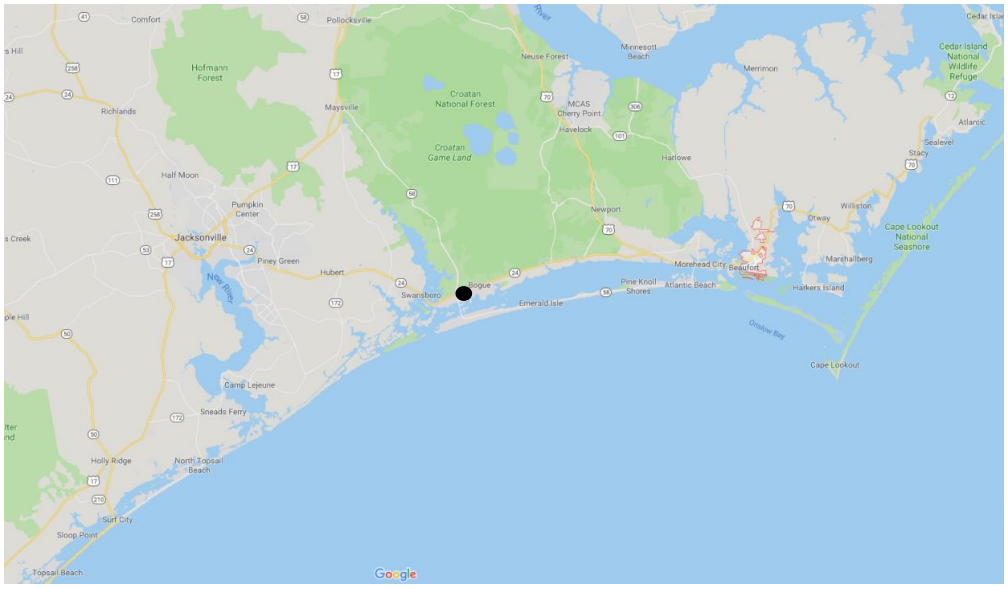

Figure 1-3. The White Oak River on the coast of North Carolina.

Location of station H, black circle, at the White Oak River estuary.

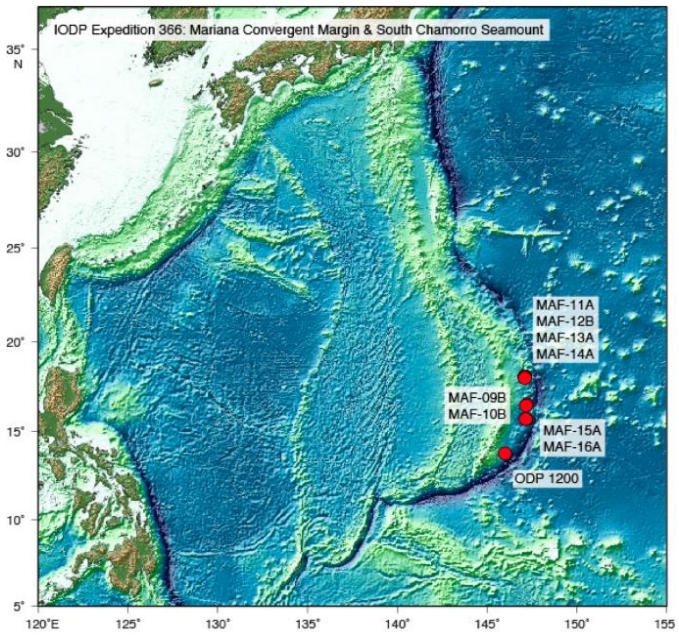

Figure 1-4. Drill sites for the IODP 366 expedition.

Sample sites for IODP 366 along the Marianas forearc. ODP 1200 has been previously sampled in 2003. Figure reproduced from Expedition 366 Preliminary Report. Drill sites used in this work are: MAF-15A, MAF-11A, and MAF-12B.

Figure 1-5. JOIDES Resolution.

The drilling platform that was used to retrieve sample in EX366. Credit: William Crawford and IODP.

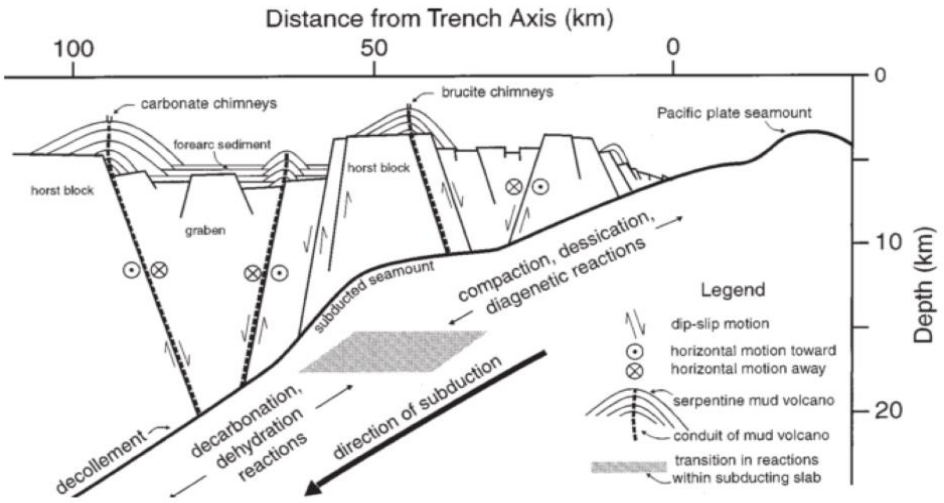

Figure 1-6. Subduction of Pacific plate beneath the Philipine plate results in serpentinization.

Schematic of typical settings for mud volcanoes at the Marianas forearc. Reprinted from Fryer et al. 1999.

CHAPTER 2

UNCULTURED ANME-1 ARCHAEA GAIN ENERGY FROM EITHER METHANOGENESIS OR ANAEROBIC OXIDATION OF METHANE

A version of this chapter has been prepared for submission as a peer-reviewed article by Richard Kevorkian and authors: Richard Kevorkian, Sean Callahan, Rachel Winstead, and Karen G. Lloyd. “ANME-1 archaea drive methane accumulation and removal in globally common marine sediments.” *Proceedings of the National Academy of Sciences”* (2019).

Richard Kevorkian and Karen G. Lloyd designed the study. All analyses were completed by Richard Kevorkian. Other Data collection occurred with assistance from Sean Callahan and Rachel Winstead. The manuscript was written by Richard Kevorkian with inputs from Karen G. Lloyd.

Abstract

Uncultured archaea in the Methanomicrobia (ANME-1) perform the anaerobic oxidation of methane (AOM), or reverse methanogenesis. The majority of marine sediments lack advective transport of methane, so AOM occurs in the sulfate methane transition zone (SMTZ) where sulfate-reducing bacteria make methanogenesis exergonic in the reverse direction by consuming hydrogen. When sulfate is depleted, fermentative hydrogen increases and forward methanogenesis becomes energy-yielding. We found that ANME-1 comprised 99.24% of 16S rRNA genes from Methanomicrobia in the SMTZ and 99.95% in the methanogenesis zone in White Oak River estuarine sediments. Each of the 16 ANME-1 OTUs (97%) had peaks in the SMTZ that coincided with peaks of sulfate reducing bacteria *Desulfatiglans sp.* and SEEP-SRB1. In the methane production zone, ANME-1, but no putative sulfate-reducing bacteria, increased with depth. We re-analyzed public genomic DNA to show that ANME-1 was the only potential methanogen present in hydrogen-dependent methane-producing enrichments. We conclude that ANME-1 reverses between AOM in the SMTZ and methane production the methanogenic zone of non-seep marine sediments. This may give ANME-1 a competitive advantage over cultured methanogenic clades in marine sediments, explaining their dominance in methanogenic sediments worldwide.

Importance

Many microbes are difficult or yet to be isolated in pure culture to determine their preferential growth conditions and environmental relevance. We successfully generated a high-resolution diagenetic profile for a marine sediment environment. This allowed for the observation of the microbial community shift caused by the natural progression from sulfate reduction to methanogenesis. Our research provides evidence for the production of methane by microbial taxa believed to also be responsible for its anaerobic oxidation as well as evidence supporting cryptic methane cycling within the SMTZ. Furthermore, we utilize a novel method for calculating population turnover rates of individual OTUs in a natural setting, providing insight into microbial population dynamics in relation to geochemical processes.

Introduction

Non-seep marine sediments are the third largest producers of methane on Earth, after rice production and wetlands (10). However, very little of this methane is emitted to the atmosphere because abundant uncultured archaea of the Methanomicrobia group, ANME-1, catalyze the anaerobic oxidation of methane (AOM) (43, 44, 78). However, it is unknown whether ANME-1 are also responsible for the production of this globally massive amount of methane.

The majority of marine sediment microbes belong to uncultured genera or higher taxonomic groups (79), making it necessary to infer their geochemical functions in a natural setting rather than in axenic cultures. These microbes drive sulfate reduction, methanogenesis, and the anaerobic oxidation of methane (AOM), which are the key respiratory processes oxidizing organic matter in marine sediments. The balance between diffusion and biological respiration drives a downcore shift from sulfate reduction to methanogenesis, with net removal of methane through AOM in the sulfate methane transition zone (SMTZ) at intermediate depths (49). In the SMTZ, sulfate reducers keep hydrogen concentrations low enough to make reverse methanogenesis exergonic (10, 37). This is possible because methanogenesis, unlike almost all other respiratory mechanisms can be made to be exergonic in the reverse direction. This is because hydrogenotrophic methanogenesis has a Gibbs Free Energy (ΔG) close to equilibrium in the standard state (ΔG° = -137 kJ/mol, compared to about -3000 kJ/mol for aerobic heterotrophy), and 2) has a stoichiometry of 4 molecules of hydrogen per reaction. This means that the direction of exergonicity (designated by a negative ΔG value) is reversed when H_2 concentrations are very

low. In situ measurements of porewater chemistry have shown that the ΔG of methanogenesis reverses between the SMTZ and the methanogenic zone, as predicted by thermodynamic theory (39).

Although many metabolic pathways are amphibolic, it is unknown whether a single methanogen can gain energy from either methanogenesis or AOM, depending on which direction is exergonic. Although cultured methanogens catalyze reverse methanogenesis, they cannot sustain the process (80). This is most likely because most cultured methanogens operate at very high energy yields and cannot survive on the paucity of energy afforded by reverse methanogenesis. ANME-1 archaea, however, have low energy requirements (81), making them good candidates for reversible methanogens. ANME-1 are present and active in both AOM and methanogenic zones. ANME-1 are phylogenetically related to cultured methanogens, falling in the Methanomicrobia, a group for which all cultured strains are methanogens. Initial incomplete genomes from ANME-1 contained all of the genes required for methane production except for N5, N10-methylene-tetrahydromethanopterin reductase (*Mer*) (41–43). More recently, *Mer* has been found in ANME-1 genomes (43). Enrichments of ANME-1 have been shown to perform methanogenesis when hydrogen concentrations increase or when sulfate is depleted (25, 32, 36). However, evidence that ANME-1 sustainably reverses between methanogenesis and AOM in marine sediments is lacking.

We hypothesized that if ANME-1 are capable of reversing between AOM and methanogenesis, then they would dominate the total population of methanogen-like archaea in AOM and methanogenic zones in a diffusion-dominated sediment, where these zones can be clearly differentiated by depth. We examined 16S rRNA gene sequence libraries with high depth resolution (1 cm intervals) throughout a diagenetic sequence indicated by concentrations of methane, sulfate, and hydrogen and $\delta^{13}C$ values of methane in sediments of the marine-influenced White Oak River estuary. To calculate variation in total population sizes of particular clades with depth, we multiplied the fraction of read abundance for a particular clade by the total cell abundance of that sample, or FRAxC (Fraction of Read Abundance times Cells) (18). FRAxC is not absolutely quantitative, since the outcomes are biased by DNA extraction and primer-based amplification (82, 83), but relative changes in population sizes can be calculated from this because the bias factor occurs in both the numerator and denominator.

Results

Geochemistry

Sulfate concentrations in core 1 decreased rapidly for the first ~50 cm from an initial concentration of 11.2 mM before approaching a steady concentration of ~0.1 mM at 60 cm (Fig. 2-1e). This concave decrease in sulfate is consistent with it being consumed microbially, probably by sulfate-reducing bacteria as the sediment is typically anoxic within a few millimeters below the surface (46). Although sulfate was rapidly reduced it never reached zero nor below our limit of detection, either because the concentration was too low for the sulfate-reducing bacteria to use or the resultant sulfide was reoxidized with iron back to sulfate (84).

Aqueous methane concentrations in core 1 ranged from 0.003 mM at the surface to 0.05 mM at 53.5 cm, below which it increased to 0.73 mM in the 75-78 cm depth interval. Aqueous methane concentrations in core 6 ranged from 0.005 mM at the surface to 0.08 mM at 27.5 cm, below which it increased to 0.87 mM at 75-78 cm.

Hydrogen concentrations in core 1 as the mean measured in the headspace at the water/ sediment interface was 2.9 nM. Between the 2.5cm and 64.5 cm downcore the concentrations ranged from 0.07 nM and 2.05 nM with a standard deviation of 0.45 nM. These values are consistent with those predicted for sulfate reducers operating at their minimum energy (1.22 ± 0.45 nM) (16). After sulfate is depleted at ~60cm, hydrogen begins to increase in concentration with two of the three deepest datapoints then exceeded 6 nM. These values approach or are as high than the value measured for methanogen maintenance energy of 5.11 nM (16).

Stable carbon isotopes of methane were measured for both cores. In core 1 measurements progressed from -41‰ ± 1.17 at 41.5cm to -72‰ ± 0.10 at 73.5 cm (Fig. 2-1 c,g). Core 6 values moved from -46‰ ± 0.20 at 29.5 cm to -74‰ ± 0.02 at 67.5 cm. These values are consistent with the biogenic production of methane at deeper sediment depths resulting in enrichment of the lighter carbon isotope, C^{12}, resulting in values ranging from -40 ‰ to -90 ‰ (85). The values at higher sediment horizons, including those in the SMTZ, are depleted in the lighter carbon isotope, which is further consistent with the presence of AOM (15, 86). This is because biological AOM has a preference for ^{12}C over ^{13}C, leaving the residual methane ^{13}C-enriched (87, 88).

As classically applied to porous sediments, Fick's Second Law of Diffusion, a concave-down section would signify a zone of net methane production and a concave-up section signifying net methane oxidation (14). The inflection point is not readily apparent in our samples,

so we choose the area between 60 and 76.5 as the methane production zone in core 1 because sulfate is depleted at 60 cm and 45 to 76.5 cm in core 6 due to the variability in concentrations measured there (49). Furthermore, there is no apparent plateau in either core suggesting that our core did not reach the full methane production zone, combined with difficulties in measuring methane above the saturation concentration (~1.2 mM) limits the ability to accurately constrain the depth limit of methane production (44). This leaves the resultant area above the methane production zone and into that of sulfate reduction as the SMTZ. Previous studies applied to this site have suggested that the sulfate/ methane transition zone occurs over a broad depth interval and is not readily confined (14).

For every sample downcore in core 6 total cellular abundance remained below the order of 10^9 cells/g sediment as determined by direct cell counts (Fig. 2-1A) but decreased rapidly within the first 10 cm from 2.0×10^8 to 2.6×10^7 cells/g where the concentration of cells was reasonably steady with a standard deviation of 1.27×10^7 for the rest of the core.

Methane cycling communities

ANME-1 ranged from 0.00026 % to 0.199 % of 16S rRNA gene sequence relative abundance, comprising six OTUs of ANME-1a, nine OTUs of ANME-1b, and one OTU that could not be placed into one of those two subgroups. Methanobacterales ranged from below detection to 0.0026 % relative sequence abundance and comprised one OTU. No other groups that have been shown through cultures or enrichments to perform methanogenesis or AOM (ANME-2, ANME-3, Methanosarcinales, Methanomicrobiales, Methanococcales, or Methanopyrales) were found after quality filtering.

All three subclassifications of ANME-1 were present in the SMTZ (25-50 cm) and methanogenic zones (50-75 cm) (Fig. 2-2C). Vertical patterns of individual OTUs differed, but all had one or more peaks in the SMTZ that were defined by at least three depths for each peak. These peaks did not coincide with peaks in methane or hydrogen. The vast majority of ANME-1 sequences (three ANME-1a and four ANME-1b OTUs, comprising 88% of total ANME-1 FRAxC) had large populations (13-46% of FRAxC for each OTU) in the methanogenic zone below 50 cm. The remaining 12% of the ANME-1 (one ANME-1_unclassified, three ANME-1a, and five ANME-1b OTUs) had only 1-5% of their FRAxC in the methanogenic zone. Only 9% of ANME-1 FRAxC were found in sediments with less than 0.03 mM of methane. The Methanobacteriales OTU increased threefold in relative abundance within the first ten

centimeters downcore followed by a period of much lower abundance until it quickly rose to a similar peak in abundance at 51.5 cm, with 40% of its FRAxC in the methanogenic zone.

Three ANME-1 OTUs exponentially increased between 33.5 and 39.5 cm downcore with population turnovers ranging from 0.721 to 0.837 cm, corresponding to 2.8 to 3.3 years (Table 1). Significant exponential increases for ANME-1 at other depths were not detected using our parameters.

Sulfate reducing bacteria

Families with cultured sulfate reducing bacteria comprised 83 OTUs and 0.14% and 0.02% of 16S rRNA gene sequence relative abundance. They were dominated by OTU's of the genus Desulfatiglans in the Desulfoarculaceae (90% of SRB FRAxC, and 54 OTUs), followed by SEEP-SRB1 in the Desulfobacteraceae (6% of SRB FRAxC, and 10 OTUs). The remaining ~4% included all OTUs from Desulfobulbaceae (Desulfobulbus) and the Sva0081 sediment group in the Desulfobacteraceae, and decreased rapidly with depth, such that >72% of their FRAxC values were in the upper 10 cm (Fig. 2-2D).

The four most abundant SRB's, which were identified as Desulfatiglans OTU's, demonstrated their highest abundance in the SMTZ and not near the surface where sulfate was at its highest concentrations. Two do generally decline in abundance with depth until the SMTZ while the other two show little response to the first 40 cm and only increase briefly in abundance in the SMTZ. These 3-5 fold spikes in abundance coincide with a similar spike in abundance alongside the four most abundant ANME-1 OTU's. These increases in abundance were spatially distinct and did not occur over a period which would have allowed for the calculation of a turnover time.

Eleven OTUs were identified as SEEP-SRB1 and the main increases in relative abundance occurred between 30-50 cm downcore (Fig. 2-2D). These increases manifest in 3-4 distinct spikes shared across multiple OTUs that match peaks seen in ANME-1, which has been shown previously to form syntrophies with ANME-1, with both demonstrating a 3-5 fold increase in abundance at those points (32, 33). This increase in abundance also made it possible to calculate a turnover time of 1.08 cm for the period between 33-37cm (Table 1). OTUs containing sulfide-oxidizing bacteria such as *Sulfurimonas*, *Thiotrichales*, and *Thiomicrospira* were either low in abundance, not detected, or demonstrated no significant increases in abundance over time. Thirty-one OTUs of the phylum Defferibacteres were identified, of which all belonged to the

genus *Caldithrix*, which is an organoheterotroph and is not likely an iron reducing bacteria, and declined rapidly with depth (89). Otherwise, obligate iron and manganese reducing bacteria either did not meet abundance thresholds or were not detected in our sequence libraries.

Uncultured taxa

Throughout the downcore, bacteria represented ~60% of total amplicon sequences and archaea ~27%, the remaining amplicons failed to classify on the domain level. The relative abundance of bacteria declined steadily downcore as the abundance of archaea increased eventually replacing bacteria as the most abundant domain (Fig. 2-2A). There was a sustained increase in the phylum Euryarchaeota between 30 and 50 cm before decreasing slightly. Bathyarchareota was the most abundant archaeal phyla and increased in total abundance throughout the entire length of the core. Thaumarchaeota demonstrated a similar tend and increased slowly throughout the core. The archaeal phyla WSA2 and Hadesarcheota both briefly increase in relative abundance between 27.5 and 29.5 cm with Hadesarcheota beginning a steady increase with depth beginning at 41.5 cm downcore. Lokiarchaeota and Woesearchaeota both decrease in relative abundance rapidly with depth. Acidobacteria, Bacteroidetes, Latescibacteria, Nitrospirae, Deferribacteres and Gemmatimonadetes all demonstrated a rapid decline in relative abundance and accounted for less than 1% of total reads per sample each within ~20 cm downcore. Proteobacteria declined steadily throughout the core from ~25% of total reads initially to ~4% by the end of the core (Fig. 2-2B). Chloroflexi, Aminicenantes and Planctomycetes all declined throughout the core profile, but only very modestly. A Bathyarchaeota OTU also demonstrated an exponential increase which allowed for the calculation of a 1.085 cm turnover between 24.5 and 27.5 cm, which is however not in the methane production zone. Two separate OTUs of Hadesarchaea exhibited this trend as well with one from 17.5-25.5 cm and the other 48.5-51.5 cm and turnovers of 1.03 and 0.93 cm respectively (Table 1). An OTU of Dehalococcodia also demonstrated an increase in abundance that made it possible to calculate a turnover of 0.84 cm between 10.5 and 13.5 cm.

Discussion

ANME-1, with both a and b subgroups, dominated the Methanomicrobia in both the AOM and methanogenesis zones (99.24 and 99.95%, respectively). This agrees with previous observations from Aarhus Bay, Denmark, White Oak River estuary, and Gulf of Mexico deep-sea

slope sediments that cultured methanogens were either absent or in too low abundance to account for methane production (43, 44, 78) Each of these analyses utilized 16S rRNA primers capable of amplifying cultured methanogens, so their absence was not likely to be an artifact of primer bias. However, primer bias can greatly skew the relative abundance of different clades (90), so we analyzed 16S rRNA gene sequences from previously published high-depth-read metagenomes from the same station in the White Oak River estuary (45, 71). When free from primer bias, ANME-1 comprised 100% of the Methanomicrobia in the AOM zone and 92.86% in the methanogenic zone, corroborating the findings of the other studies.

The only other potentially methane-producing archaeal group detected in our samples that increased in the methane production zone was Bathyarchaeota (Fig. 2-5B) (27, 70). However, the inference that Bathyarchaeota perform methanogenesis is based on the presence of a highly evolutionarily-divergent *mcrA* gene found in genomes from a terrestrial coal bed. Orthologs to this *mcrA* have subsequently been shown to catalyze reactions with butane, rather than methane (26) and none of the Bathyarchaeota genomes obtained from the White Oak River estuary sediments have this gene (71). Bathyarchaeota in marine sediments appear to perform acetogenesis and fermentation of organic substrates such as proteins and lignin (91). They have also been suggested, based on their lipid stable carbon content to be autotrophic (73) . Additionally, ten OTUs identifying as Hadesarchaeota were detected in our samples and increased in FRAxC in the methane production zone (Fig. 2-5A). This archaeal phylum has numerous carbon metabolism genes in common with Methanomicrobia but do not have a methanogenic pathway. Instead they are hypothesized to have a heterotrophic and/or nitrogen cycling lifestyle (74). A proposed methyl-reducing methanogenic archaeal lineage, WSA2, was also detected in our samples. However, the 11 OTUs were only at any appreciable abundance in the sulfate reducing zone between 27-30 cm and declined below that (92). Since Methanobacteraceae, Bathyarchaeota, Hadesarchaeota, and WSA2 showed no peaks in the SMTZ, and were either in much lower abundance than ANME-1 or contained no genes for methanogenesis, we cannot reasonably conclude that they are responsible for AOM or methanogenesis in White Oak River estuary sediments. Collectively this provides very strong evidence that ANME-1 reverses between AOM in the AOM zone and methanogenesis in the methanogenic zone, simply because it is the only organism present with the genetic capability to do so.

Further evidence that ANME-1 reverse between AOM and methanogenesis with sediment depth comes from changes in cell abundance with depth. A higher cell density of AOM-performing microbes is expected in the AOM zone than methanogenesis-performing microbes in the methanogenesis zone because the amount of methane that is consumed over just a few centimeters sediment depth in the AOM zone is produced over the many tens of centimeters of methanogenesis. In agreement with this trend, maximum ANME-1a and ANME-1b FRAxC values were three- and five-fold higher in the AOM zone than the maxima in the methanogenesis zone. ANME-1b FRAxC increased steadily between 56 and 70 cm in the methanogenesis zone (Fig. 2-2C), coinciding with increasing hydrogen concentrations (Fig. 2-1D). This is consistent with hydrogenotrophic methanogenesis supporting the growth of this population. Although ANME-1a did not increase with depth in the methanogenic zone, its cell abundance did not decrease, suggesting that it, too, was capable of sustaining a viable population throughout the methanogenic zone. The only other member of Methanomicrobia present, *Methanobacterium sp*., representing 0.15% of Methanomicrobia with one OTU, did not increase with depth in the methanogenic zone. In contrast to ANME-1, sulfate reducing bacteria decreased in FRAxC throughout the methanogenic zone, suggesting that successively smaller populations were capable of meeting their energetic needs on either cryptic sulfur cycling or fermentation as substrates were depleted with depth. This also suggests that ANME-1 populations were not dependent on sulfate reducing bacteria in the methanogenic zone, consistent with ANME-1 performing methanogenesis.

In the AOM zone, however, ANME-1 variations coincided with those of *Desulfatiglans sp.* and SEEP-SRB1. The four most abundant OTUs of ANME-1 and *Desulfatiglans sp.* (comprising 96% and 63% of total sequences from each of the two clades) had three discrete and coinciding peaks in the SMTZ (Fig. 2-3). Similarly, coinciding spikes in abundance in the SMTZ were demonstrated by SEEP-SRB1. Although this group was much less abundant than Desulfatiglans, it has been shown to form syntrophies with ANME-1 (32, 35, 93, 94). These sulfate reducing bacteria in the SMTZ were different from the dominant clades present in the upper, methane-free sulfate reduction zone, which were dominated by *Desulfobulbus sp.* and the uncultured Sva0081 clade within the Desulfobacteraceae. This suggests that *Desulfatiglans sp.* and SEEP-SRB1 may be adapted to syntrophy with ANME-1 and are out-competed by *Desulfobulbus sp.* and Sva0081 when sulfate is plentiful in the upper 4 cm of the core.

The presence of population peaks of ANME-1 and sulfate reducing bacteria in the AOM zone has a couple of potential explanations. The first explanation is that a random distribution of these populations throughout the AOM zone results in some areas having more cells than others due to non-uniform clonal growth. Support for this hypothesis comes from the fact that these peaks did not coincide with measurable changes in sulfate, methane, or hydrogen concentrations. The second explanation is that these peaks represent population oscillations similar to a Lotka-Volterra model in which a reversible chemical reaction oscillates in direction as it approaches equilibrium. This model has been used to describe predator-prey interactions (95), and here it would describe microniches of methanogenesis followed by methanotrophy in the AOM zone, as sulfate becomes extremely limiting and sulfate reducing bacteria start to lose thermodynamic control of the hydrogen that is being continuously produced by fermenters (96). This is similar to the oscillations of subpopulations under extreme catabolic substrate limitation called the growth advantage in stationary phase (GASP) response (97). Such a mechanism could explain the cryptic methane cycling proposed by Beulig et al., 2018, who explained their simultaneous methanogenesis and AOM rates by presuming these processes alternated on smaller time or space scales than were measured (43). A third possibility is that these peaks could be leftover from previous locations of the SMTZ, which has been demonstrated to migrate up and down the sediment column over time (46, 48). If this were the case, one would expect that ANME-1/SRB peaks would be present below the present-day SMTZ as well as above it, but this was not observed in our study. Even though core 1 had a deeper base of the SMTZ than core 6, demonstrating the likelihood that the SMTZ in core 1 has probably been deeper than it is present-day, core 6 had no ANME-1/SRB below the present-day SMTZ. Therefore, the third possibility is unlikely, meaning that either of the other two possibilities are more likely.

The best support that ANME-1 archaea perform AOM comes from enrichments of ANME-1 that drive equimolar decreases in methane and sulfate, with concomitant increases in sulfide, and gradual ^{13}C-enrichment of the remaining methane due to a preference for the ^{12}C isotope during AOM (88, 98). These geochemical changes over time provide solid evidence of AOM occurring in an enrichment where the only reported member of the Methanomicrobia is ANME-1. If ANME-1 are capable of reversing metabolism to methanogenesis, then these same ANME-1 enrichments should produce methane when hydrogen is added. In support of our conclusions, adding H_2 to the headspace of these ANME-1 enrichments caused methane concentrations to increase (35). When the H_2 was consumed, methane concentrations decreased

since sulfate was available to drive AOM. The rates of the net methanogenesis and net AOM were equivalent. If ANME-1 was the only organism in these enrichments with the genetic capability of producing and oxidizing methane, then this is extremely good evidence that ANME-1 reverse their metabolism between methanogenesis and AOM, depending on the H_2 concentration.

It is possible, however, that in these experiments, ANME-1 performed AOM, and a different organism that was previously missed by the researchers performed methanogenesis. However, a Blast search of all known genes for methyl coenzyme M reductase against the transcriptomes from this experiment showed that only ANME-1 had hits at an e-value cutoff of 1×10^{-10}, under every experimental condition, with the exception of <0.01% hits to ANME-2 in two of the methane incubations. Therefore, the only organism with the genes capable of methane metabolism in each of these incubations was ANME-1. Wegener et al. point out that the cessation of AOM under conditions of high hydrogen may simply reflect a metabolic decoupling of ANME-1 and sulfate reducers, since the sulfate reducers prefer electrons from hydrogen.

These enrichments were made with thermophilic organisms from Guaymas Basin, but enrichments of mesophiles from Hydrate Ridge and Amon Mud Volcano show similar H_2-dependent reversibility (101). Simply washing the ANME-1 enrichments free of sulfate was sufficient to see steady methane increases over a period of 30 days, presumably fueled by organic matter present in the enrichments. The fact that methane started being produced in less than a day and did not increase in production rate over 30 days suggests that the methane was produced by the ANME-1 that were already there, not a subpopulation that grew which would have caused an exponential methane increase and a substantial lag time. Adding H_2 to the headspace increased the rate 100-fold. The rate of methanogenesis was much lower than that of AOM, likely because some ANME-1 cells were washed out of the system along with the sulfate.

If ANME-1 cells perform AOM through an interspecific hydrogen transfer to SRB cells, then they must contain hydrogenases, which are enzymes capable of metabolizing hydrogen. Although ANME-1 genomes contain homologs for the hydrogenases of cultured methanogens, they have thus far been found to lack the active site (35, 41, 102, 103). One possible explanation is that the active subunit of a typical methanogenic hydrogenase is present in ANME-1 genomes, but has not yet been sequenced because the genomes are incomplete, in a similar situation to the *mer* gene (43). Another possibility is that ANME-1 contain an evolutionarily-divergent hydrogenase that has yet to be described. All methanogenic hydrogenases that have been

characterized came from cultured methanogens growing under conditions of extremely high hydrogen (usually 80% gas). However, ANME-1 is adapted to a low energy, slow-growing lifestyle, and may have an evolutionarily-divergent hydrogenase with high substrate affinity, similar to *Escherichia coli*, which employs the high affinity cytochrome bd under conditions of O_2 limitation (104). Evidence that methanogens undertake major cellular rearrangements due to hydrogen limitation have been shown for *Methanocaldococcus jannaschii*, which produces flagella when hydrogen is low (105). One potential candidate for this high-affinity hydrogenase in ANME-1 was found by Beulig et al. 2018, who hypothesized that an F420-reducing hydrogenase could access electrons from hydrogen either alone or in combinations with an adjacent heterodisulfide reductase. However, this function still remains to be proven.

If ANME-1 has a reversible metabolism, then all the enzymes in the pathway must be reversible. Cells often ensure that metabolic reactions that are essential to the cell, yet operate at ΔG close to zero, only flow forward by employing "irreversible" enzymes. Such enzymes, such as phosphofructokinase in glycolysis, bind their product at an allosteric site away from the active site in order to disable the enzyme activity when product builds up, in order to prevent back-flow that would decrease the efficiency of the reaction. However, none of the genes of methanogenesis have this property (30); they appear well-poised to catalyze whichever direction is exergonic. This may be an advantage to ANME-1, since they can gain energy when AOM is favored, increasing their relative cell abundance over other methanogens that are not able to catalyze the reverse process. Then, when hydrogen concentrations increase, they have a head start on these other methanogens, and can outcompete them for available resources.

High depth-resolution analysis of FRAxC relative abundance of ANME-1 and sulfate reducing bacteria enabled us to visualize ANME-1 growth in the SMTZ, and also in the methanogenic zone. Concurrent increases of Desulfatiglans, SEEP-SRB1, and ANME-1 over the depth profile suggest a syntrophic relationship. The lack of any cultured methanogen in high abundance in the methane production zone or SMTZ other than ANME-1 suggest that ANME-1 can perform both methane oxidation and methane production. This shift in metabolism also appears to be mediated by the concentration of molecular hydrogen dictating the direction, consistent with previous studies and the genetic capabilities of ANME-1. The results of this study also indicate that ANME-1 should not be used as an indicator of AOM, since they could equally likely be performing methanogenesis.

This metabolic reversal of ANME-1 methanogens, dependent upon sulfate-reducing bacterial control of hydrogen concentrations, agrees with the original hypothesis for AOM in marine sediments (16, 37), as well as more recent literature demonstrating hydrogen-dependent net methane production in ANME-1 enrichments, measurable methanogenesis in the SMTZ (43) and genes in ANME-1 that are plausibly hypothesized to utilize hydrogen (96). Non-seep marine sediments are the third largest producers of methane on Earth, after rice production and wetlands, but they are only the ninth largest emitters of methane on Earth (10). ANME-1 are the dominant Methanomicrobia in environments that cover the full range of environment types that contribute to these budgets: coastal marine sediments (Aarhus Bay), brackish estuarine sediments (White Oak River estuary), and offshore deep-water sediments (Gulf of Mexico slope). Therefore, ANME-1 may be one of the greatest emitters of methane on Earth and are also responsible for consuming it as well. In the search for habitable zones on Earth and extraterrestrially, researchers should look for further examples of metabolic reversals, which may be a general feature of organisms specialized to survive in ultra-low energy environments.

Methods

Sample collection

Two push cores (core 1 was 78 cm deep and core 6 was 75 cm deep) were collected in May 2017 (1 m) at the White Oak River Estuary Station H (34 44.490’ N, 77 07.44’ W), in 1.5 m water depth. Using a plunger inserted from the bottom to push the core up, sediment intervals were sectioned in 1 cm intervals from 0 to 60 cm and in 3 cm intervals below that.

Sampling and geochemical measurements

To measure methane, sediment was quickly sub-cored with a plastic cut-off 4 ml syringe, placed into glass serum vial containing 1 ml 0.1 M KOH, sealed with a butyl rubber stopper, and shaken to mix. with a negative bottle only containing KOH. Methane was determined by injecting 100 µl of gas from the headspace, after shaking the bottle vigorously for 1 min, into a gas chromatograph with a flame ionization detector (Agilent, Santa Clara, CA). The formula for determining methane concentration was peak area of sample multiplied by the volume of the bottle headspace, which was divided by gas constant times temperature, porosity, volume of sediment. To measure $\delta^{13}C$ values of methane, 4 ml of headspace from the vial used for methane

measurements was removed via syringe and injected into a gas bag containing hydrocarbon free zero gas (Airgas, Radnor, PA). This was then measured on a cavity ring down spectrometer using a small sample introduction module (Picarro, Santa Clara, CA). To measure hydrogen, 2 ml of carefully sub-cored sediment was placed into a 10ml brown glass vial being careful to disturb the sediment as little as possible, sealed with a black butyl stopper, and gassed with helium. Negative control was an empty bottle gassed with helium. After 4 days equilibration at near *in situ* temperature (21°C), 500µl of headspace gas was injected into a Peak Performer 1 Reducing Compound Photometer (Peak Laboratories, Mountain View, CA). Premixed hydrogen ppm lab bottles (Airgas) were used as standards. This method has shown to result in headspace hydrogen concentrations that are equilibrated between with porewater (37) For cell abundance, 1 ml of sediment was placed in a 2 ml screw cap tube with 3% paraformaldehyde. To measure sulfate, a 15 ml plastic tube was filled completely with sediment and centrifuged at 5 000 xg for 5 minutes. A syringe was used to remove the supernatant below the air interface. The porewater was filtered using a 0.2 µm syringe filter into 100 µl of 10% HCl to a final volume of 1 ml. Porewater sulfate concentrations were determined by ion chromatography (Dionex, Sunnyvale, CA). A 10 ml cut off syringe was filled, capped with parafilm, and frozen at -80°C for later molecular analysis.

Cell quantification

Total cell counts were determined by direct epifluorescence microscopy using SYBRGold DNA stain (Invitrogen, Carlsbad, CA). Sediments were sonicated at 20% power for 40 seconds to disaggregate cells from sediments and diluted 40-fold into PBS prior to filtration onto a 0.2 µm polycarbonate filter (Fisher Scientific, Waltham, MA) and mounted onto a slide.

16S ribosomal RNA gene amplicons

DNA was extracted from frozen sediments using the Fast DNA kit for Soil (MP Bio, Santa Ana, CA). Autoclaved sediment and water blanks were used as negative controls. The V4 region of each DNA extraction was amplified using primers 806r and 515f (106), as a universal primer pair for Bacteria and Archaea. Library preparations via Nexterra kit and sequencing using an Illumina MiSeq were performed at the Center for Environmental Biotechnology at the University of Tennessee in Knoxville. At total of 14 162 094 reads were produced as a result of sequencing. The CLC Genomic Workbench 10.0 (CLC Bio, a QIAGEN Company, Aarhus, Denmark) was used to trim adaptors and make contigs of bidirectional sequences, cluster

operational taxonomic units (OTUs) at 97% similarity, and classify them with the Silva reference set 132 (107). 36.4% of a total of 866 834 unique sequences were removed as chimeric. with a total of 9 165 958 reads in 25 116 OTUs. Approximately 5% of the remaining sequences were removed for not classifying as Archaea or Bacteria. Reads were then randomly subset from sample libraries to the size of the smallest library (77 609). Further analyses were considered for OTUs with at least an average of 2 reads per sample, leaving 2 307 OTUs across 59 libraries. A negative sample containing DNA extracted from autoclaved sediment control yielded no amplification. Estimates of community coverage were determined for a rarefied set of 20 922 OTUs using the CLC software.

Fractional Read Abundance times Cells (FRAxC)

Relative read abundance of 16S rRNA sequences were calculated by dividing the number of sequences for a particular OTU by the sum of bacterial and archaeal reads. The FRAxC values were calculated by multiplying the relative read abundance values by the total cell counts determined by direct epifluorescence microscopy. Turnover times were determined for OTUs that exhibited exponential increases in relative cell abundance for a minimum of four time points and an $R^2 \geq 0.9$ as described previously (18). Sedimentation rate at this site is 0.26 cm/year (108).

Data archiving

16S rRNA gene sequences can be found at the NCBI Genbank short read archive with accession numbers (###). Geochemistry data can be found at www.bco-dmo.org with project number ###.

Appendix

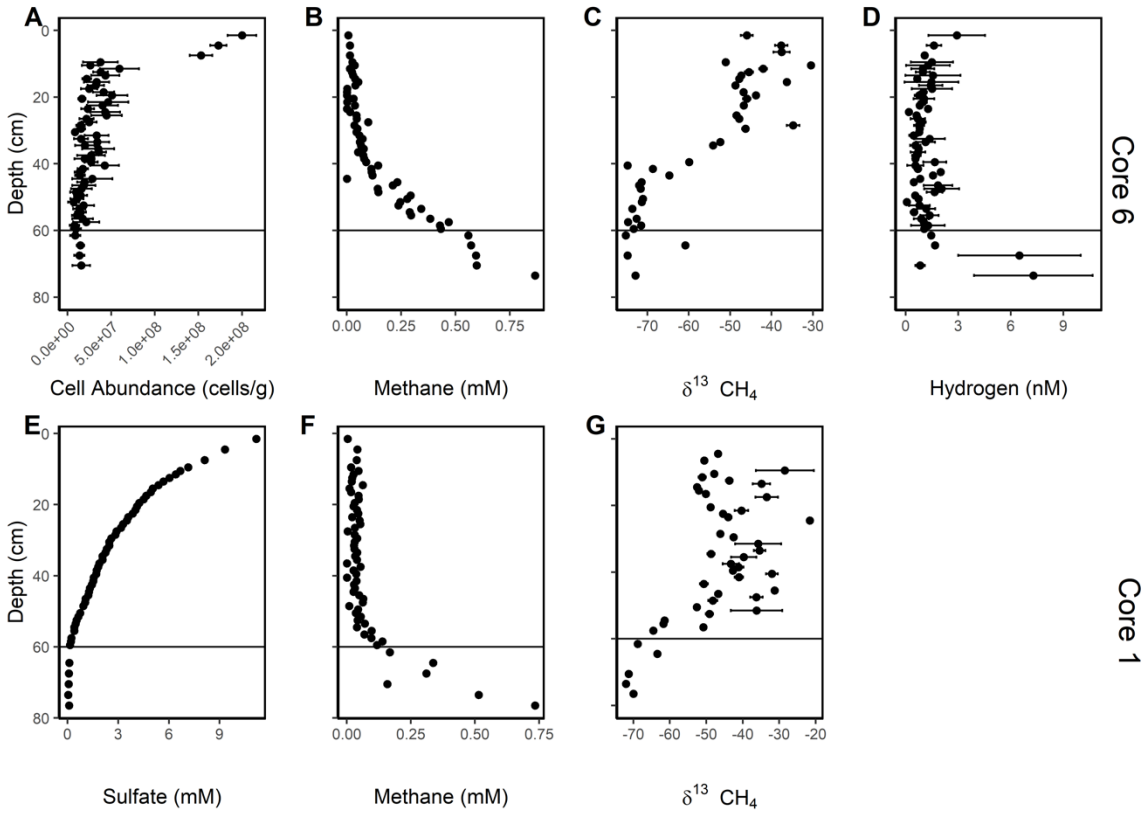

Figure 2-1. White Oak River estuary cores show methane-consuming or AOM sediments in the SMTZ and methane-producing or methanogenic sediments below it.

Aqueous geochemistry for cores 6 (top row) and 1 (bottom row), with A) cell abundance, B and F) methane concentration, C and G) δ13C of CH4, D) hydrogen concentration, and E) sulfate concentration. Black line shows approximate transition from AOM to methanogenesis.

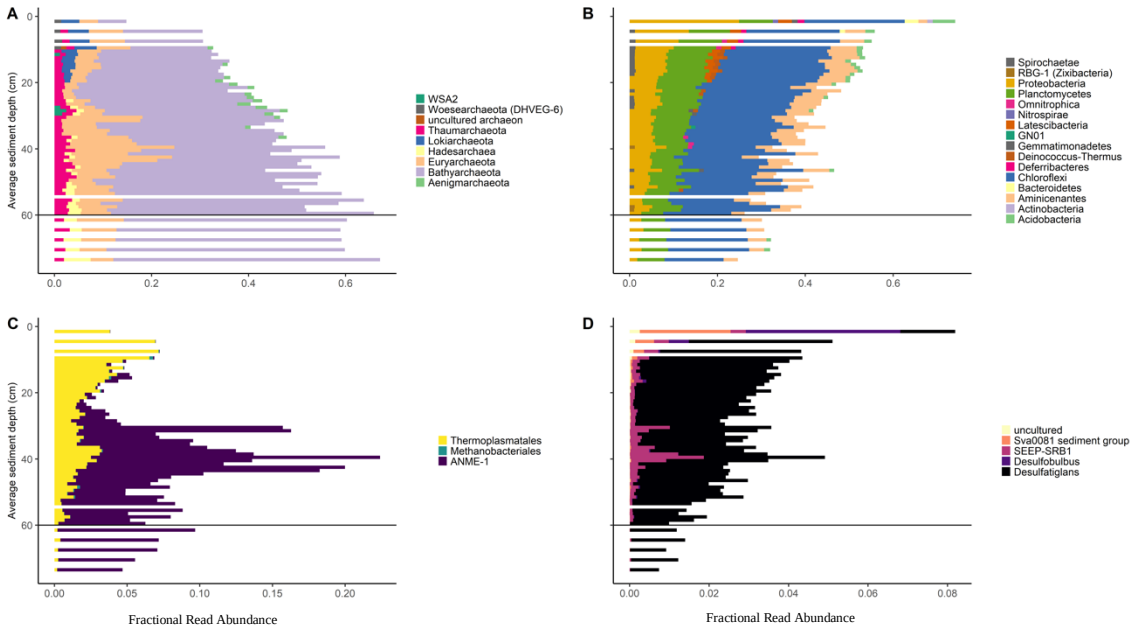

Figure 2-2. ANME-1 and *Desulfatiglans sp.* dominate methane- and sulfur-cycling organisms in both methane-consuming and methane-producing sediments.

Relative abundance of 16S rRNA gene sequences for all archaea (left panels A and C) and all bacteria (right panels B and D), grouped at the phylum level. Bottom panels show only putative sulfate reducing bacteria and Euryarchaeota, grouped at the family level. Phyla with <1% relative 16S rRNA gene sequence abundance for bacteria and < 0.1% for archaea, were not included. Black line denotes the point where methane production begins.

Table 1. Turnover Times

Putative Metabolism	OTU	Taxon	Period of Exponential Growth (cm)	Turnover Time (years)	R^2
Organoheterotrophy	OTU843	Hadesarchaea-unclassified	48.5- 51.5	3.72	0.99
	OTU8190	Hadesarchaea-unclassified	17.5- 25.5	4.12	0.93
	OTU6809	Dehalococcoidia	10.5-13.5	3.35	0.98
	OTU3056	ANME-1-unclassified	35.5- 39.5	2.88	0.99
Methane Oxidation	OTU3059	ANME-1b	33.5- 36.5	3.35	0.98
	OTU6146	ANME-1b	33.5- 36.5	3.18	0.98
Butane Oxidation	OTU2300	Bathyarchaeota	24.5-27.5	4.34	0.99
Sulfate Reduction	OTU5032	Seep-SRB1	33.5-36.5	4.32	0.90

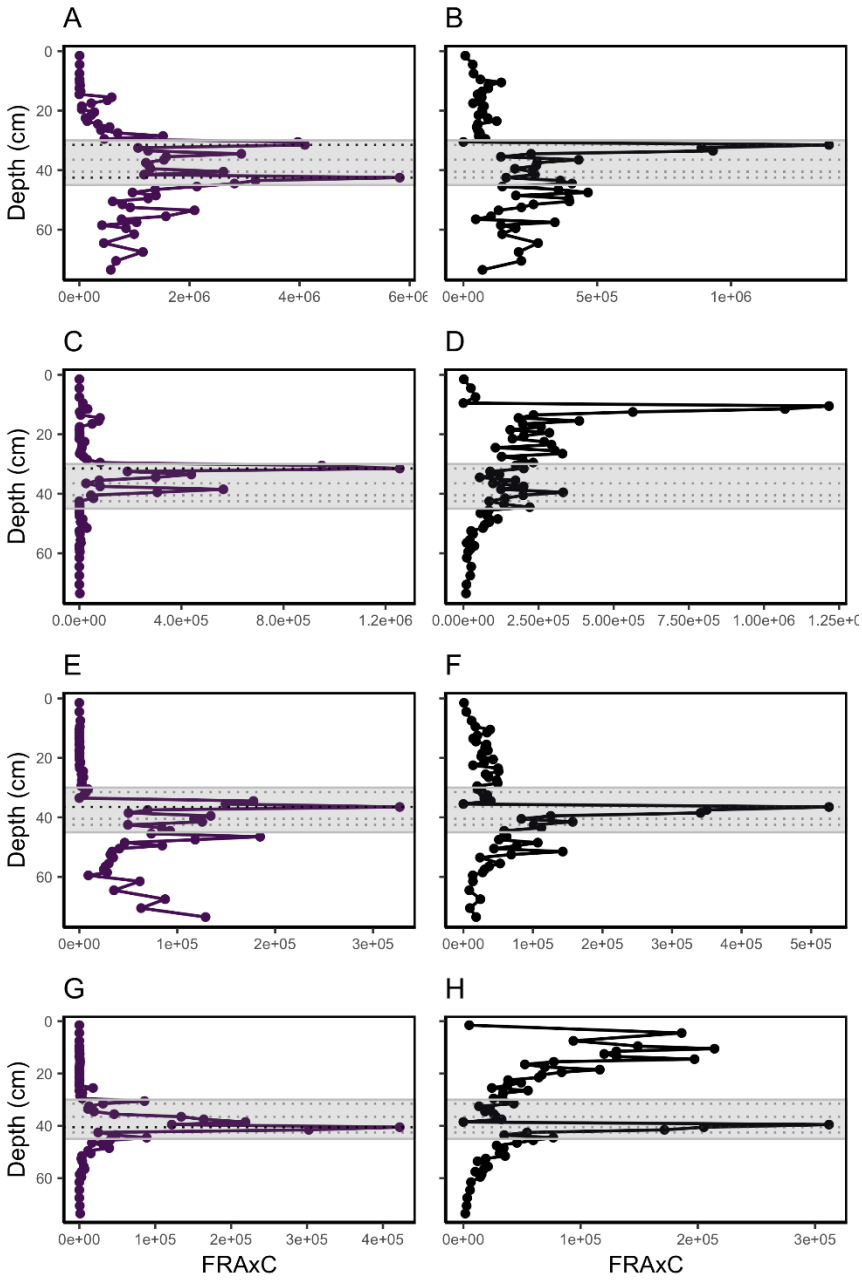

Figure 2-3. FRAxC of most abundant ANME-1 and sulfate reducing bacteria have co-occurring peaks during AOM but not methanogenesis.

FRAxC values for the four most abundant OTUs of ANME-1 (left panels, A, C, E, and G) and Desulfatiglans (right panels, B, D, F, and H) with depth. OTUs decrease in relative sequence abundance from top to bottom panels. Collectively, these OTUs contain X and Y percentages of the total sequences from ANME-1 and Desulfatiglans, respectively. Grey boxes show SMTZ, and dotted lines show peaks of ANME-1 and Desulfatiglans.

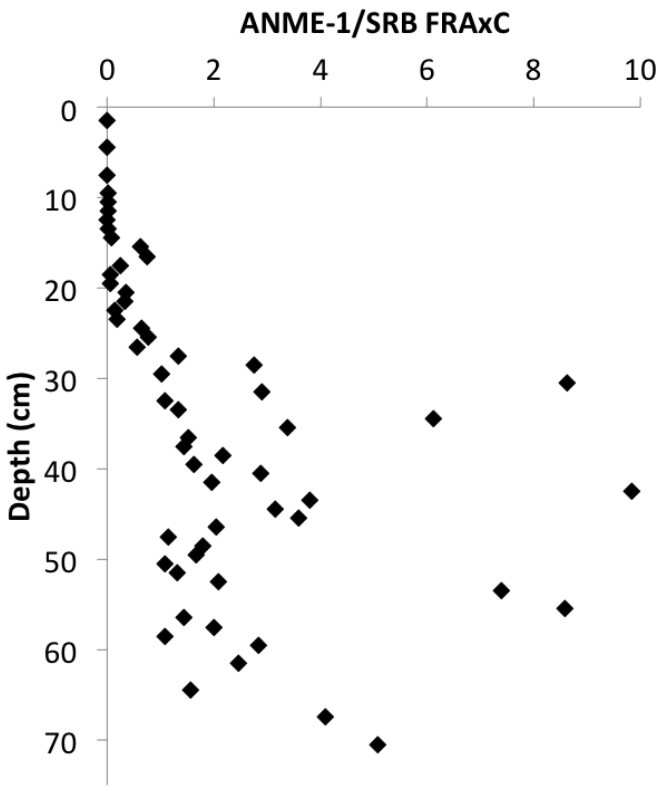

Figure 2-4. ANME-1 increased relative to sulfate reducing bacteria throughout the SMTZ and below.

ANME-1 increase relative to sulfate reducing bacteria throughout the SMTZ and below. Ratio of total ANME-1 16S rRNA gene abundance to total sulfate reducing bacteria 16S rRNA gene abundance with depth.

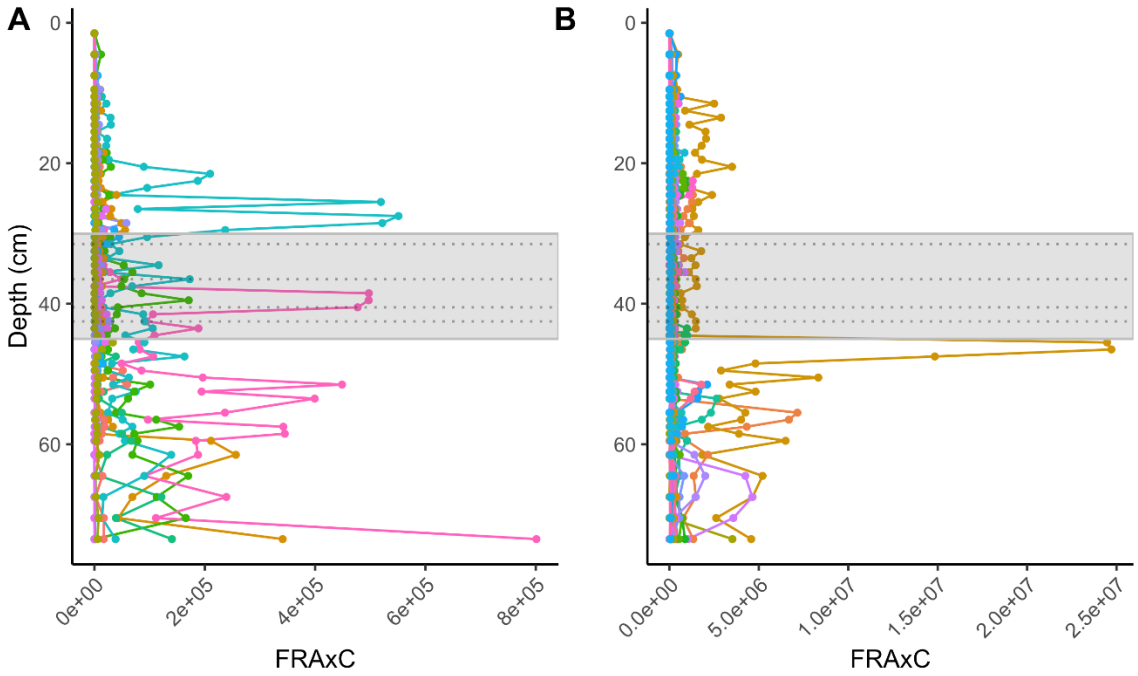

Figure 2-5. FRAxC values of dominant archaea taxa Bathyarchaeota and Hadesarcheota don't respond to AOM.

FRAxC values for OTU's of Hadesarchaeota (A) and Bathyarchaeota (B). Grey box denotes the range of the SMTZ and the dotted lines the peaks in ANME abundance shown in Fig. 2-3.

Table S2-1. Geochemistry from sediment core

Depth Interval	Avg Depth	[CH4] mM	Methane ppm	[mM] sulfate	nM hydrogen	h2 stdev
0-3	1.50	3.41E-06	43.64322	11.17495	2.918932	1.620687
3-6	4.50	3.63E-05	463.5042	9.311088	1.611648	0.41849
6-9	7.50	3.47E-05	441.5595	8.114083	1.084967	0.172459
9-10	9.50	1.52E-05	193.1951	7.144323	1.500408	1.200862
10-11	10.50	4.09E-05	519.2887	6.668035	1.278659	1.245708
11-12	11.50	2.41E-05	305.3795	6.404114	0.979366	0.661193
12-13	12.50	1.91E-05	242.4168	6.030932	0.986222	0.401442
13-14	13.50	1.74E-05	220.267	5.677755	1.559423	1.565765
14-15	14.50	5.56E-05	703.0497	5.37408	0.653051	0.096208
15-16	15.50	9.25E-06	116.84	5.046808	1.47447	1.539437
16-17	16.50	1.48E-05	186.4271	4.925235	1.429919	0.671528
17-18	17.50	4.06E-05	511.9055	4.650799	1.5036	1.156599
18-19	18.50	4.09E-05	514.9818	4.495627	1.003698	0.208958
19-20	19.50	2.7E-05	339.6296	4.247352	0.778767	0.260744
20-21	20.50	2.29E-05	287.3316	4.107825	1.044683	0.587242
21-22	21.50	3.55E-05	446.0715	4.016005	0.983455	0.233306
22-23	22.50	4.09E-05	513.136	3.861089	0.802244	0.158408
23-24	23.50	1.94E-05	243.6473	3.591013	1.277452	0.113243
24-25	24.50	4.51E-05	564.2035	3.514068	0.179872	0.049118
25-26	25.50	4.77E-05	596.8129	3.282721	0.623812	0.099613
26-27	26.50	2.83E-05	353.7808	3.161661	0.695829	0.413058
27-28	27.50	2.84E-06	35.47037	2.895689	0.913329	0.234541
28-29	28.50	2.71E-05	337.7838	2.826438	0.764192	0.287717
29-30	29.50	3.57E-05	444.841	2.589192	0.805934	0.071394
30-31	30.50	2.78E-05	345.7823	2.46685	0.776997	0.154109
31-32	31.50	2.51E-05	311.9424	2.468901	0.454597	0.244142
32-33	32.50	2.7E-05	334.7074	2.318346	1.364447	0.872386
33-34	33.50	3.55E-05	439.9188	2.243453	1.133516	0.542585
34-35	34.50	2.91E-05	360.5488	2.069045	0.558413	0.298242
35-36	35.50	3.51E-05	434.9966	2.070584	0.738916	0.174901
36-37	36.50	7.01E-07	8.675321	1.885147	0.704883	0.418788
37-38	37.50	4.83E-05	596.8129	1.818462	0.623735	0.244564
38-39	38.50	2.4E-05	296.5606	1.718433	0.552124	0.125366
39-40	39.50	3.39E-05	417.769	1.69535	1.659653	0.657295
40-41	40.50	1E-06	12.36695	1.549155	0.553537	0.459592
41-42	41.50	3.43E-05	422.0759	1.523507	0.696258	0.196757
42-43	42.50	2.49E-05	306.405	1.436046	1.996081	0.134374

Table S2-1 Continued.

Depth Interval	Avg Depth	[CH4] mM	Methane ppm	[mM] sulfate	nM hydrogen	h2 stdev
43-44	43.50	2.82E-05	346.3976	1.315756	1.560013	0.142328
44-45	44.50	2.35E-05	288.5621	1.268306	0.827696	0.107728
45-46	45.50	4.36E-05	534.6705	1.228039	0.463027	0.101733
46-47	46.50	5.79E-05	708.7922	1.066968	1.84818	0.813745
47-48	47.50	5.6E-05	684.7967	1.03106	2.054772	1.002545
48-49	48.50	8.51E-06	103.9808	0.933597	1.650023	0.450098
49-50	49.50	3.95E-05	482.3725		0.546356	0.154487
50-51	50.50	3.2E-05	390.0818	0.741235	0.740029	0.023836
51-52	51.50	4.96E-05	604.8114	0.632743	0.066565	0.025181
52-53	52.50	3.91E-05	476.2198	0.528354	0.78709	0.593129
53-54	53.50	6.5E-05	790.008	0.477058	1.172213	0.521304
54-55	54.50	3.65E-05	442.9951	0.400113	0.47454	0.19118
55-56	55.50	9.01E-05	1093.337	0.397548	1.360977	0.527022
56-57	56.50	6.4E-05	776.472		0.893101	0.432298
57-58	57.50	9.04E-05	1094.567	0.22827	1.036358	0.071613
58-59	58.50	0.000131	1583.708	0.197492	1.274194	0.960808
59-60	59.50	0.000111	1342.521	0.138501	1.061512	0.036265
60-63	61.50	0.000159	1916.569		1.454021	0.117633
63-66	64.50	0.000318	3823.294	0.100028	1.675691	0.098033
66-69	67.50	0.000296	3548.268	0.071815	6.498111	3.491216
69-72	70.50	0.000151	1800.283	0.058991	0.823565	0.27001
72-75	73.50	0.000489	5821.694	0.033343	7.288062	3.390407
75-78	76.5	0.0007	8314.157	0.087204		

CHAPTER 3

METHANE PRODUCTION IN LONG-TERM SEDIMENT MESOCOSM EXPERIMENTS REVEAL ANME-3 AS A METHANOGEN

This chapter has been prepared for submission as a peer-reviewed article by Richard Kevorkian and authors: Richard Kevorkian, Brandi Barber, Rachel Winstead, Raegan Paul, and Karen G. Lloyd. “Methane production in long-term sediment mesocosm experiments reveal ANME-3 as a methanogen.” *Applied and Environmental Microbiology”*.(2019).

Richard Kevorkian and Karen G. Lloyd designed the study. All analyses were completed by Richard Kevorkian. Other data collection occurred with assistance from Brandi Barber, Raegan Paul, and Rachel Winstead. The manuscript was written by Richard Kevorkian with inputs from Karen G. Lloyd.

Abstract

Long-term (895 days) microcosm experiments of anoxic sediments from the White Oak River estuary, NC simulated the natural transition of marine-influenced sediments from sulfate reduction to methane production without the complicating factor of the sulfate/methane transition zone (SMTZ). In situ, the SMTZ is caused by methane produced in underlying sediments diffusing upward into the sulfate containing zone, stimulating microbial anaerobic methane oxidation. Removing the SMTZ allows for the distinction between methane oxidizing and methane producing communities in sediments containing diverse populations of microbes. We elucidated the methanogenic and methanotrophic microbial community diversity and abundance in real-time by 16S rRNA gene analysis. Stable carbon isotopes suggest that methane was biotically oxidized while sulfate reduction was actively occurring. Adding methane to sulfate rich sediment did not stimulate anaerobic methanotrophs (ANME's) previously observed in these sediments. Rather, both incubations demonstrated growth of putative methanogens after sulfate was depleted and methane was being produced. Likely methanogens included *Methanolinea* spp. and *Methanosaeta* spp., and ANME-3, the latter of which has only previously been implicated in anaerobic methanotrophy. The incubations were dominated by the archaeal phylum Bathyarchaeota which has been shown to be an organoheterotroph, but otherwise demonstrated little phylum level changes, with bacteria consistently comprising 75-80% of total reads and archaea the remainder. By isolating the sulfate methane transition zone from the methane production, we were able to characterize the microbial community responsible for methane production without being primed by methane oxidation, as they are in natural sediments.

Importance

The environmental relevance and impact of many microbes is difficult to determine without the ability to be isolated in pure culture. We successfully generated two long term mesocosm incubations to simulate a diagenetic profile of marine sediments. This allowed for the observation of the microbial community shift caused by the natural progression from sulfate reduction to methanogenesis. Our research provides evidence for the production of methane by microbial taxa believed to be responsible for its anaerobic oxidation. Furthermore, we provide evidence that anaerobic oxidation of methane could not be stimulated in sulfate reducing

sediments in microbial taxa that are believed to utilize this metabolism as their sole energy source.

Introduction

Marine sediment microbial communities are phylogenetically diverse and abundant, totaling ~10^{29} cells globally (2, 12, 13, 109, 110). The majority of these cells belong to taxonomic groups that have no cultured representatives at the genus level or higher, making it necessary to infer their geochemical functions in a natural setting. Microbes surviving in marine sediments have been shown to grow on the order of weeks, months, or even longer in low energy environments, and therefore require a long duration of study (75). These microbes drive sulfate reduction, methanogenesis, and the anaerobic oxidation of methane (AOM), which are the key respiratory processes oxidizing organic matter in marine sediments. Enormous quantities of methane are produced globally in marine sediments (10). AOM is responsible for at least 80% (45-61 Tg) of methane removal before it reaches the atmosphere (10, 21). The balance between diffusion and biological respiration over time as sediments are buried drives a downcore shift from sulfate reduction to methanogenesis, with net removal of methane through AOM in the sulfate/methane transition zone (SMTZ) at intermediate depths (49). In the SMTZ, sulfate reducers are believed to keep hydrogen concentrations low enough to make reverse methanogenesis exergonic (10, 18, 37). Methanogenesis and AOM appear to be mediated by uncultured anaerobic methanotrophic (ANME) archaea (43, 44, 78), which are phylogenetically related to cultured methanogens, include many of the genes required for methane production (41–43), and have been associated with both methanogenesis and AOM in laboratory enrichments (101, 111). They have also been shown to form syntrophies with sulfate reducing bacteria (SRB), with whom they share electrons or some other reducing equivalent to perform AOM (25, 32, 36). ANME's comprise multiple non-monophyletic groups within the Methanomicrobia. The class Methanomicrobia has many cultured representatives, all of which are obligate methanogens (40). ANME-1 is its own order in the Methanomicrobia, ANME-2a/b and ANME-2c are families within the order Methanosarcinales, and ANME-3 is a species within the *Methanococcoides* genus of the order Methanosarcinales. However, despite the presence and activity of ANME's in methanogenic sediments, direct evidence that ANME archaea either are capable of methanogenesis or shift between methanogenesis and AOM in marine sediments is lacking (36).

Recent studies have suggested that methanogenesis and AOM occur simultaneously in marine sediments dominated by ANME-1 archaea in a "cryptic" methane cycle, were the pool of methane may be observed to change when in fact it is being constantly created and destroyed (43) . However, it is difficult to distinguish between the methanogenic and methanotrophic zones of marine sediments due to free diffusion methane and environmental heterogeneity. This obfuscates the active metabolism of microbes and encourages their potential misclassification, especially in the case of methane cycling if the same pathway is used for two types of energy production. Several attempts have been made to incubate sulfate rich marine sediments until sulfate is depleted and methane produced (18, 112). These incubations were conducted on much more active sediments and over shorter periods of time (≤122 days) than would be found in many marine sediments.

To study methanogenesis in isolation from anaerobic methanotrophy in extremely slow-growing natural populations over a long time period, we conducted two long term mesocosm incubations to investigate the microorganisms responsible for methanogenesis and AOM in marine-influenced sediments from the White Oak River estuary, NC. The White Oak river estuary has an annual sedimentation rate of 0.26 cm / yr^{-1}, is anoxic within a few millimeters, and has well characterized geochemical gradients (48). The first incubation, WOR 5.16, involved subsampling from three incubation chambers monthly over 895 days, without adding any substrates to alter the system. The second incubation, WOR 5.17, occurred in separate incubation vials, three of which were destroyed at each monthly timepoint over 586 days, and methane was added to the headspaces on day 45. We examined 16S rRNA gene sequence libraries as well as concentrations of methane, sulfate, and hydrogen and $\delta^{13}C$ values of methane. This allowed us to create a temporal analog for depth by incubating the near surface, sulfate-rich sediments over extended periods of time, allowing dissolved porewater sulfate to deplete via sulfate reducing bacteria and subsequently methane production to occur without the diffusion that would create an SMTZ. No significant amount of sequences identified as ANME-1 were detected, however, sequences identified as ANME-3 were shown to increase in abundance only in the methane production zone, alongside other traditionally classified methanogenic archaea.

Results

Geochemistry

Sulfate concentrations in the WOR5.16 incubation decreased over 312 days from an initial concentration of 12.9 ± 0.2 mM before approaching a more stable concentration at or below 1 mM (Fig. 3-1D). Sulfate concentrations in WOR5.17 decreased over 323 days from an initial concentration of 10.8 ± 0.7 mM before reaching a stable average concentration near or below 1 mM (Fig. 3-2D). This is consistent with sulfate being consumed biotically, probably by sulfate-reducing bacteria. Although sulfate was reduced constantly in that time the concentration never reached zero, indicating that the concentration was too low for sulfate-reducing bacteria to use or it reached equilibrium with sulfide being reoxidized back to sulfate (84).

Aqueous methane concentrations in WOR5.16 ranged from 0.002-0.009 mM at the first measured timepoint, 7 days, to a maximum of 1.7 mM at 487 days (Fig. 3-1B). The concentration remained below 0.07 mM until sulfate was limiting at 312 days. Methane concentrations in the first two timepoints, 1 and 44 days, prior to the addition of methane to 5.11 mM, averaged 0.014 ± 0.011 mM in WOR5.17. Subsequent time points demonstrated a sustained decrease in methane concentration to 0.02 mM at 200 days (Fig. 3-2B), this was followed by an increase in methane to a maximum 1.9 mM by 278 days, before declining to 2.0e-4 mM at 363 days. After this point, methane increased steadily for the rest of the incubation reaching a maximum of 4.86 mM at 397 days.

The mean hydrogen concentration in the headspace of WOR5.16 at the first time point was 0.118 ± 0.401 nM (Fig. 3-1C). Concentrations remained below 1.0 nM until sulfate was depleted at 312 days and the concentration rose as high as 10.1 ± 0.36 nM at day 375, before declining and reaching a new equilibrium around 1 nM and a final concentration of 0.19 ± .03 nM at day 895. The mean concentration in the first time point of WOR5.17 was 0.136 ± 0.054nM (Fig. 3-2C). Subsequent mean concentrations up to 431 days were greater, ranging from 0.36 to 0.92 nM, at which point the concentrations dropped to under 0.24 nM for the remaining incubation. Following the depletion of sulfate, the replicate variability decreased from a high of 5.7 nM at 276 elapsed days to an average of 0.05 nM between 431-586 days.

Stable carbon isotopes of methane were measured only for WOR5.17. The value for the methane added experimentally on day 45 was -34.9 ‰. The fractionation values depleted in the

lighter isotope slightly at 111 and 323 days, which corresponded with a depletion of aqueous methane concentrations (Fig. 3-2E). This is consistent with the presence of AOM due to preference for ^{12}C over ^{13}C, leaving the residual methane ^{13}C-enriched (15, 86–88). After sulfate was depleted at 323 days the fractionation values steadily declined to -79 ‰ at 568 days. These values are consistent with the biogenic production of methane, resulting in enrichment of the lighter carbon isotope, ^{12}C, resulting in values (85).

Total cellular abundance in WOR5.16 was $2.64 \times 10^8 \pm 1.03 \times 10^8$ cells/ml initially as determined by direct cell counts, which increased to $1.22 \times 10^9 \pm 2.00 \times 10^8$ cells/ml by 35 days, before decreasing to a final $1.94 \times 10^8 \pm 3.29 \times 10^7$ (Fig. 3-1A). Total cellular abundance in WOR5.17 was $2.06 \times 10^8 \pm 1.14 \times 10^8$ cells/ml initially, increased in abundance to $8.32 \times 10^8 \pm 2.34 \times 10^8$ cells/ml at 161 days, and then declined to $2.68 \times 10^8 \pm 8.64 \times 10^7$ cells/ml at 586 days (Fig. 3-2A).

Methane cycling communities

Members of the class Methanomicrobia increased in relative 16S rRNA gene abundance as sulfate neared depletion at 312 days and methane began to increase in the WOR5.16 incubation. This class increased two orders of magnitude to 0.2% of sequences at 570 days of incubation (Fig. 3-3C). Similarly, the relative abundance of Methanomicrobia in WOR5.17 increase significantly after sulfates depletion to maximum of 0.26% of sequences at 461 days of incubation. Of the 68 total Methanomicrobia ASVs in the WOR5.17 incubation, the most abundant was an unclassified species of the genus *Methanolinea*, which peaked at 566 days, accounting for 0.08% of total sequences (Fig. 3-4C). The second most abundant Methanomicrobia ASV in WOR5.17 was ANME-3. ANME-3 was consistently present in the methane production zone of both incubations and increased in relative 16S rRNA gene sequence abundance with increasing methane concentrations in both incubations. Three ASVs of ANME-3 were detected in WOR5.17 and increased to a relative abundance of $6.7\ E^{-4}$ at 461 days. The twelve ASVs of ANME-3 in the WOR5.16 incubation peaked at $6.4\ E^{-4}$ at 895 days.

Unclassified clades of Methanosarcinales and Methanomicrobiales were well represented in the methane producing zone, with 33 and 26 ASVs respectively. No sustained increase in abundance was observed for any Methanomicrobia ASVs during the first 312 days of the WOR5.16 incubation or the first 363 days of the WOR5.17 incubation, even though methane was added to the headspace in WOR5.17. Five ASVs of ANME-1 were detected at three timepoints in

WOR5.16 and five timepoints in WOR5.17 with relative abundances at or below 1.0 E^{-5}. Due to its low abundance and absence in the majority of time points, ANME-1 was not considered in further analyses.

Sulfate reducing bacteria

Bacteria closely related to cultured sulfate reducing bacteria were represented by 1563 unique ASV's in the WOR5.17 incubation accounting for as much as 11% of the total sequence abundance. The three most abundant ASVs were unclassified members of the family Desulfobulbaceae, which together accounted for ~2% of total sequences. Classified and unclassified members of the family Desulfobulbaceae (242 ASVs) accounted for ~3.5% of total sequences observed throughout the incubation. The Sva0081 sediment group had 121 ASV's consistently accounting for ~2-3% of sequence abundance. Many putative sulfate reducing bacteria decreased in abundance following the depletion of sulfate, but later rebounded to their previous abundance levels, or in some cases above previous levels, suggesting that they either switch metabolisms or have other roles in the community. In both incubations the immediate decrease in abundance after sulfates depletion appears to be replaced by an increase in methanogens. The genus *Desulfatiglans* represented 1.5% of sequence abundance and 353 ASVs. Although *Desulfatiglans* are putative sulfate reducing bacteria and potential syntrophs with methane oxidizers, they were in some cases slightly more abundant after sulfate was depleted and potentially could be replacing bacteria that appear to decline steadily overtime. SEEP-SRB1, another putative SRB and partner with methane oxidizers, accounted for ~0.5% of total sequences and 141 unique ASVs and showed little to no response to the depletion of sulfate.

Uncultured taxa

Bacteria in the WOR5.16 incubation, began the incubation with ~92% of sequences and ended with ~89% after 895 days (Fig. 3-3B). Archaea represented the remaining sequences with ~8% at the start of the incubation, increasing slightly over time to ~10% after 895 days of incubation (Fig. 3-3A). Proteobacteria was the most abundant bacterial phylum and accounted for approximately 40% of sequences throughout the timepoints. Bathyarchaeaota were consistently one of the most abundant archaeal clades in the WOR5.16 incubation and increased over time from 2% of sequences to ~6% sequences after 895 days (Fig. 3-5A).

Throughout the WOR5.17 incubation, bacteria represented the majority of total amplicon sequences with a slight decrease over time, beginning at ~78% and ending at ~73% of sequences (Fig. 3-4B). Archaeal sequences represented ~12% of total microbial abundance at the beginning of the incubation and ~17% of abundance after 586 days (Fig. 3-4A). Proteobacteria was the most abundant bacterial phylum, accounting for approximately 38% of sequences throughout the incubation. Bathyarchaeaota were the most abundant archaeal phylum in the WOR5.17 incubation and increased over time from 5% of sequences to 8% of sequences after 586 days; although population turnover times were slow and likely not in response to any shift in geochemistry (Fig. 3-5B).

Transcriptomics

24.6% of the predicted proteins in the publicly available metagenome from WOR samples could be assigned to a KEGG pathway. mRNA transcripts mapping to 41 methane cycling genes increased in abundance as sulfate approached depletion at 312 days and peaked shortly afterward at 375 days (Fig. 3-6). This agrees with previous studies showing that the highest rate of methane production occurs prior to sulfate depletion (96). The gene encoding methyl coenzyme M reductase (*mcrA*), a key gene in methane production, was not detected. Transcripts mapped to only three genes in two time points in sulfur cycling pathways, one of which was exclusive to dissimilatory sulfate reduction, adenylylsulfate reductase subunit A (*aprA*), at 375 days of incubation. Five transcripts mapped to genes related to nitrogen cycling metabolism across 3 samples; and none of them were exclusive to energy generation and included amino acid synthesis genes such as glutamine synthase (*glnA*) and glutamate dehydrogenase (*gdhA*). This agrees with the observations that the sediments lack free oxygen and nitrate at these depths. Transcripts mapped to 42 genes related to carbon fixation and peaked in expression at 194 days but remained actively expressed throughout. This suggests that microbes may be actively utilizing other carbon pathways, such as the reductive citrate cycle and the reductive acetyl-CoA pathway, however we cannot accurately distinguish between them since these genes are commonly shared with methanogenesis. However, it is difficult to separate these metabolic pathways considering many of the detected expressed genes play a role in several pathways, and key proteins often used as indicators for distinct pathways were absent.

Six mRNA transcripts were associated with pyrimidine metabolism with the highest expression occurring after 375 days. Conversely, 13 purine metabolism associated genes were

more evenly distributed between 63-532 days (Fig. 3-6). The expression of genes associated with DNA replication were not detected and only 4 genes associated with DNA mismatch repair were detected while the two highest expression levels were both on day 194; proliferating cell nuclear antigen and replication factor A1 respectively. The expression of only one gene, *motB*, associated with flagellar motility was detected at 124 days. This gene plays an important part in the utilization of the proton motive force for flagellar motility. No other genes recruited mRNA reads in more than a sample or two.

Discussion

In both incubations, methane production was never observed when sulfate was greater than 2 mM for the first 231 days of WOR5.16 and 200 days of WOR5.17. This was likely due to thermodynamic control of hydrogen by sulfate reducers, since hydrogen concentrations remained well under 1 nM during this time. These results agree with a previous incubation of marine sediments with more labile organic matter, where hydrogen concentrations were under 1 nM until sulfate decreased below 2 mM (18). Sulfate reduction sequesters hydrogen to a concentration below the maintenance energy requirements of methanogens, excluding them from growth during active sulfate reduction (16, 113). Our results suggest that this principle applies when porewater sulfate concentrations are greater than about 2 mM in these experiments. In further support for this conclusion, members of the Methanomicrobia comprised less than 0.05% of the total 16S rRNA gene sequence abundance, and methanogenic genes were not transcribed (only WOR5.17 was tested for gene transcription) during this interval.

After sulfate decreased below about 2 mM in the WOR5.16 incubation, hydrogen and methane concentrations increased, suggesting that, even though sulfate was not completely gone, the sulfate reducers were less able to out-compete methanogens for hydrogen. These timepoints had increases in the relative 16S rRNA gene abundance of the Methanomicrobia, driven primarily by the Methanosaeta sp. , Methanolinea sp., the ANME-3 clade within the *Methanococcoides* sp., and *Methanoregula* sp. Methane concentrations and the Methanomicrobia remained elevated throughout the duration of the experiment, however, methane concentrations were not sustained at saturating values around 1 mM. This suggests that either methane was leaking out of the incubation vessels or biological methane oxidation was occurring. We conclude that both were likely responsible for the lack of significant methane accumulation for the following reasons. At this point in the experiment, the sediments became very difficult to remove through the wide-bore

Teflon stopcock (timepoints where this was impossible have no porewater or 16S rRNA gene data), so sampling required forceful action that resulted in a sulfide smell leaking out of the bottle. Methane would have leaked out as well, and oxygen would have been introduced through this open conduit. Evidence that oxygen leaked into the three incubation vessels comes from the increase in sulfate concentrations after 500 days. This could have resulted from the biotic or abiotic oxidation of sulfide to sulfate, although there is no apparent increase or response to changing geochemistry from putative sulfide oxidizing bacteria from clades within *Thiobacilliaceae* or *Beggiatoaceae* in either incubation. Given the large volume of sediment many centimeters in diameter and depth, and the long-time intervals between sampling where sediments remained undisturbed, it is likely that the low sulfate concentrations allowed sulfate gradients to occur. In areas of low sulfate, methane may have been produced, and in areas of high sulfate, perhaps due to proximity to the sampling port, some of that methane may have been oxidized. Therefore, it is impossible to know which members of the Methanomicrobia were involved in methanogenesis and which were involved in AOM, since they were all mixed together at each timepoint.

The WOR5.17 incubation was designed to decrease the likelihood of gas leaks by allowing each incubation chamber to remain undisturbed until it was destroyed for a timepoint. The addition of methane on day 45 in WOR5.17, when sulfate concentrations were about 10 mM, coincided with an increase in the rate of sulfate removal and an increase in the $\delta^{13}C$ value of headspace methane. This suggests that the methane removal was through AOM, rather than a leak. Since hydrogen concentrations were very low at this time due to the action of sulfate reducing bacteria operating in high sulfate concentrations, this exogenously added methane was likely removed via AOM through reverse methanogenesis. No large increase in 16S rRNA gene abundance for any clade was observed during this time, but *Methanoregula* sp., *Methanolina* sp., and ANME-3 within the *Methanococcoides* sp. all increased slightly. Therefore, these three groups were the most likely candidates for performing AOM in these incubations.

A decrease in $\delta^{13}C$ of methane to -80‰ did not occur until sulfate was fully depleted at 524 days. Here, hydrogen had a slight increase of about 0.3 nM, suggesting that thermodynamic control may have shifted from that of sulfate reducers to methanogens. This coincided with methane concentrations around the saturation values for methane at 1 atm, suggesting that any additional methane would have been pushed out of the stopper through over pressure from the headspace. Likewise, the relative 16S rRNA gene abundance of *Methanosaeta* sp., *Methanolinea*

sp., the ANME-3 clade within the *Methanococcoides* sp., and *Methanoregula* sp. increased steadily over the four timepoints during this net methanogenic interval. This suggests that the same microbes participated in AOM during the ~100-day time period, and methanogenesis during the ~500-day time period.

The intervening time between the 100-day AOM event and the 500-day methanogenesis event is less straightforward to interpret. A month after AOM removed the exogenously added methane in incubation WOR5.17 in the 100-day event, hydrogen and methane concentrations increased because sulfate concentrations decreased below about 2 mM and became limiting to sulfate reducing microbes. However, this methane was quickly removed, possibly also through AOM, since it coincided with another transient increase in $\delta^{13}C$ of methane and subtle increase in the sulfate removal rate. No identifiable increase in the relative 16S rRNA gene abundance of any group was observed at this time, although the same members of the Methanomicrobia that were implicated in the earlier AOM were present throughout the whole interval, bolstering the conclusion that they are capable of either methanogenesis or AOM.

The next methane increase occurred at 396 days and coincided with another high hydrogen concentration and the presence of the same groups within the Methanomicrobia. At this interval, the subsequent methane decrease did not coincide with a change in $\delta^{13}C$ of methane, so it may have been a leak due to overpressure from the headspace. In total, it appears that when sulfate is still present, but is in low concentrations (< 2 mM), sediments alternate between methane production and consumption, so the dynamics are impossible to sort out with our current experimental design.

The proliferation of *Methanosaeta* sp., *Methanoregula* sp., and *Methanolinea* sp. during periods of methanogenesis is unsurprising considering they are closely related to cultured hydrogenotrophic and acetoclastic methanogens (20, 114–116). Furthermore, RNA expression of methane cycling genes in the WOR5.16 incubation begins prior to sulfate being depleted confirming previous work suggesting that the highest rate of methane production occurs prior to sulfate depletion (43). However, what was surprising was the increase in abundance and presence of ANME-3 in both incubations only after sulfate was depleted and not when AOM was possible in WOR5.17. This taxon falls within the genus *Methanococcoides* and is implicated as an obligate methanotrophs based on its presence in methane seeps performing AOM (117, 118). We provide evidence here that ANME-3 is indeed a methanogen because it increases in relative abundance along with the other three members of the Methanomicrobia during the period of net

methanogenesis after 524 days in incubation WOR5.17, and during transient methanogenic periods of incubations WOR5.16 and WOR5.17. Each of these Methanomicrobia may also be anaerobic methanotrophs, since they were the only members of the Methanomicrobia present during periods of AOM in the WOR5.17 incubation.

Despite previous observations that ANME-1 plays an important role in both the oxidation and production of methane in sediments associated with the White Oak river (44) and Kevorkian in prep, sequences associated with this group were not consistently detected in any significant abundance. This could be due to several factors. First, ANME-1 may not have been present in the first 3 cm that were used to create the incubations. They were previously detected in anoxic sediments at depths in excess of 30 cm. Oxygen is typically depleted within several millimeters of the sediment-water interface alongside nitrate and is not likely to be inhabited by a diversity of methanogens (14). Second, the growth rates of ANME-1 or microbes utilizing AOM have never been properly elucidated and could have resulted in their lack of detection or lack of competition in our mesocosm. Lastly, if the pathway for methane production and oxidation is reversible it could be a preferential for slow growing microbes to gain an advantage by utilizing AOM as a way to get a head start on population growth. As the population is buried the geochemistry eventually flips from sulfate reduction to methanogenesis, and if other putative methanogens which may grow at a faster rate, thus AOM allows ANME's to get ahead of the competition.

Sulfate reducing bacteria, although putatively active and abundant in these systems, did not consistently increase in abundance throughout the zone of sulfate reduction. The lack of RNA transcripts mapping to dissimilatory sulfate reduction genes limit what can be determined about this pathway in the incubation as well. The lack of active expression of sulfate reduction genes is consistent with the possibility that the population of sulfate reducing bacteria is not actively growing. It is believed that oxygen was introduced into the later timepoints, which was followed by rises in sulfate concentrations. If AOM was occurring in the WOR5.17 incubation with an ANME/SRB partnership it would be expected to see an increase in abundance or cessation of decline in abundance from the SRB partner. Despite the present taxa previously shown to form syntrophies with ANME such as *Desulfatiglans* and SEEP-SRB1, there was no increase in abundance detected suggesting no syntrophy occurred (32) and Kevorkian et al (submitted). Sulfate depletion also had little immediate effect on the abundance of any sulfate reducers, possibly due to their ability to ferment short-chain fatty acids or aromatics (119). Additionally, there was an increase in abundance in several taxa of sulfate reducing bacteria after sulfate was

depleted, further suggesting a transition and utilization of some other metabolism and terminal electron acceptor.

Our results further indicate that the majority of observed microbes, including clades of sulfate reducers, do not increase or decrease abruptly in response to the major redox shift from sulfate reduction to methanogenesis, agreeing with previous studies (18). Our results also support environmental observations that Bathyarchaeota is a major archaeal taxon in these sediments and steadily increases in abundance throughout the course of our incubation irrespective of geochemical shifts seen in downcore analysis. This suggests that future studies should focus on metabolisms other than sulfate reduction and methanogenesis for characterization of the uncultured majority. Our work suggests that members of the *Methanoregula* sp., *Methanolinea* sp., and the ANME-3 clade within the *Methanococcoides* sp. are methanogens that are capable of reversing to AOM, depending on which process is exergonic.

Methods

Sample collection

Plunger cores were collected in May 2016 (30 cm; WOR5.16) and May 2017 (1 m; WOR5.17) at the White Oak River estuary station H (34 44.490’ N, 77 07.44’ W), in 1.5 m water depth. Using a plunger inserted from the bottom, the first three centimeters of sediment from each core was placed in three 2L Erlenmeyer flasks from the 30 cm cores as previously described in Kevorkian et al 2018. About 100 ml of sediment were autoclaved and incubated alongside the experiments under anoxic conditions as a negative control. Meter long cores were subsampled at 1 cm intervals for further analysis described below.

Sampling and geochemical measurements

Each of the three WOR5.16 flasks were fitted with a custom butyl rubber stopper with a hole drilled through the center to accommodate a wide bore (6 mm) glass and Teflon stopcock for the removal of samples. Two 18-gauge needles with stainless steel stopcocks were inserted into the stopper as well. Using the luer-lock fitting on the needles, ultra-high purity nitrogen gas (99.999%) that had been scrubbed of oxygen using heated copper fillings was flowed through the bottles using the second needle for the outflow to make the headspace anoxic. Then the flasks were let stand at constant room temperature (21.4°C) in the dark (Fig. 3-7A).

The WOR5.16 incubations were turned over once every month just before sampling. Prior to gas sampling, 2 ml of anoxic N_2 gas (99.999%) was used to blow the needle clear of sediment. Separate hydrogen and methane gas samples were collected in glass gastight Hamilton syringes using the steel needle ports in the custom stopper. About 32 ml of sediment was removed through the glass and Teflon stopcock using a sterile 60 ml plastic catheter tip syringe. After sampling, 30 ml of oxygen- and hydrogen-scrubbed N_2 was injected into the bottle to replace the lost volume.

The WOR5.17 incubation bottles were sampled destructively in triplicate on a monthly basis. The crimp seal and butyl stopper were removed after sampling the headspace for hydrogen, methane, and stable carbon isotopes (Fig. 3-7B).

From both incubations, two 15ml conical centrifuge tubes were filled and capped, one used for porewater analysis and the other frozen at -80°C for later molecular analysis. One ml of sediment was placed in a 2 ml screw cap tube with 3% paraformaldehyde. The 15 ml tube destined for porewater analysis was centrifuged at 5 000 xg for 5 minutes. A syringe was used to remove the supernatant not in contact with the air. The porewater was then filtered using a 0.2 µm syringe filter into 100 µl of 10% HCl to a final volume of 1 ml. Porewater sulfate concentrations were determined by ion chromatography (Dionex, Sunnyvale, CA).

500µl of headspace gas was injected into a Peak Performer 1 Reducing Compound Photometer (Peak Laboratories, Mountain View, CA). Premixed hydrogen ppm lab bottles (Airgas, Radnor, PA) were used as standards. Hydrogen was assumed to be equilibrated between headspace and porewater. Methane was determined by injecting 500 µl of gas from the headspace into an evacuated glass bottle to be later analyzed on a gas chromatograph with a flame ionization detector (Agilent, Santa Clara, CA). Methane concentrations were not assumed to be equilibrated with the aqueous phase; therefore, concentrations are presented as headspace partial pressures. The formula for determining methane concentration was peak area of sample multiplied by the volume of the bottle headspace, which was divided by gas constant times temperature, porosity, volume of sediment.

To measure $\delta^{13}C$ values of methane, 4 ml of headspace from the vial used for methane measurements was removed via syringe and injected into a gas bag containing hydrocarbon free zero gas (Airgas, Radnor, PA). This was then measured on a cavity ring down spectrometer using a small sample introduction module (Picarro, Santa Clara, CA).

Cell quantification

Total cell counts were determined by direct epifluorescence microscopy SYBRGold DNA stain (Invitrogen, Carlsbad, CA). Sediments were sonicated at 20% power for 40 seconds to disaggregates cells from sediments and diluted 40-fold into PBS prior to filtration onto a 0.2 μm polycarbonate filter (Fisher Scientific, Waltham, MA) and mounted onto a slide.

16S ribosomal RNA gene amplicons

DNA was extracted from WOR5.16 frozen sediments using the Qiagen Powersoil Total DNA extraction kit (Qiagen, place, country. DNA was extracted from WOR5.17 frozen sediments using a protocol modified from Mills et al 2008 (120). Autoclaved sediment and water blanks were used as negative controls. The V4 region of each DNA extraction was amplified using primers 806r and 515f (106), as a universal primer pair for Bacteria and Archaea. Library preparations via Nextera kit and sequencing using an Illumina MiSeq were performed at the Center for Environmental Biotechnology at the University of Tennessee in Knoxville. At total of 22,477,189 reads were produced as a result of 2 Miseq sequencing runs.

Qiime2 was used to trim adaptors and make contigs of bidirectional sequences, denoised using Dada2, and generate Amplicon Sequence Variants (ASVs) at 99% similarity, and classify them with the Silva reference set 132 (107). Following quality control 16,632,317 (74%) of original reads surviving containing 72,445 unique sequences. Samples with fewer than 20,000 reads were removed from further analysis and ASV's appearing in fewer than 3 samples were also removed. All remaining samples were then scaled to even depth of the smallest sequence library size, which was 20,000 reads (121). Sequences that identified as chloroplast, eukaryote, or failed to classify on the domain level were removed from further analysis. ASV's for WOR5.16 incubation were agglomerated to the species (97% similarity) level using the command taxa_glom() in the package phyloseq (121) due to the sequences being produced using two separate Miseq runs.

Transcriptomic analysis

RNA was extracted from WOR5.16 frozen sediments using the Qiagen Powersoil Total DNA extraction kit. Samples were shipped on dry ice to Mr. DNA (Shallowater, Texas) for sequencing. The concentration of total RNA was determined (Table 2) using the Qubit® RNA Assay Kit (Life Technologies). 200ng-500ng of total RNA was used to remove the DNA

contamination using Baseline-ZERO™ DNase (Epicentre) following the manufacturer's instructions followed by purification using the RNA Clean & Concentrator columns (Zymo Research). DNA free RNA samples were used for library preparation using the TruSeq™ RNA LT Sample Preparation Kit (Illumina) according to the manufacturer's instructions. Following the library preparation, the final concentration of all the libraries (Table 2) were measured using the Qubit® dsDNA HS Assay Kit (Life Technologies), and the average library size was determined using the Agilent 2100 Bioanalyzer (Agilent Technologies). The libraries were then pooled in equimolar ratios of 2nM, and 5.5pM of the library pool was clustered using the cBot (Illumina) and sequenced paired end for 500 cycles using the HiSeq 2500 system (Illumina).

Reads were trimmed using Trimmomatic in paired-end read mode with a minimum quality score of 25 and a maximum of 4 low-quality bases (122). There was an average of 3185420 (minimum = 616402, maximum = 7063586) RNA reads across the ten samples after quality filtering from 0 – 647 days of incubation. A metagenome produced from the White Oak River estuary sediments Genbank Accession: PRJNA366356 was used for further analysis. Transcriptomic reads were mapped were mapped to the assembled metagenomic contigs using Bowtie version 2.3.5 using the "sensitive" end-to-end setting (123). Resulting files were converted to bam files using SAMtools version 1.9 and an anvi'o v5.3.0 database was created and each sample profiled against the metagenomic contigs using the anvi'o command anvi-profile and ORF determined by Prodigal (124–126). Gene coverage and detection files were exported using the anvi'o command anvi-export-gene-converage-and-detection, resulting in reads per kilobase per million (RPKM). ORFs were exported as amino acid sequences using anvi'o command anvi-get-aa-sequences-for-gene-calls and function was assigned using GhostKOALA and parsed in R(127, 128).

Data archiving

16S rRNA gene sequences can be found at the NCBI Genbank short read archive with accession numbers (###). Geochemistry and qPCR data can be found at www.bco-dmo.org with project number ###.

Acknowledgments. We thank Andrew Steen, Jordan Bird, Lauren Mullen, Taylor Royalty, Katherine Sipes, Katherine Fullerton, and Joy Altom for assistance retrieving the sediment samples, Michael Piehler for the use of his laboratory at the UNC Institute of Marine Sciences,

Frank Löffler for use of ion and flame ionized detector chromatographs, Robert Murdoch and the University of Tennessee Knoxville Bioinformatics Resource Center for computational resources, and Christopher G. Kevorkian and Alexandra Emmons for aid in analytical analysis. This work was funded by Alfred P. Sloan Foundation Fellowship (FG-2015-65399) and NASA Exobiology (NNX16AL59G).

The authors declare no conflicts of interest.

Appendix

Table 2. Concentration of total RNA, final library concentration and average library size.

Sample	RNA Concentration (ng/uL)	Library Concentration (ng/uL)	Avg Library size (bp)
03012018-2	15.8	41.40	426
11032017-2	23.4	41.20	413
09192017-2	18.1	43.20	411
05302017-2	7.94	39.00	407
03282017-2	18.2	39.60	394
01062017-2	22.8	38.40	414
11302016-2	13.4	40.40	441
09212016-2	22.0	43.20	429
07222016-2	20.2	39.60	442
05202016-3	16.4	39.80	435

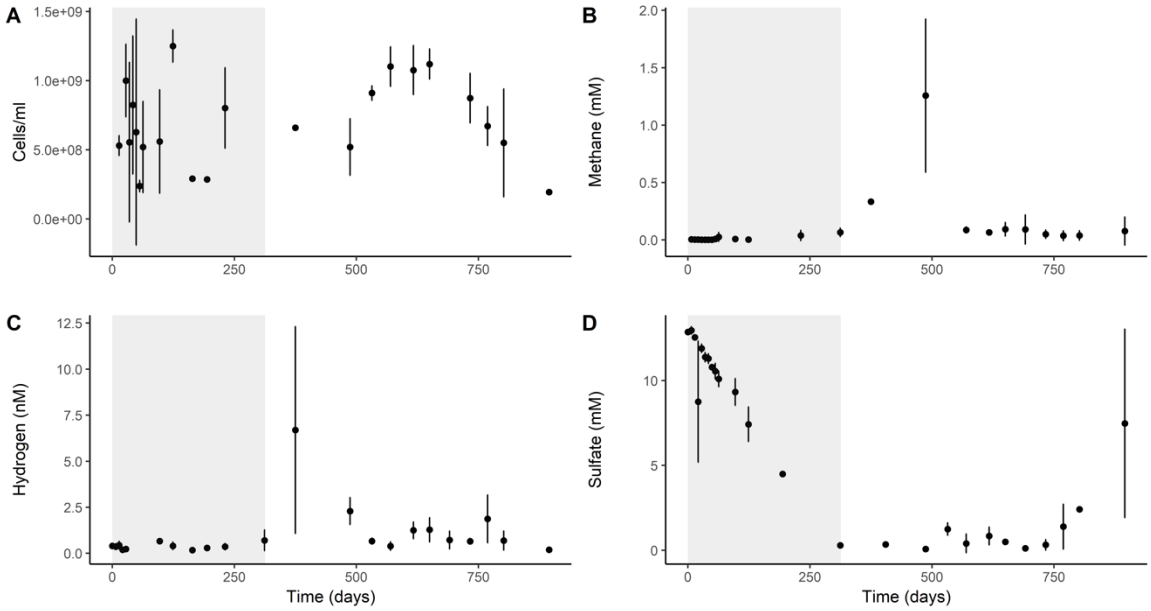

Figure 3-1. WOR5.16 incubation geochemistry demonstrates methane is only produced after sulfate is depleted.

Geochemistry for WOR5.16 incubation, with A) cell abundance, B) headspace methane concentration, C) aqueous hydrogen concentration, and D) sulfate concentration. The grey box shows range of sulfate reduction. Error bars represent the standard deviation between the three bottles.

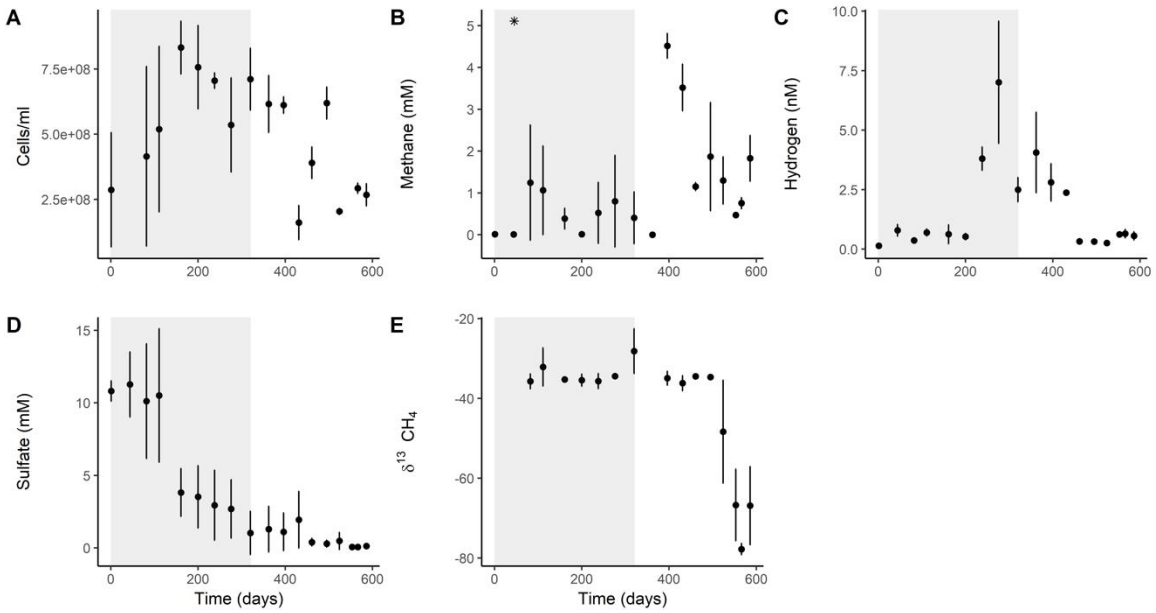

Figure 3-2. WOR5.17 incubation geochemistry demonstrates methane is only produced after sulfate is depleted and AOM may of occurred.

Geochemistry for WOR5.17 incubation, with A) cell abundance, B) headspace methane concentration; with the star representing the time and concentration of methane added to bottles, C) aqueous hydrogen concentration, D) sulfate concentration, and E) $\delta^{13}CH_4$ fractionation of methane. The grey box shows range of sulfate reduction. Error bars represent the standard deviation between the three bottles.

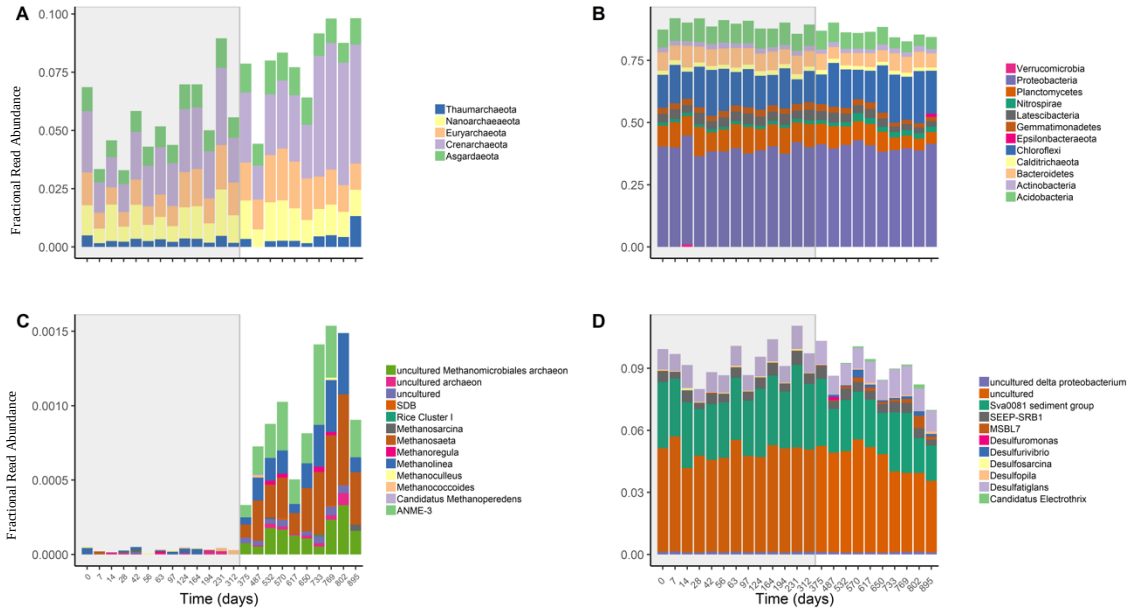

Figure 3-3. ANME-3 only increased in abundance after sulfate was depleted and methane was produced.

Relative abundance of 16S rRNA gene sequences in the WOR5.16 incubation for all archaea (left panels A and C) and all bacteria (right panels B and D), grouped at the phylum level. Bottom panels show only putative sulfate reducing bacteria and Methanomicrobia, grouped at the family level. Phyla with <0.1% relative 16S rRNA gene sequence abundance for bacteria and archaea, were not included. The grey box shows range of sulfate reduction.

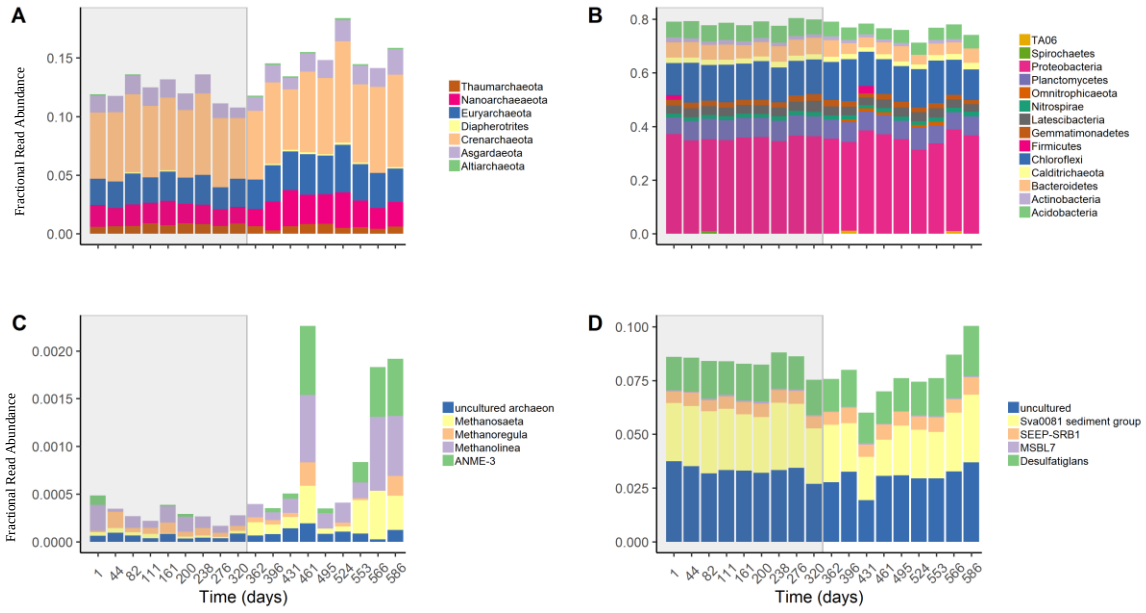

Figure 3-4. ANME-3 only increased in abundance after sulfate was depleted and methane was produced, not when AOM was potentially occuring.

Relative abundance of 16S rRNA gene sequences in the WOR5.17 incubation for all archaea (left panels A and C) and all bacteria (right panels B and D), grouped at the phylum level. Bottom panels show only putative sulfate reducing bacteria and Methanomicrobia, grouped at the family level. Phyla with <0.1% relative 16S rRNA gene sequence abundance for bacteria and archaea, were not included. The grey box shows range of sulfate reduction.

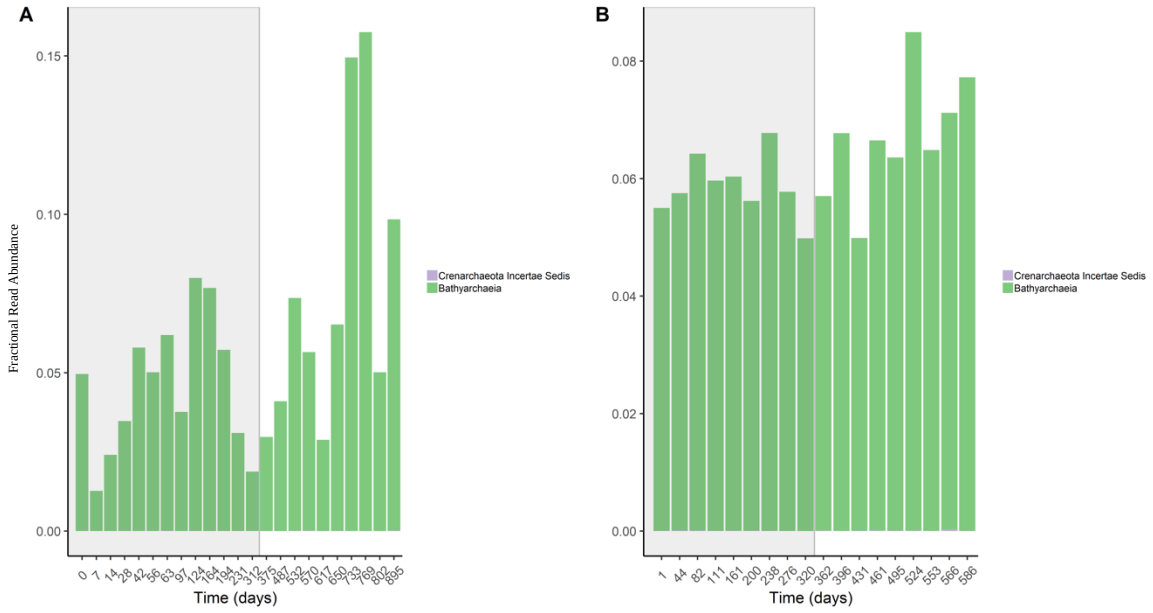

Figure 3-5. Bathyarcheota did not respond to methane being produced and was not considered to be a methanogen.

Relative abundance of 16S rRNA gene sequences in the WOR5.16 (A) and WOR5.17 (B) incubations for all detected members of the order Bathyarchaeota. The grey box shows range of sulfate reduction.

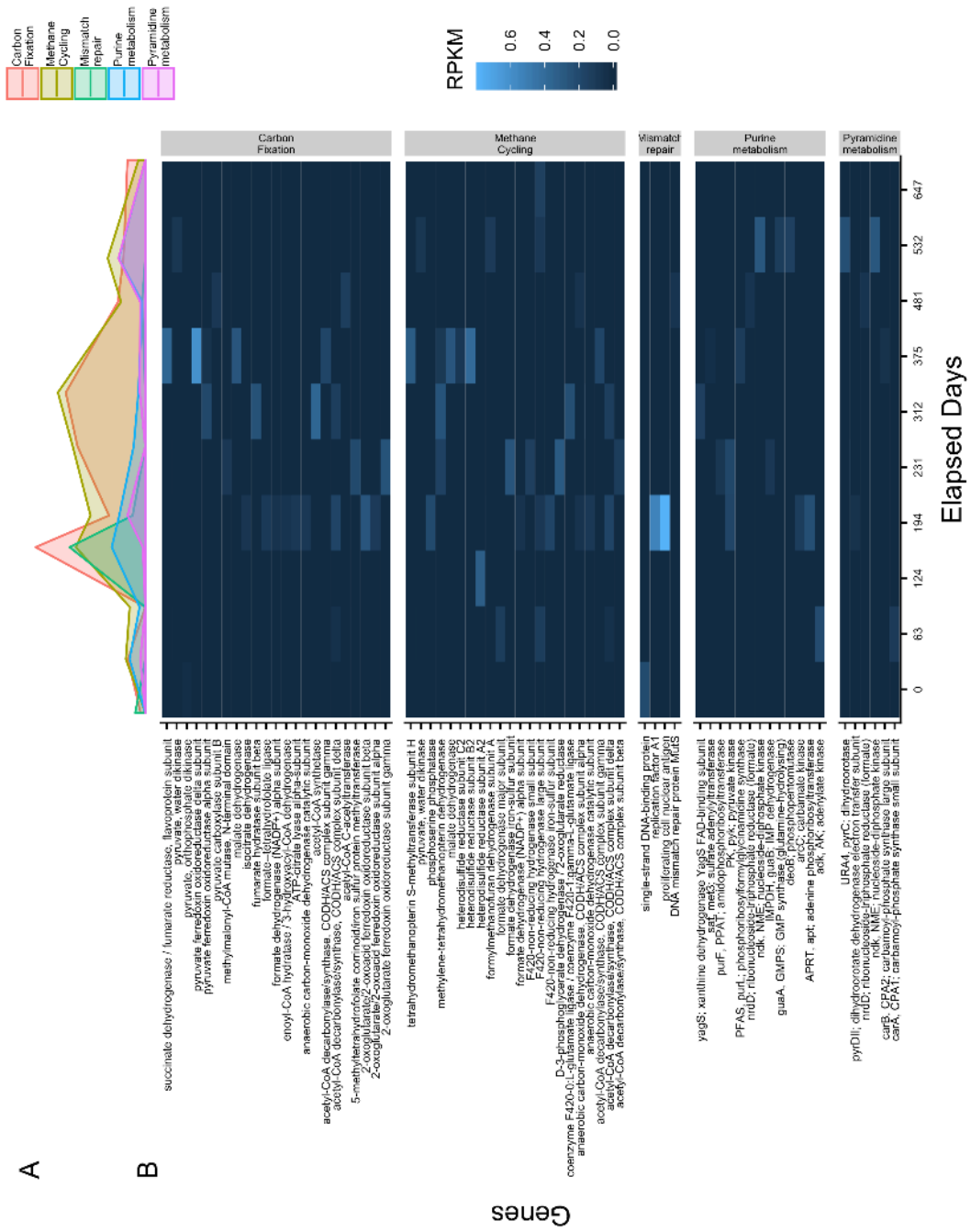

Figure 3-6. Transcrips reveal the highest level of carbon fixation related gene expression occurs prior to sulfates depletion.

Abundance of ORF which putatively encode cellular processes in the WOR5.17 incubation. (A) represents the summed value of each pathway over time. (B) The individual genes detected in each pathway. Heatmap color corresponding to RPKM (Reads Per Kilobase Mapped).

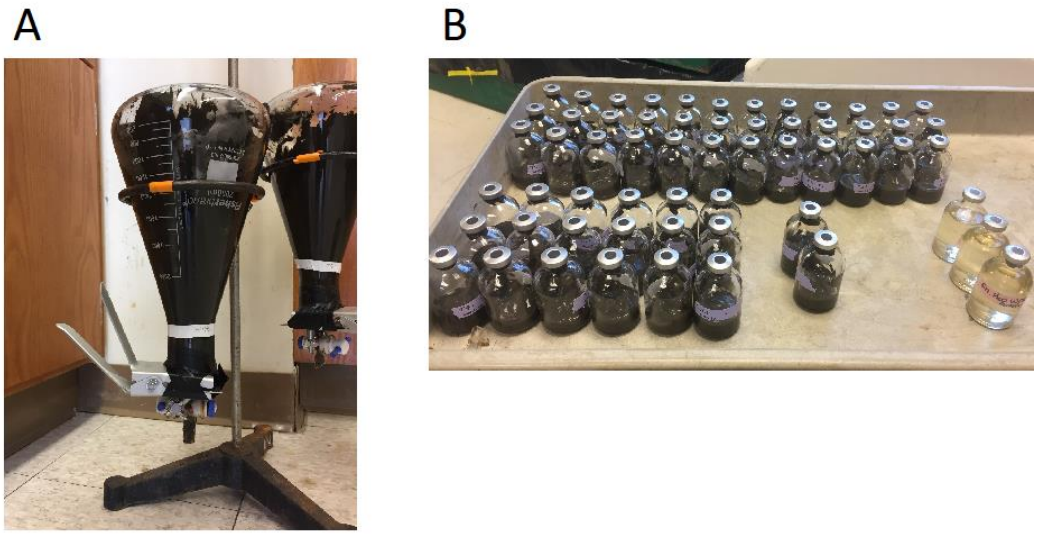

Figure 3-7. Incubation set up for both WOR5.16 and WOR5.17.

Experimental design of the long-term incubation bottles. (A) WOR5.16 incubation in 2-liter flasks. (B) WOR5.17 incubation using individual bottles destructively sampled, clear bottles represent negative controls.

Table S3-1. Data used for incubation analysis.

ID	Miseq Run	Experiment	Date	Elapsed time	Replicate	H2 nM	H2 std	CH4 mM	CH4 STD	Isotope ch4	Iso std	so4 mM	Cells ml	Std dev cells
0_0	2	WOR5.17	5/26/2017	1	0	3.6807714	0.6608 9945	0.0045 7544				9.4206 0581	228666 667	1043642 31
0_1	2	WOR5.17	5/26/2017	1	1	0.1727 4549	0.0135 1508	0.0197 0958				11.500 6797	346266 667	1358036 22
0_2	2	WOR5.17	5/26/2017	1	2	0.1606 3981	0.0420 5351	0.0066 8718				10.087 4606	435555 55.6	1023467 67
0_3	2	WOR5.17	5/26/2017	1	3	0.0734 7361	0.0150 3713	0.0112 6261				10.856 9084	470400 000	1437026 09
1_1	2	WOR5.17	7/8/2017	44	1	1.0507 7966	0.6818 1677	0.0151 3414				9.1897 7147	366955 556	1919563 08
1_2	2	WOR5.17	7/8/2017	44	2	0.7405 3341	0.0032 4932	0.0102 0674				13.665 3928		
1_3	2	WOR5.17	7/8/2017	44	3	0.5623 1261	0.2684 4975	0.0066 8718				10.949 2421	216688 889	2340713 77
3_1	2	WOR5.17	8/15/2017	82	1	0.3852 1972	0.0775 8887	0.2386 2664		-37.1366	0.2900 3845	7.9099 2331	356066 667	2052351 12
3_2	2	WOR5.17	8/15/2017	82	2	0.3578 3024	0.1150 6268	0.6827 9599		-33.6164	0.0745 0705	7.7627 023	104533 333	2034433 39
3_3	2	WOR5.17	8/15/2017	82	3	0.3552 012	0.0751 1895	2.8156 5359		-36.457	0.0528 583	14.693 888	785088 889	3032396 97
4_1	2	WOR5.17	9/13/2017	111	1	0.5532 7516	0.3273 9973	0.0516 7898	0.0001 0354	-34.772	0.1675 2512	7.2276 796	605422 222	1645081 12
4_2	2	WOR5.17	9/13/2017	111	2	0.8557 4289	0.4181 0063	0.9655 3454	0.0011 7904	-26.607	0.1822 2514	15.781 3742	785088 889	3470376 65
4_3	2	WOR5.17	9/13/2017	111	3	0.6840 7488	0.2716 8433	2.1706 6947	0.0027 2772	-34.994	0.0406 8784	8.5306 112	167688 889	1915821 39
5_1	2	WOR5.17	11/2/2017	161	1	1.0796 358	1.1010 6095	0.2144 5895	0.0003 8777	-35.26	0.1445 4296	2.9828 9261	721933 333	1846610 94
5_2	2	WOR5.17	11/2/2017	161	2	0.3951 2993	0.0432 8312	0.2726 4912	0.0028 56	-35.367	0.0466 9582	2.7476 9807	850422 222	1635547 16
5_3	2	WOR5.17	11/2/2017	161	3	0.3930 1462	0.0361 1717	0.6687 1773	0.0023 5992	-35.105	0.0328 5575	5.7272 5641	923377 778	1987838 07

Table S3-1 Continued.

ID	Miseq Run	Experiment	Date	Elapsed time	Replicate	H2 nM	H2 std	CH4 mM	CH4 STD	Isotope ch4	Iso std	so4 mM	Cells ml	Std dev cells
6_1	2	WOR5.17	12/11/2017	200	1	0.4823 3233	0.1146 5513	0.0461 5326	0.0010 6844	-36.3248	0.3159 4256	2.3519 4542	838444 444	1945553 40
6_2	2	WOR5.17	12/11/2017	200	2	0.6726 3811	0.1644 8056	0	0	-36.3468	0.1643 2955	2.2083 1517	572755 556	1654004 07
6_3	2	WOR5.17	12/11/2017	200	3	0.4124 0318	0.0774 9539	0	0	-33.677	0.0869 885	6.0016 9279	859133 333	1881746 27
7_1	2	WOR5.17	1/18/2018	238	1	4.1578 716	0.7274 1865	0.1769 169	0.0018 8306	-36.3614	0.3314 6991	5.6990 4332	671844 444	1477635 77
7_2	2	WOR5.17	1/18/2018	238	2	3.9973 2712	1.0996 9242	0.0326 1465	6.6561 E-05	-37.156	0.1655 7023	1.1772 5512	712133 333	2302542 59
7_3	2	WOR5.17	1/18/2018	238	3	3.2431 3292	0.4726 6769	1.3621 8974	0.0045 183	-33.5484	0.0761 4985	1.9338 7879	731733 333	1497220 52
8_1	2	WOR5.17	2/26/2018	276	1	6.1051 5359	1.3225 9303	2.0533 1538	0.0013 0677	-34.186	0.2677 7976	4.8372 6179	732822 222	1869058 14
8_2	2	WOR5.17	2/26/2018	276	2	9.9189 324	5.7395 5423	0.3443 3097	0.0005 0075	-34.7356	0.0509 6371	2.3904 1781	495444 444	2124127 47
8_3	2	WOR5.17	2/26/2018	276	3	5.0121 6577	1.3802 7457	0.0060 8885	7.5978 E-05	-34.4482	0.0527 3708	0.8335 6844	378933 333	1013592 83
9_1	2	WOR5.17	4/11/2018	320	1	2.3066 0956	0.1504 0234	0.0876 3722	0.0006 7065	-28.7504	0.2693 0893	0	768755 556	2358332 90
9_2	2	WOR5.17	4/11/2018	320	2	3.0725 0756	0.1917 627	0.0101 0116	0.0002 042	-22.2618	0.1393 6355	0.3231 6807	573844 444	1635997 06
9_3	2	WOR5.17	4/11/2018	320	3	2.1054 1889	0.5088 6701	1.1174 6252	0.0039 2049	-33.4748	0.0175 6986	2.7520 5827	790533 333	2102040 90
10_1	2	WOR5.17	5/23/2018	362	1	5.4949 2395	1.4947 1916	0.0002 2056	1.4092 E-06			0.0243 6585	492177 778	1717737 92
10_2	2	WOR5.17	5/23/2018	362	2	4.4954 5187	5.0993 9613	0.0001 1849	1.4454 E-06	-31.796	0.2439 1187	3.0511 1698	654422 222	1903779 25
10_3	2	WOR5.17	5/23/2018	362	3	2.1937 9115	0.1684 832	0	0	-37.1868	0.1062 2241	0.7899 664	700155 556	2020428 00
11_1	2	WOR5.17	6/26/2018	396	1	3.2575 035	0.6544 481	4.3144 0252	0.0056 7562	-36.9868	0.7174 6861	0.0248 7881	620666 667	1933537 84
11_2	2	WOR5.17	6/26/2018	396	2	3.2551 4101	0.7388 5805	4.3709 5023	0.0025 9726	-33.6876	0.1524 2802	2.5443 0737	638088 889	1500003 30

Table S3-1 Continued.

ID	Miseq Run	Experiment	Date	Elapsed time	Replicate	H2 nM	H2 std	CH4 mM	CH4 STD	Isotope ch4	Iso std	so4 mM	Cells ml	Std dev cells
11_3	2	WOR5.17	6/26/2018	396	3	1.8935 1689	1.1794 6562	4.8602 8736	0.0019 8612	-34.2054	0.1157 0653	0.7309 754	576022 222	1330342 03
12_1	2	WOR5.17	7/31/2018	431	1	2.3282 9004	0.7168 2253	3.7668 7522	0.0027 4569	-35.7984	0.0421 2185	4.1729 7186	234111 111	1204330 73
12_2	2	WOR5.17	7/31/2018	431	2	2.3409 6536	0.2077 5725	3.9103 5624	0.0102 5481	-38.2966	0.1415 3904	1.1105 6965	106711 111	1141105 11
12_3	2	WOR5.17	7/31/2018	431	3	2.4519 2577	0.2111 7407	2.8761 9014	0.0058 765	-34.534	0.2112 2263	0.5334 838	143733 333	9537401 2.7
13_1	2	WOR5.17	8/30/2018	461	1	0.3828 4348	0.0612 127	1.2323 0599	0.0048 7245	-34.562	0.2230 4017	0.7104 568	332111 111	1407227 19
13_2	2	WOR5.17	8/30/2018	461	2	0.3034 4062	0.0048 4543	1.0441 382	0.0005 4924	-34.562	0.1435 0087	0.2377 5937	454066 667	1152070 07
13_3	2	WOR5.17	8/30/2018	461	3	0.2838 7145	0.0315 7657	1.1811 1975	0.0096 5441	-34.3226	0.0829 9277	0.2282 6951	385466 667	1027295 52
14_1	2	WOR5.17	10/3/2018	495	1	0.3584 8056	0.0288 2636	1.0112 8891	0.0045 3992	-34.6214	0.1736 1538	0.1513 2473	560777 778	1407227 19
14_2	2	WOR5.17	10/3/2018	495	2	0.2507 0938	0.0334 9131	3.3576 669	0.0122 4944	-34.807	0.1398 6958	0.1359 3578	682733 333	1152070 07
14_3	2	WOR5.17	10/3/2018	495	3	0.3455 4707	0.0242 8001	1.2318 4844	0.0018 4995	-34.567	0.1086 0018	0.5642 6171	614133 333	1027295 52
15_1	2	WOR5.17	11/1/2018	524	1	0.2892 9202	0.0087 2111	1.5057 8807	0.0039 4785	-34.6436	0.9878 2655	1.1516 0686	215600 000	5260351 2.3
15_2	2	WOR5.17	11/1/2018	524	2	0.2460 3121	0.0406 2653	1.7330 3478	0.0024 7925	-60.2842	0.0730 8351	0.1231 1165	2.03E+08	3.68E+07
15_3	2	WOR5.17	11/1/2018	524	3	0.2397 8081	0.0372 6528	0.6561 646	0.0047 3321	-50.1256	0.0192 9508	0.1461 9508	1.93E+08	3.36E+07
16_1	2	WOR5.17	11/30/2018	553	1	0.6505 7029	0.0308 0142	0.4454 5986	0.0013 7448	-64.3445	0.6507 0907	0.0872 0408		
16_2	2	WOR5.17	11/30/2018	553	2	0.6338 9689	0.0334 8511	0.4899 2372	0.0029 0853	-59.123	0.1322 7812	0.0051 2965	310333 333	1548328 23
16_3	2	WOR5.17	11/30/2018	553	3	0.5782 8904	0.0073 4584	0.4726 7785	0.0004 9855	-76.6734	0.0502 225	0.0872 0408	487822 222	1527231 17
17_1	2	WOR5.17	12/13/2018	566	1	0.8472 2307	0.3051 7003	0.8740 258	0.0004 2734	-78.0078	0.2274 6795	0.0153 8896	290733 333	8929667 2.9

Table S3-1 Continued.

ID	Miseq Run	Experiment	Date	Elapsed time	Replicate	H2 nM	H2 std	CH4 mM	CH4 STD	Isotope ch4	Iso std	so4 mM	Cells ml	Std dev cells
17_2	2	WOR5.17	12/13/2018	566	2	0.4947 1758	0.0463 9731	0.7813 4387	0.0004 7283	-79.068	0.0543 829	0.0179 5378	313600 000	8815618 3.2
17_3	2	WOR5.17	12/13/2018	566	3	0.6093 8422	0.0399 1032	0.6100 5828	0.0008 5469	-76.2786	0.0875 9737	0.1282 413	274400 000	8029211 0.4
18_1	2	WOR5.17	1/2/2019	586	1	0.7312 5827	0.0205 8767	2.3569 3669	0.0015 5982	-56.5672	0.1242 3734	0.1974 916	313600 000	8815618 3.24
18_2	2	WOR5.17	1/2/2019	586	2	0.5479 8397	0.0697 7394	1.8641 9731	0.0025 0509	-68.0174	0.0560 8297	0.1615 8404	260244 444	6671733 3.2
18_3	2	WOR5.17	1/2/2019	586	3	0.3815 3875	0.0722 0885	1.2611 7817	0.0012 3849	-76.079	0.0205 6696	0.0051 2965	228666 667	1043642 31
18_0	2	WOR5.17	1/2/2019	586	0	0.6243 3886	0.0624 173	0.3824 5961	0.0021 1475	-34.91	0.0333 8413	5.1322 1678	699066 667	1437026 09
RK21_S85_L001_R1_001	1	WOR5.16	5/20/2016	0	1	0.4542 7827	0.1581 776							
RK33_S99_L001_R1_001	1	WOR5.16	5/20/2016	0	2	0.2356 4106	0.0437 7693					12.918 4851		
RK22_S86_L001_R1_001	1	WOR5.16	5/20/2016	0	3	0.5139 3164	0.1510 4645					12.783 331		
		WOR5.16	5/27/2016	7	1	0.5309 7423	0.0421 4174	0.0091 8663				12.971 9837		

Table S3-1 Continued.

ID	Miseq Run	Experiment	Date	Elapsed time	Replicate	H2 nM	H2 std	CH4 mM	CH4 STD	Isotope ch4	Iso std	so4 mM	Cells ml	Std dev cells
		WOR5.16	5/27/2016	7	2	0.33184132	0.06559237	0.00238017				12.7326482		
RK6_S68_L001_R1_001	1	WOR5.16	5/27/2016	7	3	0.22307574	0.06351896	0.00246369				13.1662678		
RK42_S22_L001_R1_001	1	WOR5.16	6/3/2016	14	1	0.26750841	0.12173875	0.00233842				12.5468112	587849808	247704789
RK43_S23_L001_R1_001	1	WOR5.16	6/3/2016	14	2	0.37414223	0.08404409	0.00384168				12.4736027	449560920	199783971
RK44_S24_L001_R1_001	1	WOR5.16	6/3/2016	14	3	0.67701115	0.18632484					12.6003097	553005364	439186323
		WOR5.16	6/10/2016	21	1	0.26567935	0.04131197	0.00329884				9.56215684		
		WOR5.16	6/10/2016	21	2	0.20513081	0.0498308	0.00384168				11.845699		

Table S3-1 Continued.

ID	Miseq Run	Experiment	Date	Elapsed time	Replicate	H2 nM	H2 std	CH4 mM	CH4 STD	Isotope ch4	Iso std	so4 mM	Cells ml	Std dev cells
		WOR5.16	6/10/2016	21	3	0.10569562	0.01277318	0.00542847				4.8486555		
RK3_S65_L001_R1_001	1	WOR5.16	6/17/2016	28	1	0.20071523	0.03113766	0.00200436				11.9808532	870960920	238882160
RK1_S63_L001_R1_001	1	WOR5.16	6/17/2016	28	2	0.22489907	0.02542462	0.00190626				12.0822188	827405364	289361709
RK4_S66_L001_R1_001	1	WOR5.16	6/17/2016	28	3	0.27960607	0.06078822	0.00417574				11.6229762	130324 9808	2030963 75
		WOR5.16	6/24/2016	35	1			0.00217139				11.1445868	174072031	6346682 4.4
		WOR5.16	6/24/2016	35	2			0.00238017				11.6823877	121831 6475	2002132 72
		WOR5.16	6/24/2016	35	3							11.3163452	272072031	1080823 77

Table S3-1 Continued.

ID	Miseq Run	Experiment	Date	Elapsed time	Replicate	H2 nM	H2 std	CH4 mM	CH4 STD	Isotope ch4	Iso std	so4 mM	Cells ml	Std dev cells
RK45_S25_L001_R1_001	1	WOR5.16	7/1/2016	42	1			0.00250545				11.0488526	587849 808	2477047 89
RK46_S26_L001_R1_001	1	WOR5.16	7/1/2016	42	2			0.0025472				11.6091792	485494 253	2565013 05
RK47_S27_L001_R1_001	1	WOR5.16	7/1/2016	42	3			0.00304829				11.2177953	139798 3142	1894964 44
		WOR5.16	7/8/2016	49	1			0.00263072				10.9024356	120633 8697	1863636 24
		WOR5.16	7/8/2016	49	2							10.5969309		
		WOR5.16	7/8/2016	49	3			0.00204611				10.8573842	499386 97.3	8243280 4.8
RK2_S64_L001_R1_001	1	WOR5.16	7/15/2016	56	1			0.00922839				10.0886949	280783 142	1046927 90

Table S3-1 Continued.

ID	Miseq Run	Experiment	Date	Elapsed time	Replicate	H2 nM	H2 std	CH4 mM	CH4 STD	Isotope ch4	Iso std	so4 mM	Cells ml	Std dev cells
RK7_S69_L001_R1_001	1	WOR5.16	7/15/2016	56	2			0.00668119				11.0206955	233960920	9936104.8
RK13_76_L001_R1_001	1	WOR5.16	7/15/2016	56	3							10.5279459	198027586	8065790.8
RK17_S81_L001_R1_001	1	WOR5.16	7/22/2016	63	1			0.00542847				10.6011544	253560920	1055387.71
RK19_S83_L001_R1_001	1	WOR5.16	7/22/2016	63	2			0.00279775				9.93664649	416894253	1148871.64
RK23_S87_L001	1	WOR5.16	7/22/2016	63	3			0.07098762				9.73954667	888383142	3097052.53

Table S3-1 Continued.

ID	Miseq Run	Experiment	Date	Elapsed time	Replicate	H2 nM	H2 std	CH4 mM	CH4 STD	Isotope ch4	Iso std	so4 mM	Cells ml	Std dev cells
RK12_75_L001_R1_001	1	WOR5.16	8/25/2016	97	1	0.6177 7811	0.1179 9971					8.7681 2614	465894 253	1110600 40
		WOR5.16	8/25/2016	97	2	0.8170 7026	0.1041 026	0.0096 0421				9.8831 4797	242672 031	7263231 9.9
RK9_S72_L001_R1_001	1	WOR5.16	8/25/2016	97	3	0.5469 2082	0.0837 276	0.0075 1634					971138 697	1620289 68
RK20_S84_L001_R1_001	1	WOR5.16	9/21/2016	124	1	0.6425 0852	0.2792 2589					6.6619 7381	137620 5364	2292184 91
RK34_S100_L001_R1_001	1	WOR5.16	9/21/2016	124	2	0.2673 946	0.0107 2335					7.0308 3204	123029 4253	2038047 60

Table S3-1 Continued.

ID	Miseq Run	Experiment	Date	Elapsed time	Replicate	H2 nM	H2 std	CH4 mM	CH4 STD	Isotope ch4	Iso std	so4 mM	Cells ml	Std dev cells
RK8_S70_L001_R1_001	1	WOR5.16	9/21/2016	124	3	0.31304331	0.0315518	0.00396696				8.57665775	1144272031	206082012
RK16_S80_L001_R1_001	1	WOR5.16	10/31/2016	164	1	0.08900689	0.08537794							
RK18_S82_L001_R1_001	1	WOR5.16	10/31/2016	164	2	0.33161323	0.48886293							
RK32_S98_L001_R1_001	1	WOR5.16	10/31/2016	164	3	0.08871519	0.06805387						290733333.3	1093067 46.1
RK14_S77_L001	1	WOR5.16	11/30/2016	194	1	0.2658185	0.10572547							

Table S3-1 Continued.

ID	Miseq Run	Experiment	Date	Elapsed time	Replicate	H2 nM	H2 std	CH4 mM	CH4 STD	Isotope ch4	Iso std	so4 mM	Cells ml	Std dev cells
RK10_S73_L001_R1_001	1	WOR5.16	11/30/2016	194	2	0.3900 2857	0.1807 838							
RK5_S67_L001_R1_001	1	WOR5.16	11/30/2016	194	3	0.2289 8279	0.0497 9109					4.4938 7583	286227 586	1093067 46
		WOR5.16	1/6/2017	231	1	0.4534 8974	0.3384 2156							
RK15_S91_L001_R1_001	1	WOR5.16	1/6/2017	231	2	0.1670 7859	0.0939 2149	0.0070 9876					596560 920	9690499 3.6
RK11_S74_L001_R1_001	1	WOR5.16	1/6/2017	231	3	0.4719 1621	0.1269 456	0.0709 8762					100816 0920	1764375 44
		WOR5.16	3/28/2017	312	1	0.3131 1503	0.0521 7249							

Table S3-1 Continued.

ID	Miseq Run	Experiment	Date	Elapsed time	Replicate	H2 nM	H2 std	CH4 mM	CH4 STD	Isotope ch4	Iso std	so4 mM	Cells ml	Std dev cells
RK38_S17_L001_R1_001	1	WOR5.16	3/28/2017	312	2	0.4507 0765	0.1468 456	0.0918 6633				0.2897 3673		
		WOR5.16	3/28/2017	312	3	1.3544 785	0.5504 8347	0.0405 047						
		WOR5.16	5/30/2017	375	1	0.2105 9075	0.0983 7163							
RK35_S101_L001_R1_001	1	WOR5.16	5/30/2017	375	2	10.056 337	0.3622 9294	0.3340 5939					659716 475	1258857 15
		WOR5.16	5/30/2017	375	3	9.8126 0214	0.4311 0005							
		WOR5.16	6/29/2017	405	1									
		WOR5.16	6/29/2017	405	2							0.3491 4825		
		WOR5.16	6/29/2017	405	3									
RK39_S18_L001_R1_001	1	WOR5.16	9/19/2017	487	1	2.8117 0889	0.3568 1335	0.7850 3956				0.0422 3568	708716 475	2078598 91

Table S3-1 Continued.

ID	Miseq Run	Experiment	Date	Elapsed time	Replicate	H2 nM	H2 std	CH4 mM	CH4 STD	Isotope ch4	Iso std	so4 mM	Cells ml	Std dev cells
RK36_S15_L001_R1_001	1	WOR5.16	9/19/2017	487	2							0.05603266	548649808	249510536
RK37_S16_L001_R1_001	1	WOR5.16	9/19/2017	487	3	1.77557297	1.20731786	1.72875734				0.14078558	302560920	147742823
RK30_S96_L001_R1_001	1	WOR5.16	11/3/2017	532	1	0.48868623	0.21716683					1.22398986	894916475	194062970
RK31_S97_L001_R1_001	1	WOR5.16	11/3/2017	532	2	0.68988443	0.44438531					1.61903421	866605364	166862261
RK29_S95_L001	1	WOR5.16	11/3/2017	532	3	0.82375197	0.24318706					0.89539631	968960920	145180179

Table S3-1 Continued.

ID	Miseq Run	Experiment	Date	Elapsed time	Replicate	H2 nM	H2 std	CH4 mM	CH4 STD	Isotope ch4	Iso std	so4 mM	Cells ml	Std dev cells
RK28_S94_L001_R1_001	1	WOR5.16	12/11/2017	570	1	0.3416 2838	0.0487 3845	0.1085 693				0		
RK27_S93_L001_R1_001	1	WOR5.16	11-Dec	570	2	0.1970 8483	0.0414 3012	0.0592 9554				0.1802 0555	100053 8697	2016782 22
RK25_S89_L001_R1_001	1	WOR5.16	11-Dec	570	3	0.6466 0562	0.1197 5332	0.0952 0693				1.0305 5047	120307 2031	2690322 37
RK26_S92_L001_R1_001	1	WOR5.16	1/27/2018	617	1	0.7832 8681	0.2845 7135	0.0734 9307						
	1	WOR5.16	1/27/2018	617	2	1.2751 1282	1.2669 162	0.0576 2524				1.2135 7173	120198 3142	2222084 16
	1	WOR5.16	1/27/2018	617	3	1.6840 3552	0.9773 0234					0.4758 5527	950449 808	2162923 86

Table S3-1 Continued.

ID	Miseq Run	Experiment	Date	Elapsed time	Replicate	H2 nM	H2 std	CH4 mM	CH4 STD	Isotope ch4	Iso std	so4 mM	Cells ml	Std dev cells
RK40_S19_L001_R1_001	1	WOR5.16	3/1/2018	650	2	2.0193 5948	1.0811 6423	0.0331 2756	2.4109 E-06				120633 8697	2372644 18
RK41_S20_L001_R1_001	1	WOR5.16	3/1/2018	650	3	0.7780 4779	0.1927 9874	0.1501 8753	0.0017 3793				115516 0920	3018125 45
RK24_S88_L001_R1_001	1	WOR5.16	3/1/2018	650	1	1.0355 1141	0.2959 6793	0.0974 3399	2.4109 E-05			0.4927 4954	998360 920	2399196 64
		WOR5.16	4/11/2018	691	1	0.3154 4763	0.0312 1203	0.0336 8432	0.0003 9909					
		WOR5.16	4/11/2018	691	2	1.2530 5787	1.3312 3056	0.0034 6587	3.3083 E-05					
RK48_S28_L001_R1_001	1	WOR5.16	4/11/2018	691	3	0.6048 7614	0.1638 2067	0.2364 8621	0.0011 3474			0.1210 756		

Table S3-1 Continued.

ID	Miseq Run	Experiment	Date	Elapsed time	Replicate	H2 nM	H2 std	CH4 mM	CH4 STD	Isotope ch4	Iso std	so4 mM	Cells ml	Std dev cells
WOR_5_24_18_B1	2	WOR5.16	5/23/2018	733	1	0.5220 0057	0.1002 4004	0.0904 7442	4.8217 E-05			0.6757 708	880760 920	1420932 02
WOR_5_24_18_B2	2	WOR5.16	5/23/2018	733	2	0.6171 1295	0.2475 372	0.0181 6448	2.3373 E-05			0.0985 4991	104953 8697	2227046 52
WOR_5_24_18_B3	2	WOR5.16	5/23/2018	733	3	0.8282 4597	0.1839 1694	0.0427 596	0.0002 1376			0.1830 2126	690205 364	1372411 18
WOR_6_28_18_B1	2	WOR5.16	6/28/2018	769	1	0.6357 0104	0.1893 0431	0.0668 1188	8.3515 E-05			1.4669 8578	569338 697	1442350 87
WOR_6_28_18_B2	2	WOR5.16	6/28/2018	769	2	1.7499 7466	0.6964 0339	0.0064 028	1.2757 E-05			2.6664 7895	612894 253	1321646 89
WOR_6_28_18_B3	2	WOR5.16	6/28/2018	769	3	3.2276 1695	2.4145 3197					0.0422 3568	831760 920	1524015 27
WOR_8_1	2	WOR5.16	8/1/2018	802	1	0.4721 5626	0.2153 1593	0.0862 9868	0.0003 789					

Table S3-1 Continued.

ID	Miseq Run	Experiment	Date	Elapsed time	Replicate	H2 nM	H2 std	CH4 mM	CH4 STD	Isotope ch4	Iso std	so4 mM	Cells ml	Std dev cells
WOR_8_1_18_B2	2	WOR5.16	8/1/2018	802	2	0.3152 4201	0.0894 9674	0.0203 7762	0.0001 2842				274249 808	1599720 03
WOR_8_1_18_B3	2	WOR5.16	8/1/2018	802	3	1.2852 5899	0.1188 3562	0.0088 3865	2.4468 E-05			2.4130 649	826316 475	1569415 23
WOR_11_2_18_B1	2	WOR5.16	11/1/2018	895	1	0.2004 9527	0.0202 5325	0.2172 7779	0.0029 7455			6.9491 764	194911 111	3375616 1
WOR_11_2_18_B2	2	WOR5.16	11/1/2018	895	2	0.1610 6491	0.0526 7123	0.0127 9169	0.0001 869			13.259 1863	193822 222	3202199 1
WOR_11_2_18_B3	2	WOR5.16	11/1/2018	895	3	0.2341 9407	0.0207 5477	0.0004 4541	7.7148 E-06			2.2103 3366		

CHAPTER 4

SINGLE CELL GENOMES AND THE INFLUENCE OF SERPENTINIZATION ON MICROBIAL COMMUNITES AT THE MARIANA FOREARC

This chapter has been prepared for submission as a peer-reviewed article by Richard Kevorkian and authors: Richard Kevorkian, IODP Expedition 366 Science Party, Tingting Xu, Veronica Brown, Shawn Campagna, Eric Teague, Karen G. Lloyd. “Single Cell Genomes and Influence of Serpentinization of Microbial Communities at the Mariana Forearc.” *Applied and Environmental Microbiology”* (2019).

Richard Kevorkian and Karen G. Lloyd designed the study. All analyses were completed by Richard Kevorkian. Other Data collection occurred with assistance from Tingting Xu, Veronica Brown, Shawn Campagna, and Eric Teague. The manuscript was written by Richard Kevorkian with inputs from Karen G. Lloyd.

Abstract

Serpentinizing sediments are analogs to an early Earth environment, as well as being relevant to astrobiology, since water-rock reactions can provide energy for chemolithoautotrophic life. Sediments at the summits of three seamounts in the forearc of the Mariana Convergent Margin were sampled during IODP expedition 366. Samples had high concentrations of molecular hydrogen and methane and pH values approaching 12.5. It is not clearly understood how microbes adapt to these conditions or how the process of serpentinization might facilitate their growth and abundance. Methane is potentially abiotically produced at these seamounts, yet other sites with similar geochemistry contain archaea capable of making methane. We explored single cell amplified genomics (SAGs) and metabolomics from sediments collected from three seamount sites (Yinazao summit and Asùt Tesoro summit and flank) along the Mariana Convergent Margin. Here, we present the first single cell genomes isolated from alkaline serpentinization sourced marine mud volcanoes. These genomes appear to differ taxonomically by sample site, which was also reflected by small organic metabolic intermediates, suggesting that isolated cells are strongly influenced by the source of the serpentinization derived fluids. By investigating the interactions of serpentinization-derived fluids, single cell genomics, and metabolomics, we attempted to explore the potential roles of methanogens as well as uncultured archaea and bacteria in these serpentinizing seamounts.

Importance

Single cell genomics is a new and potentially revolutionary tool in microbiology that has never been applied to serpentinization sourced marine sediment. Though it is possible to assemble a pangenome of a microbial taxon from shotgun metagenomic amplification, these genomes are an amalgam of all the DNA that bins using certain criteria (e.g., 97% similarity) and are often subject to chimeric sequences. Additionally, pathway reconstruction is unclear. By amplifying the genome of a single sorted microbial cell, the metabolic potential of that cell can be conclusively determined, not subject to the limitations of metagenomic techniques. In addition, using the metabolomic techniques described herein it is possible to link *in situ* metabolites with metabolic pathways found in SAGs and has not yet been widely attempted in marine sediments.

Introduction

Approximately 70% of the Earth is covered by oceans, and it is underlain by the "deep subsurface biosphere", defined as an environment that exists at least one meter beneath the seafloor and in permanent darkness (4). The microbes of the deep biosphere obtain their energy from geochemical transformations and rely on geochemical conditions that are not too extreme in terms of pH, temperature, oligotrophy, or other factors. However, the full limits of where life can occur within this vast deep subsurface biosphere are unknown. Defining the habitable zone is not straightforward, since no single factor alone dictates conditions favorable for life (129). One type of deep subsurface environment that is promising for life are sites of serpentinization in subduction zones. One of these places is the Mariana convergent margin, which is formed by the Pacific plate subducting beneath the eastern edge of the Philippine plate. This produces a region of serpentinite mud volcanoes in the Mariana Forearc, between the Mariana Trench and the volcanic arc that creates the Mariana Island Chain (50). The increasing pressure and temperature of the descending slab leads to dehydration reactions (50–52). This transformation results in a hydrated serpentinite mud that is pushed upwards through fault conduits resulting in mud volcanoes 2 km in height (Figure 1) (50, 51). The process of serpentinization is a geological transformation by which iron and manganese react with water to form serpentinite rock (53). Serpentinization produces fluids rich in molecular hydrogen and light hydrocarbons, and subsequent Fischer-Tropsch type reactions produce hydrocarbons such as methane which are typically thermodynamically favored (52, 54, 55). These substrates, when mixed with sufficient oxidants such as carbon dioxide, oxidized metals, sulfate, or oxygen, create perfect geochemical conditions for supporting primary production through chemolithoautotrophy and secondary degradation of the resulting organic matter (8, 53, 130).

The drawback to serpentinization, from the perspective of supporting the deep subsurface biosphere, however, is that the fluid that is released from the formation of serpentinite is very alkaline, with a pH of up to 12.5. The highest pH environment found to support microbial life is a terrestrial serpentinization sourced spring in California (pH ~12.5) (131–134). Microbes detected here included taxa from Betaproteobacteria, Firmicutes, Chloroflexi, and Euryarchaeota; community composition was strongly dictated by the source of the spring. Other alkaline serpentinization sourced fluids from marine and terrestrial locations have similarly demonstrated dominance by these four taxa (135–137).

In the environment at the Mariana forearc, the rising fluid likely provides the electron donors and acceptors for the microbial metabolic pathways (5). Abundant molecular hydrogen in the fluid readily serves as an electron donor, and electron acceptors such as sulfate are available in higher concentrations than that found in seawater (52, 54, 61). Methane is present throughout summit and flank sites and is likely a mixture comprised of a deep subsurface abiotic source and more recent microbial production (54). Organic matter in this environment is largely free of photosynthetic input and instead derives almost exclusively from serpentinizing fluids. The majority of methanogen groups are hydrogenotrophs that reduce CO_2 with H_2 serving as the electron donor, while others, called acetoclastic methanogens, are capable of using acetate as the carbon source (20). Hydrogenotrophic methanogenesis is autotrophic and only requires salts, H_2, CO_2, and trace metals to produce energy and biomass (5). Previous research looking at the DNA present in the Mariana forearc mud volcanoes have only examined the upper 10 cm of sediments, under conditions of circumneutral pH. This work showed the presence of groups commonly associated with surficial marine sediments such as Marine Group I (*Thaumarchaeota*), Marine Benthic Group B (*Lokiarchaeota*), Methanosarcinales, and Marine Benthic Group E (51, 58). The only other study including biological material from this site was an analysis of membrane lipids, which found that archaea dominated the population when the pH increased with depth to 12.5 (51).

Despite active serpentinization occurring across large areas of the deep seafloor and numerous terrestrial sites, ecosystems of such areas remain poorly understood components of the global biosphere (135, 137). The Mariana convergent margin experiences these geological reactions that transform the deep sediment and minerals into a hydrated serpentinite mud that is pushed upwards through fault conduits resulting in mud volcanoes 2 km in height with older exhumed material pushed down its flanks [4, 5]. The fluid that is released from the formation of serpentinite mud is very alkaline and rich in molecular hydrogen and short chain hydrocarbons. Unique microbial populations dominated by methane and sulfur cycling metabolisms have been studied at marine and terrestrial sites sharing similar geological conditions to that of the Mariana convergent margin (62, 63, 131). However, this site has a unique geological and chemical composition due to the high flow rate, fluid composition, association with a submarine seamount, and isolation from terrestrial inputs. The microbial structure and function of deep biosphere microbes at serpentinizing seamounts are not fully understood, an initial study of a nearby seamount discovered uncultured and unique clades thriving on the upwelling fluid (58). By

obtaining genomes of the dominant microbes in this environment, assaying the relative abundance of bioactive metabolites, and characterizing site geochemistry we attempted to describe how microbes are able to thrive in a high pH environment lacking any inputs from photosynthetically-derived biomass.

Results

Site description

IODP Expedition 366 aboard the JOIDES Resolution used Advanced Piston Coring (APC) to sample three serpentinite mud volcanoes: Yinazao, Fantangisña, and Asùt Tesoru, which are located at distances of 55 km, 65 km and 70 km west of the Mariana Trench, respectively (138). Yinazao is about 13 km above the subducting slab at 15°43′N and 147°11′E with recovered sediments consisting of green and blue-grey serpentinite mud. Fantangisña seamount is about 14 km above the subducting plate and is located at 16°32′N and 147°13′E with recovered sediments consisted of blue-grey serpentinite mud interspersed with dark pebbles. Asùt Tesoru seamount is about 18 km above the subducting slab at 18°06′N and 147°06′E with recovered sediments also consisting of blue-grey serpentinite mud. As a control for contamination of samples during drilling, a perfluorocarbon tracer was introduced to the drilling apparatus. This tracer does not occur in nature and is easily measured aboard ship. Samples were taken from three locations on a recovered sediment core, on a transect from the center moving distal with the final sample touching the core liner, samples shown to be contaminated were excluded from further microbial analysis (54).

Geochemistry

At Yinazao, the pH increased steadily from 7.7 to 11.1 in the upper ten meters of sediment. At Asùt Tesoro, the pH increased from 11.8 to 12.4 in the upper meter of sediments (Fig. 4-2A) (54). This gradient is caused by circumneutral pH at the seawater/ sediment interface mixing with the highly alkaline serpentinizing fluids moving upward from the subsurface. Methane is present at the majority of depths in both summit and flank sites sampled in this study, and is likely to be a mixture of a deep subsurface abiotic source and more recent microbial production (54). The fluid from Yinazao is sourced from non-sterilizing subsurface temperatures (~80°C) while that of Asùt Tesoro is sourced at much greater temperatures of ~250°C. Molecular hydrogen was present in all samples, both on the flanks and at the summits. The hydrogen

concentrations at the summit site of Asùt Tesoro are in the mM range. Hydrogen at the flanks of Asùt Tesoro ranged from 1.7 to 309.0 μM. Hydrogen concentrations at the summit of Yinazao ranged 0.1 to 143.0 μM, local maxima at 14 and 81 mbsf (Table S4-1). Methane concentrations at the summit of Asùt Tesoro ranged from 0.9 to 6.8 mM, while the flank sites ranged from 0.09 to 43 μM. The summit of Yinazao ranged from below the limit of detection to 29.8 μM methane with a peak at 31 mbsf. Methane at the flanks of Yinazao were all below 0.54 μM. Ammonium concentrations at both the flank and summit of Yinazao ranged from 34 to 112 μM, while the flank of Asùt Tesoro ranged from below detection to 18 μM, and the summit had concentrations in excess of 250 μM. These are much higher than ammonia/ammonium concentrations in seawater, which are typically between 0-10 μM (Table 4) (138, 139). Pore-water sulfate concentrations at Yinazao summit and flank ranged between 24-30 mM, similar to the ~28 mM of seawater. Asùt Tesoro concentrations of sulfate at the flank sites and summit fluctuated between 14 and 28 mM demonstrating no clear change with depth.

Single cell analysis

We obtained 30 single cell amplified genomes (SAGs) from three sites at a depth where the pH had not yet reached it maximum value: 1492B-1H-6 (Yinazao summit), 1496A-2F-1 (Asùt Tesoro summit) , and 1494A-1F-3 (Asùt Tesoro flank) at 5.9, 4.3, and 3.0 mbsf, respectively (Table 4). Epifluorescence microscopy was used as verification of the single cell sorting process (Fig. 4-3). Data obtained from the FACS machine indicated that cellular abundance in these sediments is very low, which corresponds with unpublished cell count data from collaborators (Table. S4-2). Assembled genomes ranged in size from 1,032,282 bp to 6,717 bp (mean = 190,615 bp). The N50 of assembled contig libraries ranged from 16,480 bp to 728 bp (mean = 16,480bp). Genome completion, as determined by single copy conserved genes through CheckM (140), were low, ranging from 0% to 26.7% (mean = 5.2%) (Table 3). The completeness of genomes varied significantly with site with 1492B-1H-6 averaging >10% while 1496A-2F-1 and 1494A-1F-3 averaged 0% and 5%, respectively. The more neutral pH may of facilitated extraction, but the SAGs from 1492B-1H-6 were amplified at the Bigelow Single Cell Genomics Center using their proprietary WGA-X procedure while the other two were amplified using a publicly available kit, which may explain a difference in amplification (141). The key genes related to methane production and dissimilatory sulfate reduction *DsrAB* and *McrA* were not detected in any genome. Two SAGs contained one 16S rRNA gene each, which were identified

as relatives of Arthrobacter (C5) and Propionibacterium (B7) from 1496A-2F-1 and 1494A-1F-3, respectively. Two more partial 16S rRNA genes were obtained from SAGs using PCR amplification of the whole genome product following whole genome sequencing, including relatives of *Bacillus asahii* (P13) and Prosthecochloris (F2). Utilizing Clusters of Orthologous Groups (COGs) domains to determine relatedness to genomes in a public database available through the Department of Energy's online tool Kbase (142), suggests that most SAGs were members of Gammaproteobacteria, Deltaproteobacteria, and Betaproteobacteria, although Clostridia, Actinobacteria, Cytophagia, Aquificae, and Methanomicrobia may also have been present (Fig. 4-4). Because the SAGs were incomplete, taxonomic assignments are only approximations. Six SAGs contained acetyl coA synthase, while one also had carbon monoxide dehydrogenase, key enzymes in anaerobic metabolisms, all from sample 1492B-1H-6. Although the similarity between SAG B7 and cultured microbes associated with human skin suggesting that it was likely a contaminant, other single cell genomes showed close associations with microbes found in anaerobic sedimentary environments and may be novel genomes isolated from the mud volcanoes.

Small organic metabolites

We obtained profiles of the small organic metabolic intermediates in subsurface sediment cores from IODP Expedition 366, representing flank and summit sites of three mud volcanoes associated with the Mariana Forearc as well as the three sample sites used for SAGs (Fig 4-5). From a total of 33 identified metabolites in this study, 16 were found at Yinazao summit, nine at the summit of Asùt Tesoro, and twelve at the flank site of Asùt Tesoro. At the Yinazao summit 50% of recovered known metabolites were amino acids, each of which were 68 times more abundant than samples at depths above or below, at 25 mbsf where the pH had plateaued at ~11. This coincided with a peak in abundance of both methane and hydrogen at about the same depth (54, 143). Identified metabolites at the summit of Asùt Tesoro had peak concentrations at depths less than 15 mbsf, this included metabolites such trehalose, a disaccharide that can act as an osmolyte and protein stabilizer (144). There appears to be little correlation with metabolite peak concentrations and pH, with most metabolites demonstrating peaks at points when the pH was consistently high. Several of the metabolites included mono-phosphorylated variants of amino acids and nucleosides such as uridine and uridine-monophosphate. Principal component analysis (PCA) of known metabolites with geochemical factors demonstrated distinct differences by site.

Samples from site 1496, the summit of Asùt Tesoro, were strongly associated with factors such as pH, hydrocarbons, total inorganic carbon (TIC), total organic carbon (TOC), acetate, and formate, while samples from Yinazao more strongly correlated with metabolites such as amino acids salicylate and succinate/methylmalonate (Fig. 4-6A). Cystine, Isoleucine/ Leucine, and Succinate/ Methylmalonate accounted the most to the variation in PCA. Metabolites of unknown structure and composition comprised 40,028 unique signatures across samples. A canonical correspondence analysis was used prior to PCA visualization as a necessary data reduction tool yielding 106 unknown metabolites of interest (Fig. 4-6B). The PCA of these unknown metabolites demonstrates two metabolites strongly influence the model as well as the sample site. This agrees with the known PCA plot were the samples group by site as well. A network analysis of all sites, geochemistry, and known metabolites did not reveal and clear correlations (Fig. 4-7).

Discussion

The SAGs provided here are, to the authors knowledge, the first isolated from a marine serpentinization sourced mud volcano, as well as the first SAGs sequenced from a marine environment isolated near the current upper observed pH of microbial life (131, 134). These genomes suggest that the presence of microbes in serpentinization sourced springs may be closely related to those widespread in anaerobic sediments globally (145–147). Additionally, presented here are among the first analyses of small organic metabolites in marine and serpentinization sourced sediments. PC1 and PC2 of known metabolites accounted for approximately 32% of variation in the data. This improved to 52% when including unknown metabolites. Approximately 50% of the variation remained unexplained, suggesting that there are missing variable(s) of interest that are likely to emerge with further testing. Microbial community abundance and composition could play an important role in driving both the small organic metabolite changes and geochemistry and is worthy of further investigation. Furthermore, sample bias is likely influencing PCA models; not every metabolite was detected at each site for either known or unknown metabolites. Though this may reflect real site differences, this could also be due in some way to sampling / laboratory methodologies. Nevertheless, the analysis suggests that there are differences between the three sites, with Yinazao influenced more by metabolites and Asùt Tesoro more by geochemistry. One explanation for this may be due to the sterilization conditions found at the source of the latter and a more biological influence at the former, pointing to a biotic/ abiotic dichotomy.

The increasing pH gradient observed in the depth profile, likely results from the mixing of deeply sourced fluid and seawater as it heads upward towards the seafloor which is most notable at the summit sites. This gradient exists where the nutrient rich serpentinization sourced fluid, potentially carrying a microbial seed population, meets seafloor fluids that moderate pH and introduce pelagically sourced microbes (54). This gradient also creates conditions favorable for biotic and abiotic formation of biomolecules and light hydrocarbons such as methane (55, 66, 67). If Yinazao fluids are from non-sterilizing temperatures, as opposed to those from Asùt Tesoro, then it is possible that microbes from a deeply sourced seed population are carried upward with the serpentinization-sourced fluid at Yinazao (54, 148). We believe that if microbial life is abundant in these seamounts, it is most likely located at the more mesophilic conditions found along the pH gradient. The more moderate pH at Yinazao will likely allow alkaliphilic as well as methanogenic microbes, similar to those seen at South Chamorro, to proliferate due to the high presence of reduced chemicals and hydrogen in the environment. Due to the elevated pH of source fluid temperature at Asùt Tesoro relative to Yinazao, we expect the majority of the sediment column to be of very low microbial abundance, with the possible exception near the surface where possible seawater mixing reduces the pH (Fig. 4-2A). Such mixing likely facilitates sediment colonization by pelagic microbes. Yinazao, in contrast, is sourced from much more moderate temperatures and likely bears unique microbes and possibly even microbes sourced from subducted seamounts on the Pacific plate. Pelagically-sourced microbes or microbes present but inactive in the deeply sourced fluid likely take advantage of the reduced chemicals and available energy, but at a pH more conducive to metabolic activity. An example of this spatial dichotomy can be seen at a terrestrial serpentinization sourced spring in California that had unique microbial populations originating from three sources. The more deeply sourced fluid was dominated by Chloroflexi, Firmicutes, and Euryarchaeota; shallow sourced fluids, most similar to terrestrial serpentinization sites, were dominated by *Hydrogenophaga*, a clade within Betaproteobacteria, while a third spring appeared to be a mix of the two (133). SAGs isolated at the Mariana forearc appear to share this distribution, with one, SAG M21, sharing genomic similarity with a Euryarchaeota. In addition, ten SAGs shared characteristics with Gammaproteobacteria, six SAGs related to Clostridia, six to Actinobacteria, and three to Betaproteobacteria.

The upwelling fluid provides both the electron donors and acceptors for microbial growth. However, without the input of photosynthetically derived biomass to fuel growth,

chemoautotrophy must be present to produce that biomass (31, 53, 55). There are several metabolisms that are possible given the geochemistry present (e.g., methane production and sulfate reduction), which have been found to be present at similar sites (59, 131, 149). However, there have been no comprehensive microbial studies at these seamounts. There has only been limited genomic data generated from shallow sediments dominated by pelagic influences. Therefore, it is important to investigate how microbes at this site are utilizing the energy available to them and explore the role of microbes associated with marine serpentinization sourced mud volcanoes. This site may potentially serve as an analog for an early Earth. The geological processes that provide reduced chemicals and nutrients to microbes in the marine sediments, as a stable feature associated with plate tectonics (63, 150). Microbial adaptations at the Marianas Forearc may provide insights into microbial survival mechanisms in other harsh environments such as a moon of Saturn or on an early Earth, possibly influenced by the same serpentinization reactions seen here (69, 151). Microbial life can survive extreme alkaline environments (pH ~ 11-12, e.g., soda lakes), but they do so with specialized cellular machinery to mitigate the many problems associated with elevated pH (152, 153). No known analogs were detected in the genomes sequenced here, which is likely due to low genomic completion. Nevertheless, due to elevated levels of molecular hydrogen there could also be H_2-metabolizing microbes utilizing some variation of the Wood–Ljungdahl pathway, of which several genes, including acetyl-CoA synthase, were present in genomes, and could be responsible for producing the detected acetate.

Studies of nearby South Chamorro Seamount, Ocean Drilling Program (ODP) site 1200, and at Lost City Hydrothermal Field (LCHF), a serpentinite host hydrothermal site near the Mid Atlantic Ridge, discovered uncultured and unique clades, including an abundance of methanogens, hosted in highly alkaline and shallow sediment depth (8, 58, 59, 62). The methane that was sampled at South Chamorro Seamount, from the Mariana forearc suggested that it was thermogenic in origin and not from a microbial source (51). However, 16S rRNA genes were found from the *Methanococcoides* genus within the Methanosarcinales at LCHF; all cultured members of which are hydrogenotrophic methanogens (58, 154). This suggests that methanogenesis may be occurring at a low enough rate that it does not greatly shift the isotopic composition of the total pool of stable carbon isotopes. At LCHF the available carbon pool was unusually depleted in ^{12}C indicating either an abiotic source, anaerobic methane oxidation, or methanogenesis from CO_2 under extreme limitations of CO_2 concentrations due to high pH (63). Here, too, potential methanogens (SAG M21) were found to associate as a member of archaeal

taxa Methanomicrobia. In Mariana forearc sites, ^{12}C-depleted $\delta^{13}C$ values of methane and presence of other hydrocarbons depleted in ^{12}C mean that abiotic methane production must be considered here as well (personal correspondence with Ken Takai). None of the 30 SAGs contained a methyl coenzyme M reductase gene and only a single SAG was taxonomically assigned to the domain archaea, SAG M21, from site 1496. However, SAG M21 was only 1.8% complete, and had only 53 identified non-hypothetical genes, including acetyl CoA synthase. Another possibility is that these methanogens are utilizing some non-methane-related metabolism, such as sulfate reduction, formate catabolism, or acetogenesis (58). The functional potential of genes are typically described for microbes in laboratory culture; the vast majority of microbes in the deep biosphere, or in the environment in general, are as of yet unable to be isolated in pure culture (3, 155, 156). Therefore, it is possible that genes key to a microbe's metabolism and survival in this environment will go unrecognized. Unlike LCHF where the fluid is sourced from the surrounding seawater that seeps into the seafloor around the vent site, the fluid at the Mariana forearc is sourced from the subducted Pacific plate. This suggests that any microbes isolated from the sediments carried up with the fluid may have survived a subduction event and originated from the subducted plate.

Microbial, or more broadly ecological, succession is the process of change in a community structure over time. A community undergoes changes over time following an initial colonization of a new habitat. The geochemistry limits the community, but as the conditions moderate, the community begins to be replaced by colonizers. As microbes are introduced to the seamount from the surrounding marine environment, they will compete with the microbes already present. The flank sites represent older summit material that has had the chance to be colonized by pelagic microbes. These sites may reflect a microbial community succession from summit to flank. However, as these communities spend more time under more similar conditions in the older flank sediments, the seamount flank community likely converge toward a less extremophilic dominant community, such as, aerobic heterotrophs that will take advantage of the organic matter in pelagic sediment. The pelagic influence should be identical for both seamounts, however the differing subsurface geochemical profiles and seed populations will affect the pelagic microbes' ability to colonize the summits, producing very distinct community differences between the seamounts at the summits. At LCHF, inside the carbonate chimneys, the microbial population was dominated by a unique clade of Methanosarcinales, a methane producer (59), while on the more mesophillic extremity of the chimney structure anaerobic methanotrophic archaea and

sulfate reducing bacteria related to Firmicutes and Chloroflexi dominated (59). A similar trend was also observed in Cedars spring in California, as described above; the deep fluid mixed with more shallow water resulted in distinct population shifts.

Methane is produced as part of a methanogen's central metabolism utilizing many unique and complex enzymes and cofactors. A critical final step is mediated by a nickel-containing enzyme, methyl coenzyme M reductase (*mcrA*), which serves as an indicator of methane production (24). This enzyme also catalyzes the reverse pathway of methanotrophy in consortia with sulfate reducing bacteria (25), as well as possibly catalyzing butane oxidation (26). Recent evidence suggests that methane production is more widespread in the domain archaea and not only specific to the clade Euryarchaeota (27). The porewater geochemistry at South Chamorro Seamount and the Mariana forearc have elevated concentrations of short chain hydrocarbons, as well as low organic matter (51). The fluid carried up from the subduction zone is rich in methane; however, microbial presence will likely predominate in the upper 5-10 meters of the sediment subsurface (Fig. 4-2) where the pH is closer to the physiological optimum (51, 131). An alkaline pH reduces the amount of bioavailable dissolved inorganic carbon (DIC) due to its conversion to carbonate species. The typical starting block of organic molecules and primary production is carbon dioxide. The conditions at LCHF and terrestrial environments with serpentinization similarities are characterized by very low concentrations of dissolved inorganic carbon (60, 67, 133, 157). The availability of oxidized carbon may be a limiting factor affecting the habitability of serpentinization environments. It's been theorized microbes aggregating on calcite may allow for the decrease in pH in a localized microenvironment by the generation of a proton gradient, thus freeing soluble carbonate (131).

Analysis reveals distinct differences between sample sites based on geochemistry and metabolite profiles. The potentially microbial sourced production of small organic metabolites detected in sites associated with Yinazao would likely play a larger role due to the less alkaline environment being conducive to greater microbial activity, while factors at the summit of Asùt Tesoro would be driven solely by geochemical parameters. Due to the increased alkalinity and reducing environment proposed at Asùt Tesoro, the abiotic formation of formate and acetate is possible, which may not be possible to the same degree in the other sites. It has been proposed that formate, which could potentially be abiotically formed under elevated hydrogen and reducing conditions, may be an alternative organic starting material to carbon dioxide (67, 158). Formate, which is also present in LCHF fluids, is believed to be the carbon source for methanogens there,

by indirect means of a sulfate reducing bacteria converting it to CO_2 (67). Hydrocarbons and amino acids have been shown to be produced abiotically under conditions similar to serpentinization (56). Alternatively, the samples associated with the Fantangisña seamount experienced a more mesophilic environment compared with the extremities of the other sites. While such trends are curious, the presence of a metabolite in a sample does not necessarily mean that the metabolic pathway in which it is present is active and needs support from genomic evidence for further microbial analysis. It impossible to distinguish between intra and extracellular metabolites using this metabolomic method such that any results can only be used as indicators of activity when supported by other genomic evidence. This technique is also biased against metabolites with >100 m/z as well as hydrophobic, non-polar, and phosphorylated organic compounds (159), while the assembly of a complete genome is challenging and uncommon. Analysis of Unknown metabolites suggests that they correlate strongly with sample site and do not appear to be influenced in a significant way by geochemistry.

Here, we provided microbial insights into a serpentinization sourced marine mud volcano environment that is among the first to be reported. To our knowledge these are the first single cell genomes and metabolite profiles of this environment. The source fluid produced by the subducting slab of the seamount appear to be an important driver in the geochemical and small organic metabolite composition. Furthermore, the limited taxonomic diversity and composition gleaned appear to share characteristics with continental serpentinization sourced springs. Knowledge gained in this study can inform the potential life cycles and limits of life in these environments and potentially other planets.

Methods

Sediment core samples were obtained in December 2016 through February 2017 by IODP 366 at the Mariana convergent margin on the JOIDES Resolution. The drill sites focused on seamounts formed by serpentinite mud volcanoes. Sediments were recovered using Advanced Piston Coring (APC) to minimize disturbances to the sediment while sampling (54). Recovered samples were examined on-site for microbial biomass and morphology by epifluorescence microscopy; final analyses will soon be available. Samples for SAG analysis were preserved in a glycerol solution at -80°C. Whole sediment sections were frozen at -80 ˚C until further analysis. Geochemical measurements including sulfate, methane, ammonia, iron, magnesium, carbonate species, as well as others, were performed by the science party both on the ship and at home

institutions (54). As a control for contamination of samples during drilling, a perfluorocarbon tracer was introduced to the drilling apparatus. This tracer does not occur in nature and is easily measured aboard ship. Contamination samples were taken from three locations on a recovered sediment core, on a transect from the center moving distal with the final sample touching the core liner, samples shown to be contaminated were excluded from further microbial analysis (54). Porewater samples for Short Chain Organic Acid (SCOA) quantification were stored at -80°C in baked vials (6h at 450°C) immediately after retrieval and were quantified in the home laboratory using two-dimensional ion chromatography as described in Glombitza et al. (2014) (143, 160).

Single cell genome generation

Sediment samples were preserved in a glycerol/TE buffer and prepared for cell extraction according to established methods (141, 161, 162). Samples from 1492B-1H-6 were isolated and amplified at the Bigelow Single Cell Genomics Center. Single cells from 1496A-2F-1 and 1494A-1F-3 were isolated into individual wells of a 96-well plate at UTK on a FACSAria cell sorter (BD Biosciences, San Jose, CA) using SYBRGold Nucleic Acid stain (Invitrogen) alongside an extraction blank from the sediment samples using established methods (141, 163). Whole genome amplification was performed using REPLI-g Mini kit (Qiagen, Hilden, Germany), then prepared using Nextera XT DNA Library Preparation Kit, increasing the number of amplification cycles from 12 to 15. Samples were quality checked on an Agilent Bioanalyzer, multiplexed, and sequenced at 10 pM concentration on a v2 flow cell using 250 paired-end chemistry on an Illumina Miseq instrument at UTK's Center for Environmental Biotechnology (164). Sequences were processed using Trimmomatic (v0.36) (122) (seed mismatches, palindrome clip threshold, simple clip threshold; 2,30,12; Sliding window:10:20) and those that pass quality control and filtering were assembled using SPAdes (v3.13.0) (165), gene features identified using PROKKA (166), and genome quality and contamination (Table 3) assessed using CheckM (v1.0.8) (140).

The 16S rRNA gene sequences were amplified using 8F and 1492R primers from amplified whole genomes to further elucidate the identity of samples (167). PCR products were purified using EXOSap-IT Express (Applied Biosystems, Foster City, CA). Amplified products were sequenced using Sanger Sequencing at the UTK Genomics Core facility and identified using NCBI BLAST (168).

Small organic molecules

Analysis of metabolites was performed in collaboration with Dr. Shawn Campagna at the University of Tennessee. Metabolites were extracted from whole sediments onshore by grinding 0.5g subsamples in a mortar and pestle in liquid nitrogen and measured using a Dionex Ultimate 3000 UPLC with a Thermo Scientific Exactive Plus Orbitrap MS (159). Generated data was analyzed using the MAVEN software package to visualize chromatograms (169). Samples were run in biological triplicate and normalized to mass with Allantoin used as a standard. Metabolites were identified using a list of known retention times and *m/z* values. A negative control of extraction materials was used that yielded no metabolites.

Data visualization

Software packages in the R statistical language (128) including ggplot2 and cowplot were utilized to produce the figures in this study (170). The phylogenetic tree was generated using the Interactive Tree of Life (iTOL) software (v4) (171). Canonical correspondence analysis and principal component analysis was conducted using vegan and ade4 packages respectively, known and unknown metabolites were log transformed and visualized using the package factoextra (172–174). Network analysis was performed and visualized using Cytoscape (175). Relationships between variables was calculated by treating edges as undirected using the Analyze Network module in Cytoscape.

Data archiving

Genomes can be found at the NCBI Genbank short read archive with accession numbers (###).

The authors declare no conflicts of interest.

Acknowledgements

We thank the captain and crew of the JOIDES Resolution for assistance in the retrieval of samples. We thank the Scientific Party of Expedition 366 for all the hard work and companionship aboard ship during sample collection. We thank Robert Murdoch and the University of Tennessee Knoxville Bioinformatics Resource Center for computational resources, and Alexandra Emmons for help with statistical analysis. This work is in part funded by NASA grant ###### and IODP Post Expedition Award #####.

Appendix

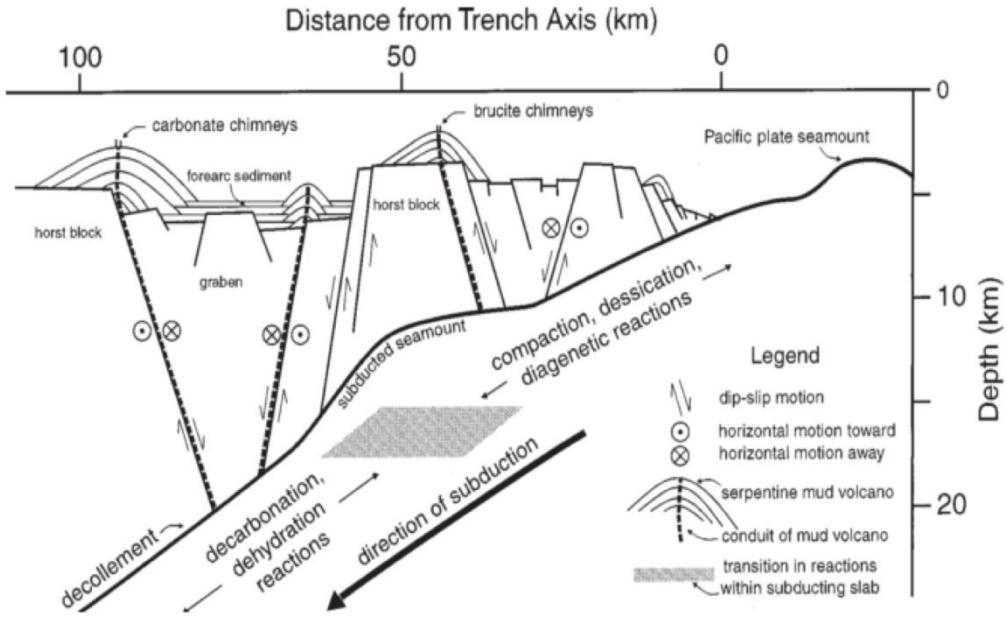

Figure 4-1. Subduction of Pacific plate beneath the Philipine plate results in serpentinization.

Schematic of typical settings for mud volcanoes at the Marianas forearc. Reprinted from Fryer et al. 1999.

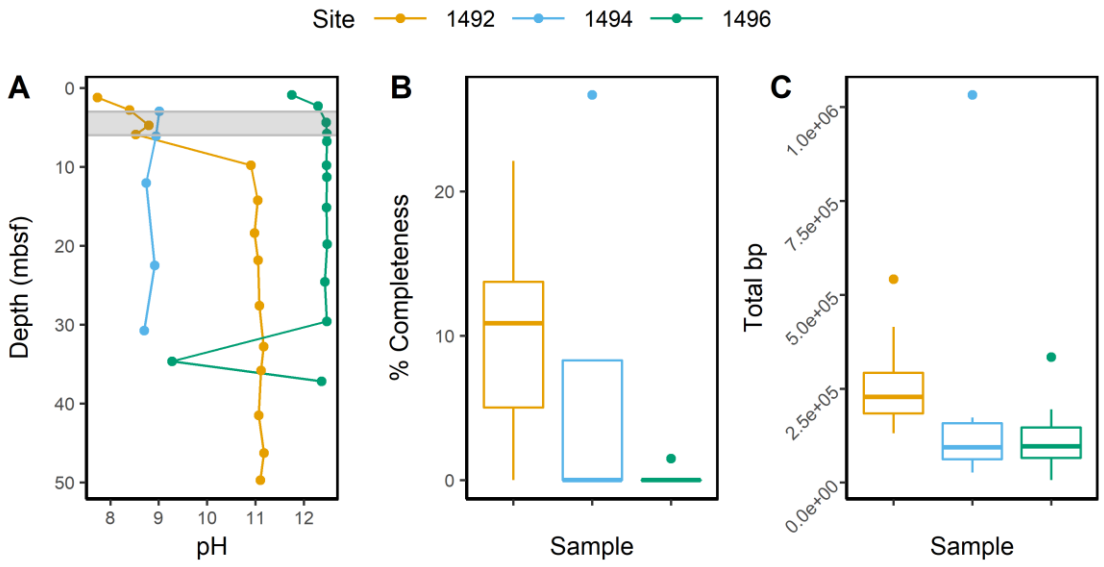

Figure 4-9. Genome completion of SAGs was on average was low.

(A) Downcore pH of sample sites, grey box shows approximate depth range of samples used for SAG analysis. (B) Approximate genome completion of SAGs and (C) box and whisker plot of total base pairs amplified per genome at each site.

Figure 4-10. It was possible to seperate indivual cells from sediments recovered from the mud volcanoes.

Single Cell identified using Epifluorescence microscopy with SYBRGold nucleic acid stain following FACS sorting.

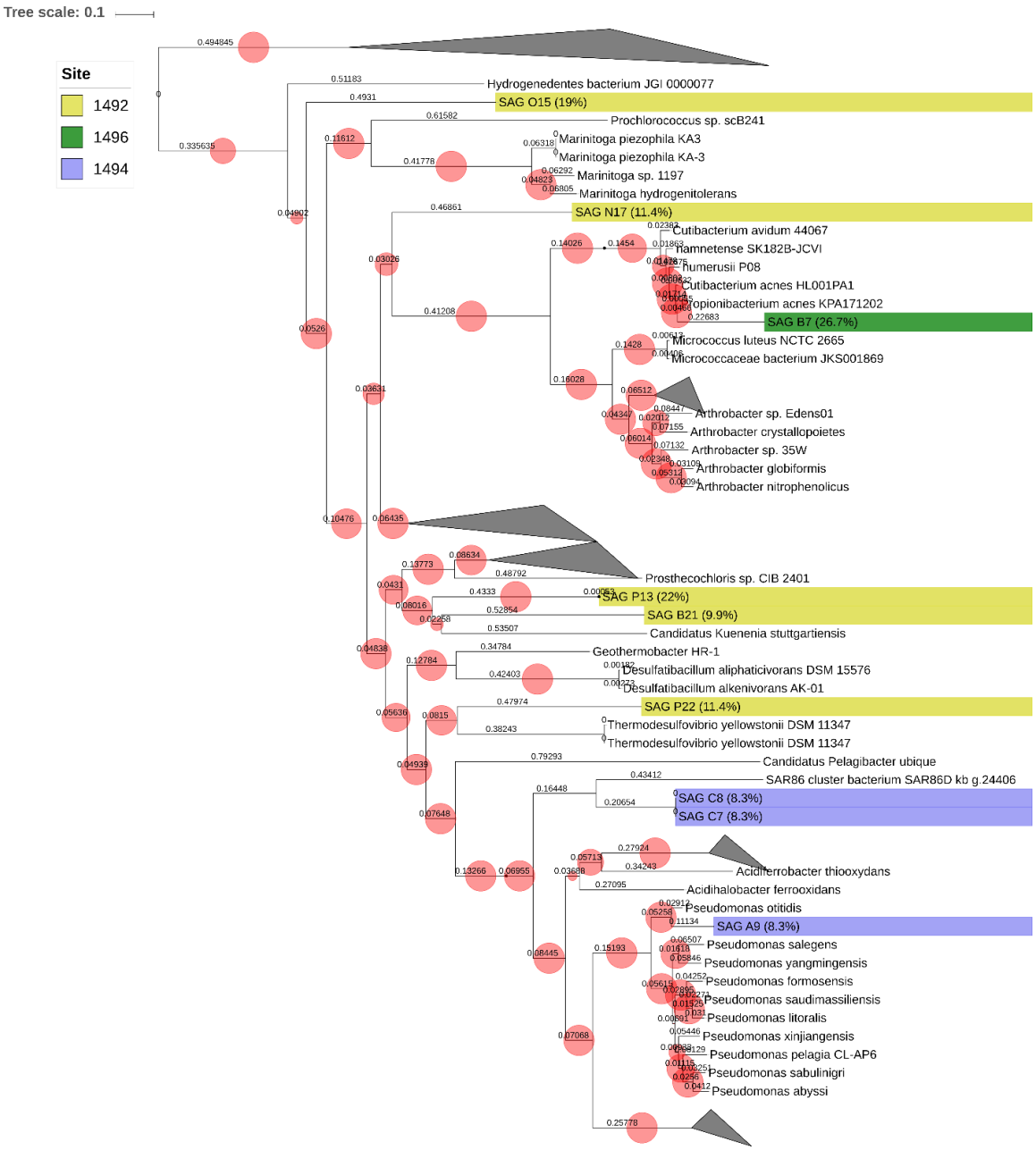

Figure 4-11. SAGs were taxonomically diverse.

Phylogenetic tree base on alignment similarity of COGs against a public library of genomes. SAG genomes with >5% completion were used. Numbers represent branch length and the size of the red circle represent bootstrap values.

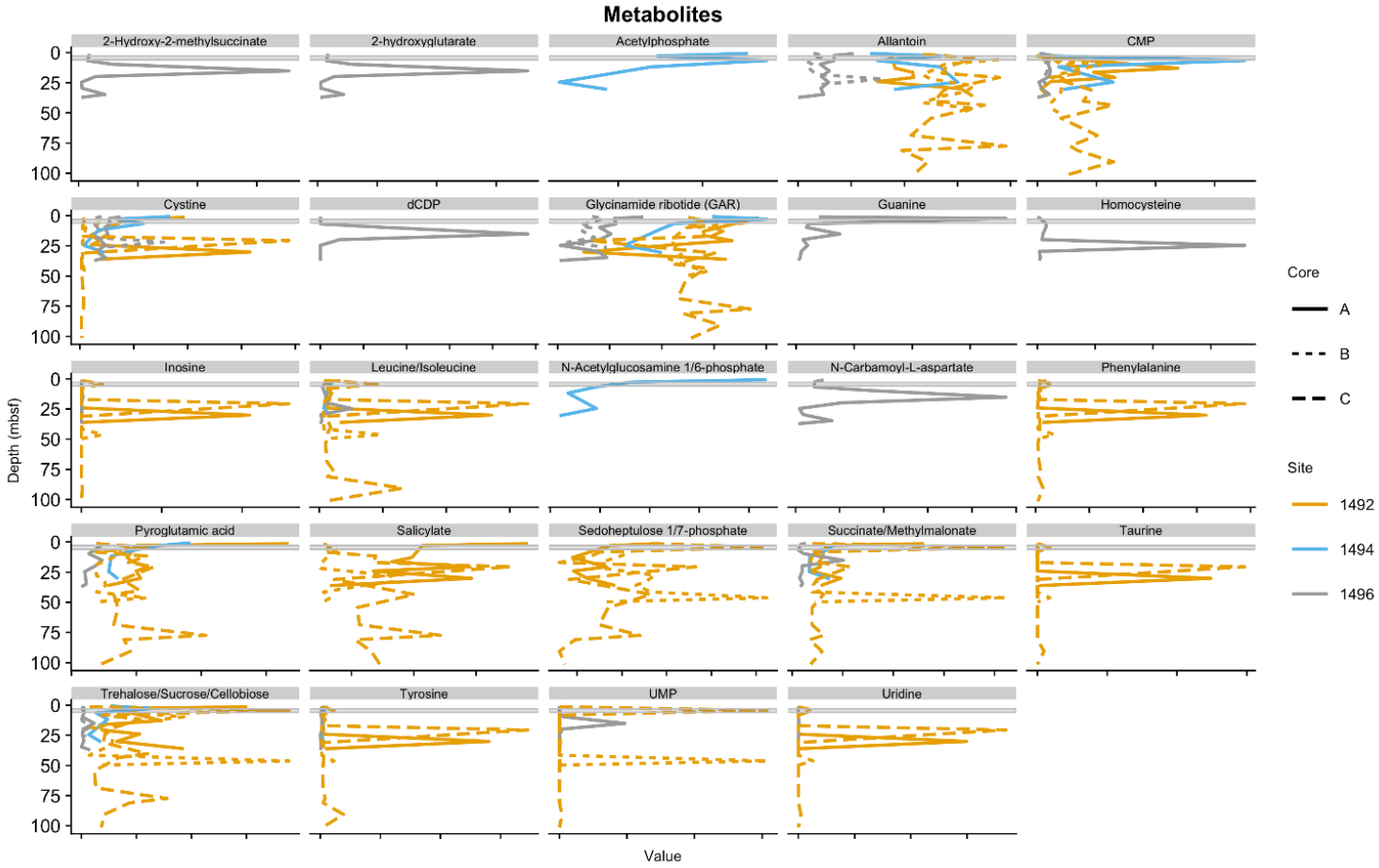

Figure 4-12. Identified metabolites demonstrated unique trends with depth.

Downcore values of known metabolites at the three sites from IODP Expedition 366 used in SAG analysis, the grey box represents the range in depth that used for SAG analysis.

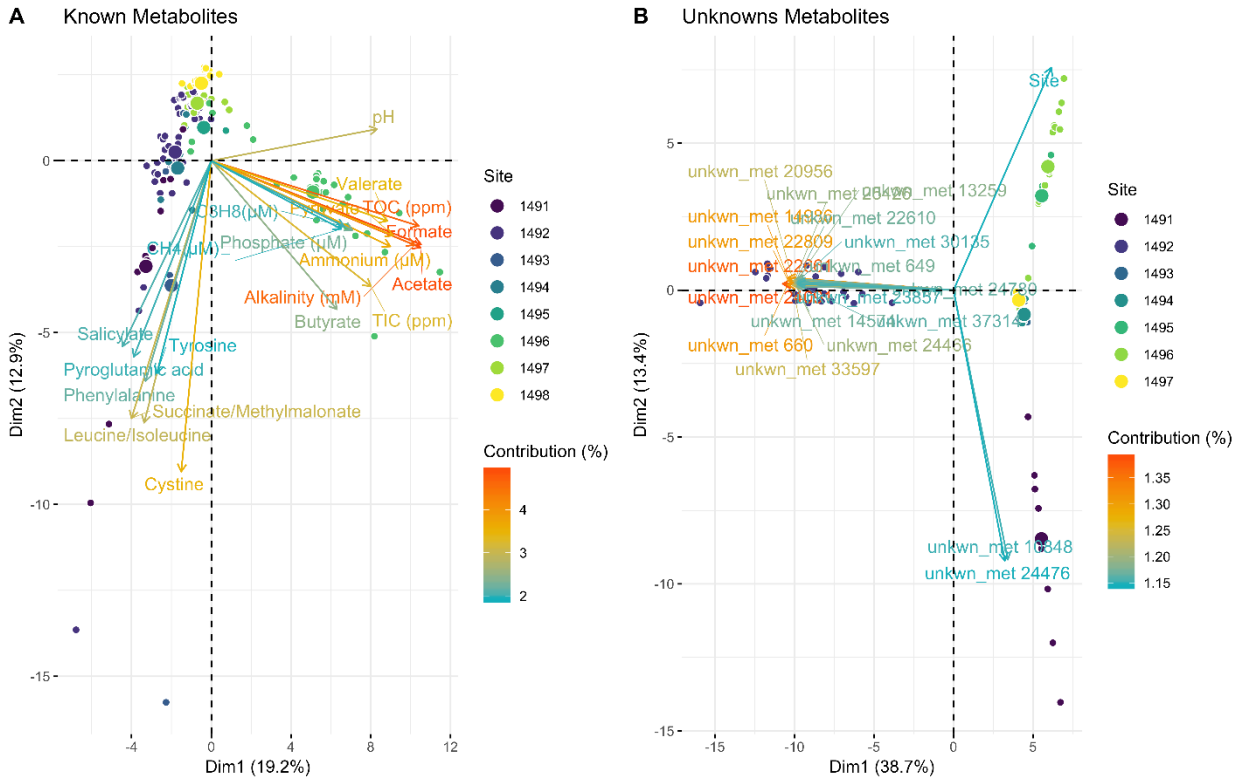

Figure 4-13. Metabolites and Geochemistry appear to be correlated by Site.

Principal Component Analysis using geochemical parameters and Known (A) as well as unknown (B) small organic molecules. Only the top twenty variables contributing to the model were labeled. The large circle of each color represents the mean of that group.

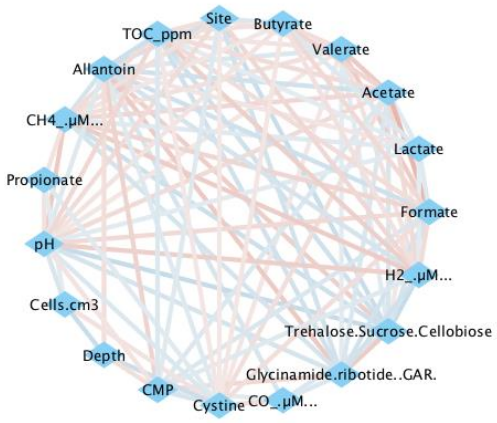

Figure 4-14. Network analysis revealed few significant insights.

Merged co-occurrence network for geochemical and small organic molecule variables at the mud volcanoes associated with the Mariana Forearc. Each node represents a variable and the edge relationship is represented with a line connected to another node. Blue indicates a negative relationship and red a positive one.

Table 3. SAG general information.

Single cell amplified genome completion and size from Exp 366. An (X) denotes positive identification of a gene in assembled genome.

Sample Site	Genome	Completion	Contigs	N50	Total bp	Carbon Monoxide Dehydrogenase	Acetyl CoA Synthase	Accession
1492B-1H-6	N17	11.4	137	1244	149651			###
1492B-1H-6	B21	9.9	121	1985	180847		X	###
1492B-1H-6	D22	10.3	257	1344	294293			###
1492B-1H-6	O19	14.5	159	2326	244328		X	###
1492B-1H-6	N21	3.4	138	2216	210931			###
1492B-1H-6	M21	1.8	87	1973	131205		X	###
1492B-1H-6	B23	0	130	2088	195439			###
1492B-1H-6	P13	22.1	283	2010	414590	X	X	###
1492B-1H-6	P22	11.4	203	1877	285905		X	###
1492B-1H-6	O15	19	293	3095	541382		X	###
1496A-2F-1	A6	0	10	728	6717			###
1496A-2F-1	C2	0	142	4623	334399			###
1496A-2F-1	D3	0	113	1658	159450			###
1496A-2F-1	D1	1.5	43	2856	77828			###
1496A-2F-1	C5	0	111	3174	194374			###
1496A-2F-1	D5	0	79	5535	108416			###
1496A-2F-1	F2	0	30	2376	53722			###
1496A-2F-1	F4	0	60	1700	87883			###
1496A-2F-1	G3	0	47	1797	61641			###
1496A-2F-1	D4	0	72	2180	104219			###
1494A-1F-3	A9	8.3	15	16480	26391			###
1494A-1F-3	A8	0	42	2106	59063			###
1494A-1F-3	B7	26.67	458	4984	1032282			###
1494A-1F-3	A11	0	40	6614	81876			###
1494A-1F-3	C8	8.3	74	7452	173181			###
1494A-1F-3	C11	0	50	5130	70795			###
1494A-1F-3	E8	0	36	1402	45834			###
1494A-1F-3	E9	0	80	1976	114091			###
1494A-1F-3	C7	8.3	74	7452	173181			###
1494A-1F-3	C10	0	48	5130	104552			###

Table 4. Porewater geochemistry for IODP 366.

Porewater geochemistry of sediment core sections from EXP 366 performed shipboard by the Science Party as part of the preliminary report.

Sample	Site	Depth (mbsf)	Alkalinity (mM)	pH	TIC (ppm)	TOC (ppm)	Salinity	Calcium (mM)	Fe (µM)	Magnesium (mM)	Mn (µM)	Ammonium (µM)	Phosphate (µM)	Sulfate (mM)
1491B-1H-2	1491	2.91	2.405	7.707	24.105		32.5	11.621	25.18	52.588	1.09	52.6	1.935	29.102
1491B-2H-2	1491	6.22	2.172	7.829			42	11.012	12.93	53.024	0	41.2	0.789	28.897
1491B-2H-4	1491	9.24	1.955	7.824	21.22	0	35	9.998	0	52.604	0	40.9	0.454	28.308
1491B-3H-2	1491	15.33	1.113	8.288	10.204	2.033	34.5	9.098	0	54.022	0	39.3	0.311	29.41
1491B-4H-3	1491	18.47	1.334	8.53	14.08	2.728	34	9.589	0	51.183	0	42.8	0.5	26.905
1491C-2H-2	1491	2.95	2.38	7.738	25.889	0.316	35	10.351	12.52	51.672	0.58	42.8	0.597	28.693
1491C-2H-4	1491	5.95	2.21	7.696	23.464	0.939	37	11.866	0.87	53.56	0	41.4	0.5	30.409
1491C-3F-2	1491	12.47	1.663	7.826	17.638	0.154	35	10.639	0	51.355	0	36.6	1.553	28.841
1491C-5F-2	1491	18.15	1.574	7.863	15.726	3.298	35	10.45	0	50.05	0	44.6	1.075	28.071
1491C-6F-2	1491	21.11	1.511	7.945	15.147	2.411	35	10.604	0	49.922	0	39	1.696	28.152
1492A-1H-1	1492	1.36	2.041	7.783	21.296	0	34	12.0	8.84			39.6	0.84	29.5
1492A-1H-3	1492	2.92	0.736	8.838	6.768	0	34	16.6			0.93	40.9	0.60	27.7
1492A-2H-2	1492	7.883	0.724	8.924	6.491	0	34	16.7			2.66	38.8	0.5	26.5
1492A-2H-7	1492	12.884	0.455	8.997	3.102	0	33.5	35.3			13.41	37.7	0.5	25.5
1492A-3F-2	1492	16.325	0.45	9.158	2.365	0	32	49.4			5.56	46.5	0.5	25.4

Table 4 Continued.

Sample	Site	Depth (mbsf)	Alkalinity (mM)	pH	TIC (ppm)	TOC (ppm)	Salinity	Calcium (mM)	Fe (µM)	Magnesium (mM)	Mn (µM)	Ammonium (µM)	Phosphate (µM)	Sulfate (mM)
1492A-4F-1	1492	20.65	0.441	8.954	2.867	0	34	33.6			15.96	41.4	1.27	25.5
1492A-5F-2	1492	24.025	0.704	9.967	5.181	0	32.5	61.7				39.3	0.5	25.0
1492A-7F-3	1492	30.077	1.225	10.574	11.757	0.5	32	69.8	1.06			45.4	0.5	26.0
1492A-9F-2	1492	36.154	0.774	10.015	8.626	0	34	65.4				45.2	0.5	26.1
1492B-1H-1	1492	1.197	1.518	7.735	12.52	0		21.3			1.74	41.4	0.5	29.3
1492B-1H-3	1492	2.773	0.385	8.395	2.085	0	35	36.1				34	0.5	29.6
1492B-1H-5	1492	4.747	0.338	8.797	1.548	0		47.7				43.6	0.5	28.2
1492B-1H-6	1492	5.893	0.241	8.522	1.511	0		49.6				38.2	0.5	27.5
1492B-2F-3	1492	9.8	2.186	10.906	5.098	0		71.9				43.8	0.5	30.0
1492B-3F-2	1492	14.241	2.825	11.048	9.208	0.151		67.4				43.6	0.5	27.4
1492B-4F-2	1492	18.374	2.617	10.982	9.25	0		67.4				51	0.5	27.9
1492B-5F-2	1492	21.816	3.053	11.051	6.371	0.709	31.5	66.7				48.9	0.5	27.9
1492B-6F-2	1492	27.603	3.22	11.084	9.526	0	30	66.9				55.8	0.5	28.2
1492B-7F-3	1492	32.78	3.625	11.171	7.777	0		69.2				66.7	0.5	29.5
1492B-9F-1	1492	35.81	3.29	11.113	6.101	1.075		63.9				42.8	0.5	27.0
1492B-10F-3	1492	41.5	3.591	11.065	6.58	0		65.3				43.6	0.5	27.5

Table 4 Continued.

Sample	Site	Depth (mbsf)	Alkalinity (mM)	pH	TIC (ppm)	TOC (ppm)	Salinity	Calcium (mM)	Fe (µM)	Magnesium (mM)	Mn (µM)	Ammonium (µM)	Phosphate (µM)	Sulfate (mM)
1492B-12F-2	1492	46.288	3.676	11.175	1.368	0.123	29	69.2				46	2.47	28.4
1492B-13F-1	1492	49.7	3.183	11.105	5.836	0.292		69.9				42.8	1.20	29.4
1492C-1H-1	1492	1.35	0.451	8.968	4.157	1.373	32.5	27.3			14.67	111	2.47	30.0
1492C-1H-2	1492	2.84	0.368	8.876	3.065	0		42.0			6.09	112	2.14	30.0
1492C-1H-3	1492	4.33	0.347	8.997	2.768	5.511	32	56.4			3.41	90.8	0.5	29.4
1492C-1H-4	1492	5.78	0.337	9.192	3.044	2.946	31.5	61.6			0.36	87.5	2.94	30.8
1492C-3F-1	1492	8.319	1.486	10.682	8.68	1.907	30	73.3				84.6	0.5	31.6
1492C-3F-2	1492	9.008	1.414	10.559	11.017	3.036	29	62.3				88.6	3.03	25.4
1492C-4F-2	1492	11.68	1.591	10.613	10.003	3.531	30	63.1				98.9	2.42	25.5
1492C-5F-2	1492	17.05	1.671	10.718	10.3	2.599	30	64.1	0.15			83.5	0.92	26.2
1492C-6F-3	1492	20.58	1.745	10.716	9.17	2.982	30	63.4				91.6	1.86	26.1
1492C-8F-3	1492	31.05	1.767	10.55	0.952	2.754	29	62.9				95.4	2.19	25.2
1492C-11F-2	1492	40.3	1.924	10.774	6.839	2.107	28	64.2				89.2	0.5	26.4
1492C-12F-1	1492	43.5	2.007	10.834	6.706	2.55	29	64.3				105	0.5	26.3
1492C-13F-1	1492	48.35	1.834	10.794	12.576	3.299	27	63.4				90.0	0.5	25.7

Table 4 Continued.

Sample	Site	Depth (mbsf)	Alkalinity (mM)	pH	TIC (ppm)	TOC (ppm)	Salinity	Calcium (mM)	Fe (µM)	Magnesium (mM)	Mn (µM)	Ammonium (µM)	Phosphate (µM)	Sulfate (mM)
1492C-14F-1	1492	54.4	1.616	10.72	8.666	2.981	29	62.2	8.68			93.2	2.28	25.3
1492C-16F-1	1492	62.39	0.438	9.563	3.829	1.726	33	54.4			0.07	94.1	1.62	27.1
1492C-17F-2	1492	68.6	1.873	10.752	7.602	1.746	29	62.0				88.4	2.23	24.4
1492C-19F-2	1492	77.4	1.435	10.619	10.325	1.655		63.0				96.2	3.08	25.9
1492C-20F-1	1492	81.06	1.645	10.657	11.911	2.14		64.0				91.9	0.5	26.3
1492C-21F-1	1492	90.6	1.506	10.655	9.795	2.907	30	63.5				107	2.94	26.1
1492C-24F-2	1492	101.5	1.254	10.555	8.686	1.731	29	60.9				91.1	0.5	25.1
1492C-26F-1	1492	109.39	1.079	9.663	9.654	4.753		62.1				96.5	0.5	24.9
1492C-27F-1	1492	114.09	1.242	10.585	9.232	2.224		63.6				97.6	0.5	25.9
1497A-2F-1	1497	2.3	0.5	9.19	3.1	2.1	32.5	28.1	0.47	20.5	0.62	3.62	0.5	17.3
1497A-2F-2	1497	3.3	0.3	9.19	3.0	3.8	31.0	37.2	0.47	6.96	0.99	2.35	0.5	13.2
1497A-2F-3	1497	4.8	0.4	9.57	3.6	3.2	30.5	41.5	0.47	0.97	0.073	1.70	0.5	11.1
1497A-2F-4	1497	5.4	0.5	9.61	3.3	5.0	30.5	40.5	2.29	0.78	0.073	3.22	0.5	10.6
1497A-5F-2	1497	14.9	2.2	10.87	1.6	2.2	32.0	70.6	0.47	0.00	0.073	4.54	0.5	7.4
1497A-5F-3	1497	16.0	1.2	10.53	8.3	6.1	32.0	64.7	0.47	0.00	0.073	3.40	0.5	9.1

Table 4 Continued.

Sample	Site	Depth (mbsf)	Alkalinity (mM)	pH	TIC (ppm)	TOC (ppm)	Salinity	Calcium (mM)	Fe (µM)	Magnesium (mM)	Mn (µM)	Ammonium (µM)	Phosphate (µM)	Sulfate (mM)
1497A-6F-1	1497	18.0	0.7	9.26	6.2	4.6	32.5	87.1	0.47	0.00	0.073	15.4	0.5	6.2
1497B-1F-1	1497	1.4	0.8	9.01	6.6	1.0	34.0	11.3	5.69	44.6	11.72	2.41	0.5	24.0
1497B-1F-2	1497	1.9	0.5	9.10	3.9	1.3	33.0	20.4	0.47	32.7	14.58	1.58	0.5	20.0
1497B-1F-3	1497	3.3	0.7	9.03	5.8	1.0	34.0	12.7	0.47	43.5	15.92	1.92	0.5	23.1
1497B-2F-1	1497	5.1	0.6	9.19	5.0	2.7	34.0	13.0	0.47	44.6	0.96	1.96	0.5	21.7
1497B-3F-2	1497	11.3	2.5	10.99	5.8	2.7	32.0	54.3	0.47	0.00	0.073	1.98	0.5	11.1
1497B-5F-2	1497	15.9	0.3	7.87	1.6	3.9	33.0	40.4	0.47	7.59	8.24	6.94	0.5	16.3
1497B-6F-2	1497	20.6	0.2	8.23	1.5	2.9	34.0	89.7	0.47	4.87	3.51	12.0	0.5	15.0
1498A-1R-3	1498	3.6	2.473	7.776	26.151	1.7	35	12.606	0.47	50.055	0.073	20.529	1.96	27.77
1498A-4R-3	1498	29.53	0.525	8.612	5.087	3.646	35	21.004	0.47	35.974	2.37	27.6	0.616	23.82
1498A-5R-2	1498	37.55	0.543	8.71	4.411	2.962	35	22.636	0.47	35.838	1.68	31.578	0.864	24.585
1498A-13R-2	1498	114.32	0.967	7.783	9.395	1.409		33.992	0.47	26.499	0.073			25.583
1498A-15R-1	1498	133.8	1.098	7.947	10.484	1.928	36	36.68	0.47	24.013	129.02	74.665	1.067	25.605
1498B-7R-2	1498	55.51	4.043	11.234	4.364	3.086	29	18.308	0.47		0.073	30.031	0.459	5.727
1498B-8R-4	1498	66.31	3.657	11.229	4.572	5.474	28.5	16.595	0.48	1.631	0.073	21.634	0.339	4.476

Table 4 Continued.

Sample	Site	Depth (mbsf)	Alkalinity (mM)	pH	TIC (ppm)	TOC (ppm)	Salinity	Calcium (mM)	Fe (µM)	Magnesium (mM)	Mn (µM)	Ammonium (µM)	Phosphate (µM)	Sulfate (mM)
1498B-9R-1	1498	74.85	3.865	11.226	6.291	3.945	28.5	17.827	0.49		0.073	26.274	0.818	4.376
1498B-10R-2	1498	84.59	2.537	10.365	4.334	8.521	29	18.593	0.5	3.053	0.073	33.345	0.662	6.361
1498B-11R-4	1498	97.31	2.402	10.985	6.809	5.011	28	15.634	0.51	1.946	0.073	29.589	0.606	5.053
1498B-12R-4	1498	109.09	3.436	11.132	7.625	4.67	27.5	12.246	0.52		0.073	55.22	0.45	4.531
1498B-13R-4	1498	115.91	5.386	11.423	5.755	5.132	26	9.136	0.53		0.073	42.184	0.634	3.36
1498B-14R-4	1498	127.32	4.748	11.354	7.316	7.021	26.5	9.624	0.54		0.073	40.858	0.588	3.737
1498B-15R-2	1498	134.26	3.413	11.202	7.604	5.607	27.5	11.845	0.55	1.606	0.073	42.184	0.606	4.539
1498B-17R-4	1498	156.62	5.002	11.376	5.935	3.908	27.5	13.879	0.56		0.073	42.184	0.404	3.672
1498B-19R-3	1498	174.95	3.434	10.991	6.459	4.911	28	15.266	0.57		0.073	42.626	0.68	3.37
1498B-22R-2	1498	193	1.968	10.875	8.717	4.683	30	11.294	0.58		0.073	43.509	0.634	3.225
1493B-3F-1	1493	11.7	1.10	8.35	9.87	4.76	34.5	9.55	0.05	52.7	0.18	11.1	0.65	28.2
1493B-3F-4	1493	14.0	0.635	8.95	4.92	3.60	34.5	9.77	0.05	44.9	0.47	0.3	0.46	26.0
1493B-4F-2	1493	17.8	0.428	9.08	3.22	3.04	33.5	11.3	0.05	32.5	2.90	0.3	0.85	21.8
1493B-5F-2	1493	22.3	0.394	8.69	3.32	0.96	32.5	12.6	0.05	19.2	0.24	1.01	0.5	18.2
1493B-6F-2	1493	26.1	0.333	9.30	2.90	7.38	31.5	15.0	0.05	7.91	0.07	0.3	0.90	16.6

Table 4 Continued.

Sample	Site	Depth (mbsf)	Alkalinity (mM)	pH	TIC (ppm)	TOC (ppm)	Salinity	Calcium (mM)	Fe (µM)	Magnesium (mM)	Mn (µM)	Ammonium (µM)	Phosphate (µM)	Sulfate (mM)
1494A-1F-3	1494	3.0	0.864	9.01	6.08	2.30	35.0	7.93	0.05	55.2	5.25	7.07	0.49	28.4
1494A-2F-2	1494	6.1	0.835	8.94	6.06	0.00	35.0	8.51	0.05	53.5	6.42	0.3	0.5	27.7
1494A-3F-3	1494	12.0	0.576	8.74	4.67	2.49	35.0	10.2	0.05	49.8	5.87	5.25	0.78	25.9
1494A-5F-4	1494	22.5	0.593	8.91	3.68	3.40	35.0	12.7	0.05	38.0	10.7	4.24	0.49	22.7
1494A-8F-4	1494	30.8	0.449	8.70	3.93	2.68	34.0	13.3	0.05	40.8	12.0	0.3	0.45	23.7
1495A-2F-1	1495	2.2	0.882	8.82	4.18	9.51	37.0	7.93	0.05	52.7	0.07	6.86	0.75	26.0
1495A-4F-2	1495	8.0	1.90	9.88	13.1	4.90	30.0	0.53	0.05	2.93	0.07	13.5	0.94	14.6
1495B-2F-2	1495	3.2	0.708	9.28	4.74	2.08	32.5	6.05	0.53	35.3	4.67	0.3	0.92	22.8
1495B-4F-2	1495	7.9	2.66	10.90	12.5	8.00	29.0	0.90	1.6	0.02	0.07	18.2	1.25	14.3
1496A-1F-1	1496	0.9	15.3	11.75	24.6	17.1	34.0	1.102	0.47	0.00	0.073	177	1.23	25.8
1496A-1F-2	1496	2.3	45.3	12.29	33.0	19.5	36.0	1.306	0.47	0.00	0.073	205	2.07	33.6
1496A-2F-1	1496	4.35	68.5	12.46	33.4	15.5	37.0	0.597	0.47	0.00	0.073	196	2.21	32.6
1496A-2F-3	1496	5.78	70.7	12.47	35.4	18.0	37.0		12.3	0.00	0.13	208	3.81	31.6
1496A-2F-4	1496	6.76	71.1	12.48	35.3	22.1	37.0		0.47	0.00	0.073	196	6.28	31.6
1496A-3F-2	1496	9.81	70.1	12.47	33.7	22.6	37.0	0.241	0.47	0.00	0.073	165	4.03	28.5

Table 4 Continued.

Sample	Site	Depth (mbsf)	Alkalinity (mM)	pH	TIC (ppm)	TOC (ppm)	Salinity	Calcium (mM)	Fe (µM)	Magnesium (mM)	Mn (µM)	Ammonium (µM)	Phosphate (µM)	Sulfate (mM)
1496A-3F-4	1496	11.28	69.7	12.47	36.8	20.9	37.0	2.06	1.07	4.20	0.073	128	2.75	31.9
1496A-4F-2	1496	15.15	70.8	12.47	14.6	16.8	37.0	1.36	0.47	0.81	0.073	258	2.08	30.0
1496A-5F-2	1496	19.81	72.6	12.48	30.6	15.9	37.0	1.45	1.02	0.10	0.073	165	3.38	29.8
1496A-6F-3	1496	24.57	71.7	12.44	20.4	20.2	37.0	0.84	1.18	0.00	0.08	189	2.06	30.1
1496A-7F-3	1496	29.58	78.5	12.48	36.2	20.4	37.0	0.18	1.54	0.00	0.073	152	3.54	29.3
1496A-8F-3	1496	34.67	1.12	9.27	7.30	3.34	34.0	14.8	6.61	26.76	4.91	11.7	0.5	26.2
1496A-9F-1	1496	37.2	58.9	12.37	22.0	20.4	36.0	4.21	0.47	2.71	0.073	96.1	5.55	31.5
1496B-1F-1	1496	0.81	38.9	12.19	26.3	23.4	37.0	2.13	0.47	0.00	0.073	158	1.57	32.1
1496B-1F-2	1496	1.55	61.8	12.39	33.9	18.2	37.5	1.37	0.47	0.00	0.073	151	1.59	31.7
1496B-2F-2	1496	2.62	58.5	12.36	30.0	23.1	37.5	1.19	0.47	0.00	0.073	188	1.29	31.9
1496B-2F-2	1496	3.71	74.4	12.46	49.3	23.4	38.5	2.69	0.66	5.28	0.073	177	2.64	32.8
1496B-3F-2	1496	8.23	69.0	12.43	53.6	17.5	38.5	0.27	0.47	1.26	0.073	118	2.04	31.8
1496B-3F-3	1496	9.28	74.3	12.46	27.4	23.3	38.5	2.23	0.47	5.08	0.073	171	2.05	31.0
1496B-3F-4	1496	10.26	74.8	12.46	48.7	17.2	38.5	0.10	0.47	1.21	0.073	184	1.98	32.3
1496B-3F-5	1496	11.04	73.3	12.45	48.2	20.8	38.5	0.02	0.47	0.49	0.073	216	2.64	32.9

Table 4 Continued.

Sample	Site	Depth (mbsf)	Alkalinity (mM)	pH	TIC (ppm)	TOC (ppm)	Salinity	Calcium (mM)	Fe (µM)	Magnesium (mM)	Mn (µM)	Ammonium (µM)	Phosphate (µM)	Sulfate (mM)
1496B-4F-2	1496	12.87	74.6	12.46	46.6	17.4	38.5	0.02	1.19	0.00	0.073	204	2.23	33.3
1496B-5F-2	1496	18.27	73.2	12.45	32.0	25.1	38.5	0.02	0.76	0.00	0.073	192	3.71	30.8
1496B-6F-1	1496	22.07	72.9	12.46	36.7	22.5	38.5	0.18	0.47	0.00	0.073	207	2.26	32.5
1496B-7F-1	1496	26.52	1.08	9.37	7.75	10.1	34.5	12.2	11.76	14.0	1.27	43.4	0.5	26.6
1496C-1R-1	1496	1.3	15.4	11.76	8.69	13.8	34.0	4.19	0.47	0.00	0.073	135	0.55	30.1
1496C-11R-5	1496	98.87	1.6	9.94	3.18	11.3	33.0	11.3	0.47	10.8	0.073	34.7	0.53	27.7
1496C-12G-3	1496	101.34	33.69	12.192			34	5.11	0.69	2.152		59.42	1.06	29.209
1496C-11G-3	1496	104.287	51.133	12.351			35	6.063		3.619		46.38	0.83	29.076

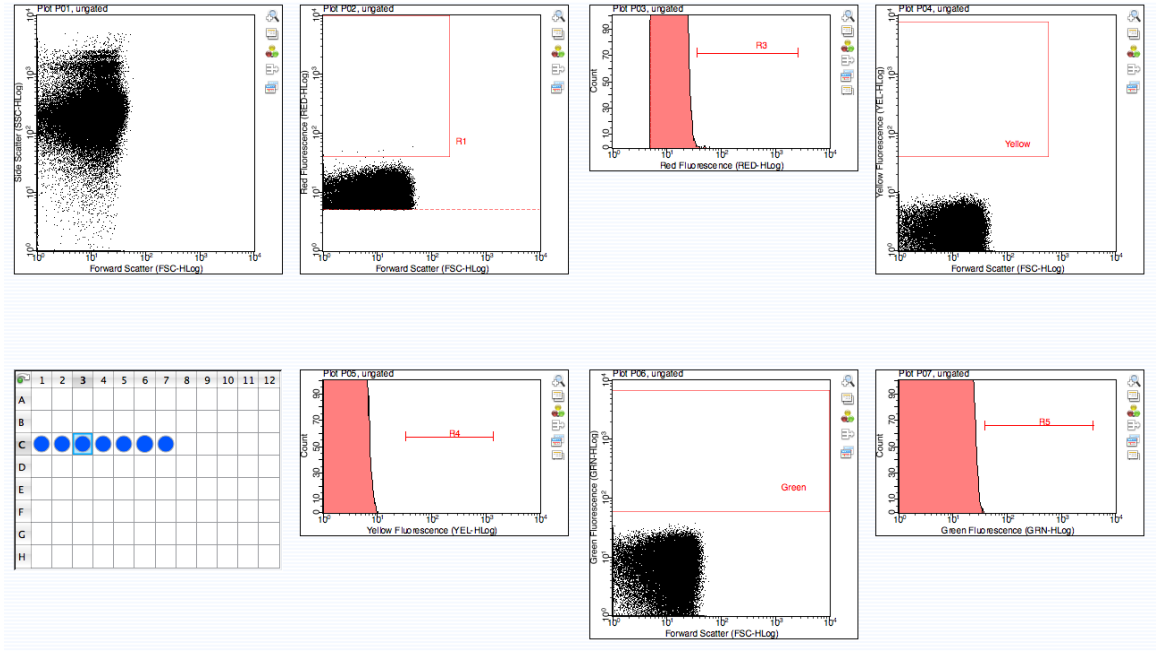

Figure S4-15. Very few cells were detected in sediment extracts.

Screenshot of the gates used in selection of cells for single cell sorting using Fluorescence Activated Cell Sorting (FACS) on a BD Aria. Selection was aided by SYBRGold nucleic acid stain.

Table S4-1. Gas data.

Short chain hydrocarbons and molecular hydrogen measured in Exp 366 sediments. Data produced by Ken Takai.

Sample	Site	Core	Depth (mbsf)	H2 (µM)	CH4 (µM)	C2H6 (µM)	CO (µM)
1491B-1H-3	1491	B	3.06		0.33		
1491B-2H-3	1491	B	6.37	1.04			
1491B-2H-5	1491	B	9.39	1.94			
1491B-3H-2	1491	B	15.05		0.44		
1491B-3H-3	1491	B	15.44	6.79			
1491B-4H-3	1491	B	18.59	23.70	0.54		
1491C-2H-3	1491	C	3.10	0.16			
1491C-2H-5	1491	C	6.10	0.69			
1491C-3F-3	1491	C	12.62	0.38			
1491C-5F-3	1491	C	18.30	0.22			
1491C-6F-3	1491	C	20.84	1.36	0.24		
1491C-7F-1	1491	C	21.90		0.16		
1491C-9X-CC	1491	C	24.52		0.22		
1492A-1H-2	1492	A	0.76				
1492A-1H-4	1492	A	3.91		0.64		
1492A-2H-3	1492	A	8.03	2.98	2.50		1.42
1492A-2H-8	1492	A	13.03		2.72		
1492A-3F-3	1492	A	17.10		7.18		
1492A-4F-2	1492	A	20.15	88.02	6.50		3.76
1492A-5F-3	1492	A	24.75	1.00	17.41		
1492A-6F-1	1492	A	27.30	15.38	26.67		1.95
1492A-7F-4	1492	A	31.07	4.64	29.82		
1492A-9F-3	1492	A	35.74	7.14	26.51		2.86
1492B-1H-2	1492	B	1.35				
1492B-1H-7	1492	B	6.04	1.19			
1492B-2F-3	1492	B	10.10	11.51	10.78		
1492B-3F-3	1492	B	14.39	31.18	6.78		
1492B-4F-3	1492	B	18.57	4.25	5.13		
1492B-5F-3	1492	B	22.44	7.19	21.81		
1492B-6F-3	1492	B	27.88	7.74	4.58		
1492B-7F-4	1492	B	33.08	2.54	2.94		
1492B-9F-3	1492	B	36.86	1.68			

Table S4-1Continued.

Sample	Site	Core	Depth (mbsf)	H2 (µM)	CH4 (µM)	C2H6 (µM)	CO (µM)
1492B-9F-4	1492	B	38.21	4.12			
1492B-10F-4	1492	B	~~42.09~~	9.08	4.92	0.17	
1492B-12F-3	1492	B	47.24	1.72	14.38		
1492B-13F-2	1492	B	49.35	2.52	4.68		
1492C-1H-2	1492	C	1.50				
1492C-1H-4	1492	C	4.48	0.98			
1492C-3F-2	1492	C	8.47	10.00			
1492C-4F-3	1492	C	11.83	2.83			
1492C-5F-3	1492	C	17.20	9.45	4.01		
1492C-6F-3	1492	C	20.73	6.25			
1492C-8F-3	1492	C	31.20	4.66	3.45		
1492C-11F-3	1492	C	40.60				
1492C-12F-2	1492	C	43.80	3.66	1.24		
1492C-13F-2	1492	C	48.50	0.50			
1492C-14F-3	1492	C	54.70	2.65	0.71		
1492C-16F-2	1492	C	62.59	2.13	0.34		
1492C-17F-3	1492	C	68.80	15.09	2.80		
1492C-19F-3	1492	C	77.55	2.46	3.47		
1492C-20F-2	1492	C	81.26	142.96	3.07		
1492C-21F-2	1492	C	85.60	4.52			
1492C-22F-2	1492	C	90.80	4.11			
1492C-23F-2	1492	C	95.49	3.66	2.88		
1492C-24F-3	1492	C	101.70	0.89	0.51		
1492C-26F-2	1492	C	109.59	3.96	1.11		
1492C-27F-2	1492	C	113.75	2.10			
1492C-31X-CC	1492	C	129.40	16.40	1.52		
1493B-1F-1	1493	A	0.00				
1493B-2X-1	1493	A	0.70				
1493B-3F-2	1493	A	11.74	60.39	0.09		20.56
1493B-3F-3	1493	A	12.22	3.67	1.09		16.45
1493B-3F-4	1493	A	12.79	32.89	0.16		14.88
1493B-4F-1	1493	A	16.44	2.95	30.24		18.50
1493B-4F-3	1493	A	18.63	6.49	43.49	0.95	9.56

Table S4-1Continued.

Sample	Site	Core	Depth (mbsf)	H2 (µM)	CH4 (µM)	C2H6 (µM)	CO (µM)
1493B-5F-3	1493	A	22.50	10.87	1.44		18.94
1493B-9X-1	1493	A	29.60				
1494A-1F-3	1494	B	2.30	103.57			21.78
1494A-1F-4	1494	B	3.10	9.78	0.03		8.10
1494A-2F-2	1494	B	5.41	1.74	0.15		9.38
1494A-2F-3	1494	B	6.91	4.77	0.09		16.54
1494A-3F-4	1494	B	12.18	5.27	0.78		8.66
1494A-5F-4	1494	B	21.98	3.80	0.65		12.44
1494A-6F-1	1494	B	23.20	16.75	1.21		12.42
1494A-8F-4	1494	B	30.12	309.03	1.11	0.18	10.16
1494A-10F-1	1494	B	32.60				
1494A-10F-2	1494	B	33.37	95.60	1.13	0.36	10.62
1494A-11X-1	1494	B	35.28				
1495A-1F-1	1495	A	1.14	47.51	0.12		8.06
1495A-2F-1	1495	A	2.28	2303.08	1.78	0.24	9.47
1495A-4F-2	1495	A	7.38	7.15	16.22	2.39	9.64
1495B-2F-1	1495	B	0.40	30.51	1.22		7.85
1495B-2F-3	1495	B	3.40	3.71	1.59	0.34	12.99
1495B-4F-3	1495	B	8.10	14.09	52.78	4.77	14.56
1495B-6F-1	1495	B	10.56				
1496A-1F-2	1496	A	0.70	1265.70	4026.79	13.10	10.02
1496A-1F-2	1496	A	1.13	866.96	1817.33	5.95	8.54
1496A-2F-2	1496	A	3.97	1830.50	2429.47	7.48	7.91
1496A-2F-4	1496	A	5.69	1638.78	2290.77	6.68	7.45
1496A-3F-5	1496	A	10.61	1470.05	1708.84	4.86	4.93
1496A-4F-1	1496	A	14.05	813.81	1315.14	4.13	7.29
1496A-4F-4	1496	A	15.68	1434.70	1539.23	4.91	6.43
1496A-5F-1	1496	A	18.51	1051.18	1723.68	5.36	2.52
1496A-6F-3	1496	A	23.94	5296.43	6869.09	19.06	6.96
1496A-7F-1	1496	A	28.08	1317.75	1568.34	5.07	5.50
1496A-8F-4	1496	A	34.01	8.04	156.86	2.45	2.65
1496A-9F-2	1496	A	37.06	739.62	2462.65	8.39	11.09
1496B-1F-2	1496	A	1.48	617.59	967.31	3.18	5.73
1496B-2F-2	1496	A	3.66	515.52	1009.62	3.62	4.18

Table S4-1Continued.

Sample	Site	Core	Depth (mbsf)	H2 (µM)	CH4 (µM)	C2H6 (µM)	CO (µM)
1496B-3F-3	1496	A	9.23	4865.97	4042.77	11.53	10.48
1496B-4F-4	1496	A	15.00	1198.31	1573.60	5.46	3.87
1496B-5F-3	1496	A	17.65	723.94	1365.57	4.97	5.20
1496B-6F-2	1496	A	21.77	687.44	1038.25	3.70	5.08
1496B-7F-2	1496	A	26.31	1485.08	1943.11	5.84	2.90
1496C-1R-2	1496	C	0.87	1210.16	3159.60	10.00	6.27
1496C-11R-6	1496	C	98.57	1063.34	1643.36	4.88	3.01
1497A-2F-2	1497	A	2.39	10.54	2.33	4.76	8.34
1497A-2F-4	1497	A	4.87	385.42	1.85	8.83	36.09
1497A-5F-3	1497	A	14.88	69.68	6.56	9.35	5.22
1497A-6F-1	1497	A	17.55	4.31	1.80	4.78	13.70
1497A-6F-3	1497	A	19.70	3.95	1.86	3.43	6.58
1497B-1F-2	1497	B	1.49	11.53	0.01		13.38
1497B-2F-2	1497	B	5.20	48.85	0.94	2.36	4.07
1497B-3F-3	1497	B	11.40	13.50	4.57	7.32	6.84
1497B-5F-3	1497	B	16.00	59.59	0.81	2.73	7.65
1497B-6F-3	1497	B	20.81	2.58	2.47	5.80	12.77
1498A-1-R3	1498	A	3.15	1.78	0.01		5.05
1498A-4-R3	1498	A	28.73	5.40	0.33		24.60
1498A-5-R2	1498	A	36.75	6.73	0.25		13.90
1498A-6-RCC	1498	A	45.40				
1498A-13-R3	1498	A	114.47	1.36	0.07		4.23
1498A-15-R2	1498	A	133.90	1.95	0.07		9.56
1498B-2-RCC	1498	B	9.74				
1498B-3-R2	1498	B	20.24	44.95	3.37		5.77
1498B-7-R2	1498	B	54.81	96.75	4.30	0.38	18.02
1498B-8-R4	1498	B	66.61	23.98	7.02	0.27	7.94
1498B-9-R1	1498	B	74.80	111.25	3.40	0.31	9.75
1498B-10-R2	1498	B	85.04	296.74	9.75	0.63	16.56
1498B-11-R4	1498	B	97.61	650.17	10.25	0.26	7.71
1498B-12-R4	1498	B	107.30	231.79	8.65	0.19	7.65
1498B-13-R4	1498	B	115.66	241.20	20.44	0.41	7.93
1498B-14-R3	1498	B	126.28	489.12	22.26	0.42	9.68
1498B-15-R3	1498	B	134.66	237.80	19.29	0.60	16.67

Table S4-1Continued.

Sample	Site	Core	Depth (mbsf)	H2 (µM)	CH4 (µM)	C2H6 (µM)	CO (µM)
1498B-16-RCC	1498	B	141.97				
1498B-17-R6	1498	B	158.52	669.15	10.92	0.41	10.82
1498B-18-R2	1498	B	161.45				
1498B-19-R1	1498	B	170.90	659.59	6.10	0.37	17.34
1498B-20-R2	1498	B	180.94				
1498B-21-RCC	1498	B	188.16	49.39	2.86		36.82
1498B-22-R3	1498	B	193.40	319.11	5.98		10.10
1498B-23-R2	1498	B	201.57	299.69	2.66		14.61
1498B-24-R1	1498	B	211.16	165.16	0.63		7.84
1498B-27-R1	1498	B	240.34	1.33	0.46		2.27

Table S4-2. Short chain organic acids.

Small chain organic acids extracted from Exp 366 sediments. Data produced by Eickenbusch et al (2019).

Sample	Formate (mM)	Acetate (mM)	Propionate (mM)	Butyrate (mM)	Pyruvate (mM)	Lactate (mM)	Valerate (mM)
1492C-1H-1	1.56017449	3.09782264	5.60952807	0.44882321		0.43691069	0.01605566
1492C-1H-2	1.36515268	2.52650289	6.17048087	0.41598248		0.9741566	0.03211132
1492C-1H-3	1.32409546	2.17101504	3.56083086	0.50355774		1.86537662	0.01605566
1492C-1H-4	1.36515268	2.0440551	4.39006544	0.52545156			0.01605566
1492C-3F-1		0.51026212	5.65135643	1.37931034		0.59037272	0.01337972
1492C-3F-2	1.96237651	1.94354616	6.0918614	1.78865406		1.15913603	0.01337972
1492C-4F-2	0.83367167	1.40728342	4.1364491	1.86874305		0.88082843	0.13379716
1492C-5F-2	0.37894167	1.35853227	6.26376578	1.61067853		0.96816163	0.01337972
1492C-6F-2	3.5620517	3.87409201	6.22078969	2.3759733		2.93474997	0.02675943
1492C-8F-2	0.48450399	1.42678389	9.19688423	1.68186874		0.8945678	0.02675943
1492C-11F-2	1.49140614	2.41155727	6.83319903	0.97886541		1.68604618	0.01337972
1492C-12F-1	0.5575856	2.50905959	8.64893903	0.57842047		1.93410449	
1492C-14F-2	1.79997293	3.29882835	7.23072791	2.07341491	1.17967332	1.276873	0.06689858
1492C-16F-1	1.37541699	1.70126325	5.28027316	1.03995621			
1492C-17F-2	0.65502774	1.5535369	5.84474886	1.89543938		0.94027709	0.06689858
1492C-19F-2	0.85803221	1.60228805	5.81251679	1.20133482		1.29458106	0.05351887
1492C-20F-1	1.5076465	2.24580334	8.28364222	1.13014461		1.31568571	0.04013915
1492C-22F-1	2.42522669	7.01366657	7.44560838	1.52169077		1.13373847	0.06689858
1492C-24F-2	1.21532007	1.30978111	2.78270212	1.29922136		0.87990683	0.02675943
1492C-26F-1	4.57707403	4.01059525	5.08192318	1.29922136		1.33907711	0.04013915
1492C-27F-1	2.23846258	2.36280612	4.24388934	1.23692992		1.18841791	0.04013915
1493B-3F-1	2.11629125	12.1336562	1.0857721	7.09631391		1.3884353	0.09410842
1493B-3F-4	1.86485071	4.12590799	1.17917186			0.84001418	

Table S4-2 Continued.

Sample	Formate (mM)	Acetate (mM)	Propionate (mM)	Butyrate (mM)	Pyruvate (mM)	Lactate (mM)	Valerate (mM)
1493B-4F-2	1.57848786	2.46392252	0.80557285			0.42393634	
1493B-5F-2	3.53413655	3.6377724	0.96902242			1.16241765	
1494A-1F-3	1.30411545	1.5488728	0.96491058			1.87567435	
1494A-2F-2	1.22572599	1.56121442	1.36017516			0.79941577	
1494A-3F-3	2.08088366	1.32672371	1.6624363			0.45042269	
1494A-8F-4	1.68181008	11.0148922	1.7438143	7.57079561		1.16113351	
1495A-2F-1	5.35626208	11.1993616	3.44961455	1.09233974	0.18188708	6.93976624	0.04899459
1495A-4F-2	2.83938058	3.56786019	8.63450889	0.96294938		0.71376898	
1495B-2F-2	4.48443645	9.11301969	3.90438689	0.21291368		3.2324865	0.04899459
1495B-4F-2	4.15508082	6.11840791	5.44301953	0.58694057		2.68330216	
1496A-1F-1	74.8575828	41.3000698	13.9994309	1.74055829		1.06147549	0.22477923
1496A-1F-2	108.514242	48.3717387	5.87780985	2.01423098	0.22988506	0.63807655	0.22477923
1496A-2F-1	110.792918	48.6764426	7.82895004	2.1893815	0.22988506		0.36928017
1496A-2F-3	111.05979	50.1745699	7.86553392	2.26600985	0.22988506	0.34275892	0.36928017
1496A-2F-4	112.989479	47.9654669	5.52416568	2.07991242	0.13409962	0.30925018	0.33716885
1496A-3F-2	108.596356	52.0281851	12.1580424	2.24411604	0.34482759	1.25842653	0.32111319
1496A-3F-4	111.439569	49.3366343	4.32909231	2.16748768	0.17241379		0.43350281
1496A-4F-2	109.294329	46.1626357	6.59729279	2.1893815	0.3256705		0.30505753
1496A-5F-2	113.338465	49.1208024	6.90215845	2.1893815	0.24904215	0.29022071	0.35322451
1496A-6F-3	116.489607	50.5046658	7.438722	2.32074439	0.28735632	0.36731209	0.32111319
1496A-7F-3	117.013087	49.7556021	6.90215845	2.27695676	0.22988506	0.32679142	0.32111319
1496A-9F-1	100.733898	45.2739161	6.59729279	2.88998358	0.22988506	0.46540451	0.36928017
1496B-1F-1	117.120969	48.2372059	2.32508574	2.24426893		0.92250428	0.38093931
1496B-1F-2	111.940139	46.2872305	1.99957373	2.15758043	0.19666973		0.33975668

Table S4-2 Continued.

Sample	Formate (mM)	Acetate (mM)	Propionate (mM)	Butyrate (mM)	Pyruvate (mM)	Lactate (mM)	Valerate (mM)
1496B-2F-1	108.697666	55.3583182	2.04607545	2.42727798	0.18355841	0.49840412	0.62803507
1496B-2F-2	116.244433	44.2014974	2.54596888	2.20574071	0.20978104		0.55596548
1496B-3F-2	112.816676	43.9299819	2.01119916	2.03236371	0.19666973	0.30915181	0.42212193
1496B-3F-3	116.451096	43.9670067	2.11582802	2.08052398	0.34089419	4.71435597	0.5250785
1496B-3F-4	93.689649	36.5003291	2.31346031	1.63744943	0.14422447	0.35417157	0.51478285
1496B-3F-5	117.341885	43.7571993	2.56921974	2.04199576	0.15733578	0.35799363	0.11325223
1496B-4F-2	117.862106	42.1527892	2.15070431	1.82045849	0.66867707		0.55596548
1496B-5F-2	114.156423	45.4233174	2.13907888	2.0130996		0.247876	0.50448719
1496B-6F-1	115.973633	43.8559322	2.24370774	1.86861876	0.19666973		0.51478285
1496C-WSTP-	55.663638	28.7497943	1.27879716	1.11731844	0.24911499	4.72103595	0.83394821
1496C-1R-1	80.2137894	46.0033734	2.33671117	1.81082643		0.49634802	
1496C-11R-5	36.707643	17.7904394	1.11604115	1.29069543			
1496C-12G-3	76.5081062	37.7344907	1.9065703	1.78193026	0.20978104	0.23635238	0.08236526
1496C-13G-3	74.0210226	37.2531677	1.67406173	1.74340204	0.24911499	0.56072462	0.08236526
1497A-2F-1	0.7731787	3.45823516	3.58271865	0.39805601		0.37975265	0.04899459
1497A-2F-2	1.31343958	3.284466	10.3286214	0.48606016		0.37657129	0.26473236
1497A-2F-4	4.02622358	5.31182444	3.63960944	1.01797506	0.26827194	1.22449817	
1497A-5F-2	4.22048924	3.161815	2.30713771	0.18514233		1.42215037	0.03674594
1497A-6F-1	7.50783177	5.04294292	3.33869447	0.98125434		0.74921933	0.88190262
1497B-1F-1	1.08511631	2.1015429	4.28151517			1.13894718	0.03674594
1497B-1F-2	0.98913551	1.74811887	4.50335533			0.85429632	0.03674594
1497B-1F-3	1.58901553	2.80839097	4.52553935	0.21291368			0.0244973
1497B-2F-1		3.26442198	6.54428484	0.93496876			0.0244973
1497B-3F-2	1.41305072	2.38656229	4.50335533	0.59245545			0.06124324

Table S4-2 Continued.

Sample	Formate (mM)	Acetate (mM)	Propionate (mM)	Butyrate (mM)	Pyruvate (mM)	Lactate (mM)	Valerate (mM)
1497B-5F-2	10.0593215	8.40617162	9.23964284	0.27771349		1.80368971	0.13473512
1497B-6F-2	1.55702193	1.83932507	4.88048361	0.61096968		1.12993037	0.2572216
1498A-1R-3	3.236686	3.91426617	6.63302091	0.24994214		0.72786222	0.06124324
1498A-4R-3	5.50023329	5.73839021	13.9426543			0.99223846	0.06124324
1498A-5R-2	5.46024129	4.16508323	6.79940103			0.89451687	0.07349189
1498A-13R-2	2.68479637	3.09341035	7.01014919	0.24994214			0.04899459
1498A-15R-1	3.3486636	2.55757392	4.27042316			0.56162103	0.06124324
1498B-7R-2	2.32395162	4.45074209	7.95686389	0.22010271		0.48266712	
1498B-8R-3	5.68780378	5.17012735	5.24628388	0.31181218		1.43429958	
1498B-9R-1	5.61320222	5.25732556	9.20285631	0.47688921		1.01730735	
1498B-10R-1	5.28766814	3.91665304	4.74351501	0.52274395		1.34272581	
1498B-11R-3	7.04419577	7.42638109	6.01136695	0.77953045		2.745912	
1498B-12R-5	5.57251046	5.98761059	5.61789566	1.66911225		6.27430341	
1498B-13R-4	6.44060133	6.43450143	6.67808219	0.61445341		5.20459459	
1498B-14R-4	11.8729513	8.38556143	5.57417662	0.64196625	0.16358045	6.54804876	
1498B-15R-2	9.76376173	8.49455919	7.11527252	0.58694057		2.13836934	0.04235718
1498B-17R-4	7.36972985	5.62791796	5.0058292	0.513573		2.97220217	
1498B-19R-3	7.27478241	5.96581103	4.52491985	0.513573		3.69047521	
1498B-22R-2	7.61388041	7.03398914	7.26828913	0.44937638		1.79691168	

Table S4-3. Metabolites.

Small organic molecules extracted from sediments and identified against a known library.

Depth (mbsf)	Site	Metabolite	Value	IODPCall
2.91	1491	Uracil	1260139.98	1491B-1H-2
2.91	1491	Trehalose/Sucrose/Cellobiose	4306172.58	1491B-1H-2
2.91	1491	Succinate/Methylmalonate	376144186.90	1491B-1H-2
2.91	1491	Pyroglutamic acid	390371204.96	1491B-1H-2
2.91	1491	Phenylalanine	5130505.63	1491B-1H-2
2.91	1491	N-Acetylglucosamine 1/6-phosphate	3608043.55	1491B-1H-2
2.91	1491	Leucine/Isoleucine	13696384.58	1491B-1H-2
2.91	1491	Glycinamide ribotide (GAR)	1187752995.6	1491B-1H-2
2.91	1491	Cystine	64311602.85	1491B-1H-2
2.91	1491	Cytidine	58235.52	1491B-1H-2
2.91	1491	CMP	1442132.92	1491B-1H-2
2.91	1491	Allantoin	32453748.94	1491B-1H-2
2.91	1491	Salicylate	267902089.56	1491B-1H-2
2.91	1491	Acetylphosphate	399599523.59	1491B-1H-2
2.91	1491	Tyrosine	3422916.19	1491B-1H-2
2.91	1491	Uridine	645311.09	1491B-1H-2
6.22	1491	Uracil	3385075.31	1491B-2H-2
6.22	1491	Trehalose/Sucrose/Cellobiose	4221738.68	1491B-2H-2
6.22	1491	Succinate/Methylmalonate	119012881.93	1491B-2H-2
6.22	1491	Pyroglutamic acid	108864386.47	1491B-2H-2
6.22	1491	Phenylalanine	5780496.21	1491B-2H-2
6.22	1491	N-Acetylglucosamine 1/6-phosphate	1474424.99	1491B-2H-2
6.22	1491	Leucine/Isoleucine	12747784.75	1491B-2H-2
6.22	1491	Glycinamide ribotide (GAR)	679413316.36	1491B-2H-2
6.22	1491	Cystine	12046798.66	1491B-2H-2
6.22	1491	Cytidine	2067248.51	1491B-2H-2
6.22	1491	CMP	530657.43	1491B-2H-2
6.22	1491	Allantoin	22087050.48	1491B-2H-2
6.22	1491	Salicylate	104506088.64	1491B-2H-2
6.22	1491	Acetylphosphate	18326623.16	1491B-2H-2
6.22	1491	Tyrosine	4214273.16	1491B-2H-2
6.22	1491	Uridine	5558441.24	1491B-2H-2
9.24	1491	Uracil	436327.33	1491B-2H-4
9.24	1491	Trehalose/Sucrose/Cellobiose	2123713.49	1491B-2H-4
9.24	1491	Succinate/Methylmalonate	67605046.24	1491B-2H-4
9.24	1491	Pyroglutamic acid	191788614.72	1491B-2H-4
9.24	1491	Phenylalanine	8409888.98	1491B-2H-4
9.24	1491	N-Acetylglucosamine 1/6-phosphate	1566918.82	1491B-2H-4
9.24	1491	Leucine/Isoleucine	15009943.33	1491B-2H-4
9.24	1491	Glycinamide ribotide (GAR)	585772213.02	1491B-2H-4
9.24	1491	Cystine	11774520.09	1491B-2H-4
9.24	1491	Cytidine	4415.35	1491B-2H-4
9.24	1491	CMP	11768.87	1491B-2H-4
9.24	1491	Allantoin	20108901.06	1491B-2H-4
9.24	1491	Salicylate	121395701.07	1491B-2H-4
9.24	1491	Acetylphosphate	6897088.08	1491B-2H-4
9.24	1491	Tyrosine	5733246.68	1491B-2H-4
9.24	1491	Uridine	294385.71	1491B-2H-4
15.33	1491	Uracil	250188.58	1491B-3H-2
15.33	1491	Trehalose/Sucrose/Cellobiose	284795.02	1491B-3H-2
15.33	1491	Succinate/Methylmalonate	57251925.09	1491B-3H-2
15.33	1491	Pyroglutamic acid	27987756.89	1491B-3H-2
15.33	1491	Phenylalanine	1175538.84	1491B-3H-2
15.33	1491	N-Acetylglucosamine 1/6-phosphate	961773.49	1491B-3H-2
15.33	1491	Leucine/Isoleucine	2419824.56	1491B-3H-2
15.33	1491	Glycinamide ribotide (GAR)	447384827.50	1491B-3H-2
15.33	1491	Cystine	3959911.03	1491B-3H-2
15.33	1491	Cytidine	3326.60	1491B-3H-2
15.33	1491	CMP	23717.51	1491B-3H-2
15.33	1491	Allantoin	15936362.25	1491B-3H-2

Table S4-3 Continued.

Depth (mbsf)	Site	Metabolite	Value	IODPCall
15.33	1491	Salicylate	62720834.57	1491B-3H-2
15.33	1491	Acetylphosphate	28808132.52	1491B-3H-2
15.33	1491	Tyrosine	703842.47	1491B-3H-2
15.33	1491	Uridine	26327.16	1491B-3H-2
2.95	1491	Uracil	178371.15	1491C-2H-2
2.95	1491	Trehalose/Sucrose/Cellobiose	1293611.04	1491C-2H-2
2.95	1491	Succinate/Methylmalonate	96249320.20	1491C-2H-2
2.95	1491	Pyroglutamic acid	102204616.74	1491C-2H-2
2.95	1491	Phenylalanine	1229311.68	1491C-2H-2
2.95	1491	N-Acetylglucosamine 1/6-phosphate	2193841.77	1491C-2H-2
2.95	1491	Leucine/Isoleucine	4707227.12	1491C-2H-2
2.95	1491	Glycinamide ribotide (GAR)	643384185.36	1491C-2H-2
2.95	1491	Cystine	10781271.68	1491C-2H-2
2.95	1491	Cytidine	5009.96	1491C-2H-2
2.95	1491	CMP	411234.30	1491C-2H-2
2.95	1491	Allantoin	19313496.04	1491C-2H-2
2.95	1491	Salicylate	73769730.39	1491C-2H-2
2.95	1491	Acetylphosphate	128612902.70	1491C-2H-2
2.95	1491	Tyrosine	1598092.65	1491C-2H-2
2.95	1491	Uridine	50600.73	1491C-2H-2
5.95	1491	Uracil	326376.73	1491C-2H-4
5.95	1491	Trehalose/Sucrose/Cellobiose	1391478.29	1491C-2H-4
5.95	1491	Succinate/Methylmalonate	142672361.31	1491C-2H-4
5.95	1491	Pyroglutamic acid	202176753.97	1491C-2H-4
5.95	1491	Phenylalanine	1385215.84	1491C-2H-4
5.95	1491	N-Acetylglucosamine 1/6-phosphate	1802733.03	1491C-2H-4
5.95	1491	Leucine/Isoleucine	6210906.28	1491C-2H-4
5.95	1491	Glycinamide ribotide (GAR)	599157350.14	1491C-2H-4
5.95	1491	Cystine	9346433.25	1491C-2H-4
5.95	1491	Cytidine	17655.71	1491C-2H-4
5.95	1491	CMP	1487219.65	1491C-2H-4
5.95	1491	Allantoin	18628482.04	1491C-2H-4
5.95	1491	Salicylate	50235677.94	1491C-2H-4
5.95	1491	Acetylphosphate	195560020.93	1491C-2H-4
5.95	1491	Tyrosine	2185812.75	1491C-2H-4
5.95	1491	Uridine	179691.78	1491C-2H-4
12.47	1491	Uracil	43769938.82	1491C-3F-2
12.47	1491	Trehalose/Sucrose/Cellobiose	46676386.98	1491C-3F-2
12.47	1491	Succinate/Methylmalonate	49945258.47	1491C-3F-2
12.47	1491	Pyroglutamic acid	50765507.55	1491C-3F-2
12.47	1491	Phenylalanine	50500497.65	1491C-3F-2
12.47	1491	N-Acetylglucosamine 1/6-phosphate	54952953.51	1491C-3F-2
12.47	1491	Leucine/Isoleucine	60333784.18	1491C-3F-2
12.47	1491	Glycinamide ribotide (GAR)	66737176.90	1491C-3F-2
12.47	1491	Cystine	13490042.09	1491C-3F-2
12.47	1491	Cytidine	14445712.33	1491C-3F-2
12.47	1491	CMP	16852765.92	1491C-3F-2
12.47	1491	Allantoin	20214662.47	1491C-3F-2
12.47	1491	Salicylate	21148850.16	1491C-3F-2
12.47	1491	Acetylphosphate	5074931.55	1491C-3F-2
12.47	1491	Tyrosine	529692.94	1491C-3F-2
12.47	1491	Uridine	30440.11	1491C-3F-2
18.15	1491	Uracil	328462.30	1491C-5F-2
18.15	1491	Trehalose/Sucrose/Cellobiose	3044709.55	1491C-5F-2
18.15	1491	Succinate/Methylmalonate	77468129.32	1491C-5F-2
18.15	1491	Pyroglutamic acid	69738834.87	1491C-5F-2
18.15	1491	Phenylalanine	1726373.53	1491C-5F-2
18.15	1491	N-Acetylglucosamine 1/6-phosphate	936206.80	1491C-5F-2
18.15	1491	Leucine/Isoleucine	3313593.60	1491C-5F-2
18.15	1491	Glycinamide ribotide (GAR)	538564120.75	1491C-5F-2
18.15	1491	Cystine	11827211.83	1491C-5F-2
18.15	1491	Cytidine	21387.91	1491C-5F-2
18.15	1491	CMP	76014.05	1491C-5F-2

Table S4-3 Continued.

Depth (mbsf)	Site	Metabolite	Value	IODPCall
18.15	1491	Allantoin	19736578.69	1491C-5F-2
18.15	1491	Salicylate	96095944.91	1491C-5F-2
18.15	1491	Acetylphosphate	12288595.82	1491C-5F-2
18.15	1491	Tyrosine	1286636.85	1491C-5F-2
18.15	1491	Uridine	152917.49	1491C-5F-2
21.11	1491	Uracil	142382.45	1491C-6F-2
21.11	1491	Trehalose/Sucrose/Cellobiose	886504.71	1491C-6F-2
21.11	1491	Succinate/Methylmalonate	44309236.35	1491C-6F-2
21.11	1491	Pyroglutamic acid	34819144.93	1491C-6F-2
21.11	1491	Phenylalanine	1080318.25	1491C-6F-2
21.11	1491	N-Acetylglucosamine 1/6-phosphate	946671.82	1491C-6F-2
21.11	1491	Leucine/Isoleucine	1803523.93	1491C-6F-2
21.11	1491	Glycinamide ribotide (GAR)	436579814.57	1491C-6F-2
21.11	1491	Cystine	3471663.47	1491C-6F-2
21.11	1491	Cytidine	13052.90	1491C-6F-2
21.11	1491	CMP	61761.39	1491C-6F-2
21.11	1491	Allantoin	14739284.20	1491C-6F-2
21.11	1491	Salicylate	50171671.47	1491C-6F-2
21.11	1491	Acetylphosphate	37396315.60	1491C-6F-2
21.11	1491	Tyrosine	709117.39	1491C-6F-2
21.11	1491	Uridine	101692.79	1491C-6F-2
1.36	1492	Succinate/Methylmalonate	130167867.76	1492A-1H-1
1.36	1492	Taurine	2986.11	1492A-1H-1
1.36	1492	Pyroglutamic acid	167509644.65	1492A-1H-1
1.36	1492	Leucine/Isoleucine	6661971.81	1492A-1H-1
1.36	1492	Salicylate	76555393.94	1492A-1H-1
1.36	1492	Allantoin	29545397.41	1492A-1H-1
1.36	1492	Phenylalanine	3895288.52	1492A-1H-1
1.36	1492	Tyrosine	3206228.13	1492A-1H-1
1.36	1492	Cystine	48615638.81	1492A-1H-1
1.36	1492	Uridine	174980.64	1492A-1H-1
1.36	1492	Inosine	210819.27	1492A-1H-1
1.36	1492	Glycinamide ribotide (GAR)	961197755.43	1492A-1H-1
1.36	1492	Sedoheptulose 1/7-phosphate	2838631.72	1492A-1H-1
1.36	1492	CMP	412831.36	1492A-1H-1
1.36	1492	UMP	131266.89	1492A-1H-1
1.36	1492	Trehalose/Sucrose/Cellobiose	3016203.12	1492A-1H-1
2.92	1492	Succinate/Methylmalonate	33707882.73	1492A-1H-3
2.92	1492	Taurine	8323.57	1492A-1H-3
2.92	1492	Pyroglutamic acid	50348344.73	1492A-1H-3
2.92	1492	Leucine/Isoleucine	3033911.66	1492A-1H-3
2.92	1492	Salicylate	42714718.22	1492A-1H-3
2.92	1492	Allantoin	35178549.32	1492A-1H-3
2.92	1492	Phenylalanine	1754873.37	1492A-1H-3
2.92	1492	Tyrosine	1412759.08	1492A-1H-3
2.92	1492	Cystine	22687653.77	1492A-1H-3
2.92	1492	Uridine	21655.92	1492A-1H-3
2.92	1492	Inosine	15537.13	1492A-1H-3
2.92	1492	Glycinamide ribotide (GAR)	935508617.03	1492A-1H-3
2.92	1492	Sedoheptulose 1/7-phosphate	1752027.12	1492A-1H-3
2.92	1492	CMP	115657.54	1492A-1H-3
2.92	1492	UMP	64479.31	1492A-1H-3
2.92	1492	Trehalose/Sucrose/Cellobiose	579455.79	1492A-1H-3
12.88	1492	Succinate/Methylmalonate	29269042.07	1492A-2H-7
12.88	1492	Taurine	1708.08	1492A-2H-7
12.88	1492	Pyroglutamic acid	42888727.24	1492A-2H-7
12.88	1492	Leucine/Isoleucine	2456224.62	1492A-2H-7
12.88	1492	Salicylate	39365995.79	1492A-2H-7
12.88	1492	Allantoin	36493987.00	1492A-2H-7
12.88	1492	Phenylalanine	941804.34	1492A-2H-7
12.88	1492	Tyrosine	1206032.02	1492A-2H-7
12.88	1492	Cystine	8602110.83	1492A-2H-7
12.88	1492	Uridine	81909.25	1492A-2H-7

Table S4-3 Continued.

Depth (mbsf)	Site	Metabolite	Value	IODPCall
12.88	1492	Inosine	22769.09	1492A-2H-7
12.88	1492	Glycinamide ribotide (GAR)	699640617.86	1492A-2H-7
12.88	1492	Sedoheptulose 1/7-phosphate	893701.82	1492A-2H-7
12.88	1492	CMP	47515959.21	1492A-2H-7
12.88	1492	UMP	48194.59	1492A-2H-7
12.88	1492	Trehalose/Sucrose/Cellobiose	1456038.03	1492A-2H-7
16.33	1492	Succinate/Methylmalonate	27111938.32	1492A-3F-2
16.33	1492	Taurine	4235.29	1492A-3F-2
16.33	1492	Pyroglutamic acid	46830647.72	1492A-3F-2
16.33	1492	Leucine/Isoleucine	2293883.28	1492A-3F-2
16.33	1492	Salicylate	32977207.47	1492A-3F-2
16.33	1492	Allantoin	43159896.42	1492A-3F-2
16.33	1492	Phenylalanine	1193869.58	1492A-3F-2
16.33	1492	Tyrosine	1118190.44	1492A-3F-2
16.33	1492	Cystine	4950588.78	1492A-3F-2
16.33	1492	Uridine	65125.05	1492A-3F-2
16.33	1492	Inosine	9445.85	1492A-3F-2
16.33	1492	Glycinamide ribotide (GAR)	699584608.30	1492A-3F-2
16.33	1492	Sedoheptulose 1/7-phosphate	1229818.13	1492A-3F-2
16.33	1492	CMP	19083972.72	1492A-3F-2
16.33	1492	UMP	46573.36	1492A-3F-2
16.33	1492	Trehalose/Sucrose/Cellobiose	332319.38	1492A-3F-2
20.65	1492	Succinate/Methylmalonate	28005193.30	1492A-4F-1
20.65	1492	Taurine	20800.93	1492A-4F-1
20.65	1492	Pyroglutamic acid	59008554.14	1492A-4F-1
20.65	1492	Leucine/Isoleucine	3087574.13	1492A-4F-1
20.65	1492	Salicylate	58009191.30	1492A-4F-1
20.65	1492	Allantoin	43444211.88	1492A-4F-1
20.65	1492	Phenylalanine	869201.10	1492A-4F-1
20.65	1492	Tyrosine	1346043.42	1492A-4F-1
20.65	1492	Cystine	9382748.75	1492A-4F-1
20.65	1492	Uridine	115369.73	1492A-4F-1
20.65	1492	Inosine	21969.76	1492A-4F-1
20.65	1492	Glycinamide ribotide (GAR)	835555931.09	1492A-4F-1
20.65	1492	Sedoheptulose 1/7-phosphate	1658976.13	1492A-4F-1
20.65	1492	CMP	26271259.56	1492A-4F-1
20.65	1492	UMP	100731.35	1492A-4F-1
20.65	1492	Trehalose/Sucrose/Cellobiose	375292.59	1492A-4F-1
24.03	1492	Succinate/Methylmalonate	18672693.04	1492A-5F-2
24.03	1492	Taurine	13713.05	1492A-5F-2
24.03	1492	Pyroglutamic acid	49962120.55	1492A-5F-2
24.03	1492	Leucine/Isoleucine	1761627.24	1492A-5F-2
24.03	1492	Salicylate	26953959.06	1492A-5F-2
24.03	1492	Allantoin	29968079.22	1492A-5F-2
24.03	1492	Phenylalanine	688764.26	1492A-5F-2
24.03	1492	Tyrosine	848932.76	1492A-5F-2
24.03	1492	Cystine	5366613.48	1492A-5F-2
24.03	1492	Uridine	31760.51	1492A-5F-2
24.03	1492	Inosine	25275.37	1492A-5F-2
24.03	1492	Glycinamide ribotide (GAR)	561106387.81	1492A-5F-2
24.03	1492	Sedoheptulose 1/7-phosphate	919672.08	1492A-5F-2
24.03	1492	CMP	4567721.25	1492A-5F-2
24.03	1492	UMP	47168.55	1492A-5F-2
24.03	1492	Trehalose/Sucrose/Cellobiose	1058420.19	1492A-5F-2
30.08	1492	Succinate/Methylmalonate	48196944.58	1492A-7F-3
30.08	1492	Taurine	49687010.71	1492A-7F-3
30.08	1492	Pyroglutamic acid	53236082.90	1492A-7F-3
30.08	1492	Leucine/Isoleucine	54172197.02	1492A-7F-3
30.08	1492	Salicylate	58523573.06	1492A-7F-3
30.08	1492	Allantoin	61342582.57	1492A-7F-3
30.08	1492	Phenylalanine	63381518.48	1492A-7F-3
30.08	1492	Tyrosine	70277258.02	1492A-7F-3
30.08	1492	Cystine	78928930.03	1492A-7F-3

Table S4-3 Continued.

Depth (mbsf)	Site	Metabolite	Value	IODPCall
30.08	1492	Uridine	89681646.75	1492A-7F-3
30.08	1492	Inosine	104624629.19	1492A-7F-3
30.08	1492	Glycinamide ribotide (GAR)	125546720.43	1492A-7F-3
30.08	1492	Sedoheptulose 1/7-phosphate	1225620.09	1492A-7F-3
30.08	1492	CMP	1198985.34	1492A-7F-3
30.08	1492	UMP	350979.40	1492A-7F-3
30.08	1492	Trehalose/Sucrose/Cellobiose	641607.04	1492A-7F-3
36.15	1492	Succinate/Methylmalonate	28282658.93	1492A-9F-2
36.15	1492	Taurine	450705.44	1492A-9F-2
36.15	1492	Pyroglutamic acid	27814941.05	1492A-9F-2
36.15	1492	Leucine/Isoleucine	6453422.80	1492A-9F-2
36.15	1492	Salicylate	13080116.85	1492A-9F-2
36.15	1492	Allantoin	65785255.93	1492A-9F-2
36.15	1492	Phenylalanine	2533234.83	1492A-9F-2
36.15	1492	Tyrosine	2067526.27	1492A-9F-2
36.15	1492	Cystine	8601801.24	1492A-9F-2
36.15	1492	Uridine	210195.71	1492A-9F-2
36.15	1492	Inosine	97634.62	1492A-9F-2
36.15	1492	Glycinamide ribotide (GAR)	810970668.78	1492A-9F-2
36.15	1492	Sedoheptulose 1/7-phosphate	1856733.52	1492A-9F-2
36.15	1492	CMP	3510606.65	1492A-9F-2
36.15	1492	UMP	63743.77	1492A-9F-2
36.15	1492	Trehalose/Sucrose/Cellobiose	1861952.53	1492A-9F-2
41.50	1492	Succinate/Methylmalonate	19756315.76	1492B-10F-3
41.50	1492	Taurine	0.00	1492B-10F-3
41.50	1492	Pyroglutamic acid	19291033.13	1492B-10F-3
41.50	1492	Leucine/Isoleucine	1433120.34	1492B-10F-3
41.50	1492	Salicylate	10994808.34	1492B-10F-3
41.50	1492	Allantoin	47045864.75	1492B-10F-3
41.50	1492	Phenylalanine	916606.94	1492B-10F-3
41.50	1492	Tyrosine	592981.49	1492B-10F-3
41.50	1492	Cystine	1616033.74	1492B-10F-3
41.50	1492	Uridine	12129.78	1492B-10F-3
41.50	1492	Inosine	13883.11	1492B-10F-3
41.50	1492	Glycinamide ribotide (GAR)	626361697.33	1492B-10F-3
41.50	1492	Sedoheptulose 1/7-phosphate	2650313.56	1492B-10F-3
41.50	1492	CMP	4781299.01	1492B-10F-3
41.50	1492	UMP	23849.63	1492B-10F-3
41.50	1492	Trehalose/Sucrose/Cellobiose	146758.72	1492B-10F-3
46.29	1492	Succinate/Methylmalonate	211119015.52	1492B-12F-1
46.29	1492	Taurine	3564901.93	1492B-12F-1
46.29	1492	Pyroglutamic acid	57997777.96	1492B-12F-1
46.29	1492	Leucine/Isoleucine	19500482.32	1492B-12F-1
46.29	1492	Salicylate	13229458.72	1492B-12F-1
46.29	1492	Allantoin	66060166.97	1492B-12F-1
46.29	1492	Phenylalanine	7001090.38	1492B-12F-1
46.29	1492	Tyrosine	5641405.21	1492B-12F-1
46.29	1492	Cystine	2037753.32	1492B-12F-1
46.29	1492	Uridine	7830531.87	1492B-12F-1
46.29	1492	Inosine	13147115.67	1492B-12F-1
46.29	1492	Glycinamide ribotide (GAR)	711602253.24	1492B-12F-1
46.29	1492	Sedoheptulose 1/7-phosphate	5237458.41	1492B-12F-1
46.29	1492	CMP	4875378.86	1492B-12F-1
46.29	1492	UMP	61390697.52	1492B-12F-1
46.29	1492	Trehalose/Sucrose/Cellobiose	3770351.69	1492B-12F-1
49.70	1492	Succinate/Methylmalonate	21891528.91	1492B-13F-1
49.70	1492	Taurine	1702.57	1492B-13F-1
49.70	1492	Pyroglutamic acid	18798486.11	1492B-13F-1
49.70	1492	Leucine/Isoleucine	1647669.40	1492B-13F-1
49.70	1492	Salicylate	10989517.04	1492B-13F-1
49.70	1492	Allantoin	61261351.93	1492B-13F-1

Table S4-3 Continued.

Depth (mbsf)	Site	Metabolite	Value	IODPCall
49.70	1492	Phenylalanine	1024455.04	1492B-13F-1
49.70	1492	Tyrosine	762222.70	1492B-13F-1
49.70	1492	Cystine	1352265.12	1492B-13F-1
49.70	1492	Uridine	35065.79	1492B-13F-1
49.70	1492	Inosine	21767.66	1492B-13F-1
49.70	1492	Glycinamide ribotide (GAR)	618848582.48	1492B-13F-1
49.70	1492	Sedoheptulose 1/7-phosphate	1513202.91	1492B-13F-1
49.70	1492	CMP	7070389.70	1492B-13F-1
49.70	1492	UMP	462438.53	1492B-13F-1
49.70	1492	Trehalose/Sucrose/Cellobiose	376937.51	1492B-13F-1
5.89	1492	Succinate/Methylmalonate	29895327.94	1492B-1H-6
5.89	1492	Taurine	5671.26	1492B-1H-6
5.89	1492	Pyroglutamic acid	36655557.41	1492B-1H-6
5.89	1492	Leucine/Isoleucine	3026883.48	1492B-1H-6
5.89	1492	Salicylate	15355229.73	1492B-1H-6
5.89	1492	Allantoin	75434147.66	1492B-1H-6
5.89	1492	Phenylalanine	1659272.56	1492B-1H-6
5.89	1492	Tyrosine	1220870.35	1492B-1H-6
5.89	1492	Cystine	9251490.54	1492B-1H-6
5.89	1492	Uridine	55311.86	1492B-1H-6
5.89	1492	Inosine	48525.32	1492B-1H-6
5.89	1492	Glycinamide ribotide (GAR)	898513145.18	1492B-1H-6
5.89	1492	Sedoheptulose 1/7-phosphate	1893829.38	1492B-1H-6
5.89	1492	CMP	1617086.56	1492B-1H-6
5.89	1492	UMP	53019.55	1492B-1H-6
5.89	1492	Trehalose/Sucrose/Cellobiose	889291.21	1492B-1H-6
9.80	1492	Succinate/Methylmalonate	20114024.89	1492B-2F-2
9.80	1492	Taurine	1494.01	1492B-2F-2
9.80	1492	Pyroglutamic acid	38749606.87	1492B-2F-2
9.80	1492	Leucine/Isoleucine	3412229.40	1492B-2F-2
9.80	1492	Salicylate	13217006.56	1492B-2F-2
9.80	1492	Allantoin	55111284.39	1492B-2F-2
9.80	1492	Phenylalanine	1799320.78	1492B-2F-2
9.80	1492	Tyrosine	1526191.21	1492B-2F-2
9.80	1492	Cystine	2688070.10	1492B-2F-2
9.80	1492	Uridine	36854.14	1492B-2F-2
9.80	1492	Inosine	33231.66	1492B-2F-2
9.80	1492	Glycinamide ribotide (GAR)	619679424.84	1492B-2F-2
9.80	1492	Sedoheptulose 1/7-phosphate	2114051.10	1492B-2F-2
9.80	1492	CMP	21332754.63	1492B-2F-2
9.80	1492	UMP	31797.30	1492B-2F-2
9.80	1492	Trehalose/Sucrose/Cellobiose	1860808.61	1492B-2F-2
18.37	1492	Succinate/Methylmalonate	17736419.97	1492B-4F-2
18.37	1492	Taurine	0.00	1492B-4F-2
18.37	1492	Pyroglutamic acid	20179513.62	1492B-4F-2
18.37	1492	Leucine/Isoleucine	1704338.69	1492B-4F-2
18.37	1492	Salicylate	10003162.76	1492B-4F-2
18.37	1492	Allantoin	46903803.57	1492B-4F-2
18.37	1492	Phenylalanine	837839.48	1492B-4F-2
18.37	1492	Tyrosine	520556.35	1492B-4F-2
18.37	1492	Cystine	1876128.33	1492B-4F-2
18.37	1492	Uridine	12211.60	1492B-4F-2
18.37	1492	Inosine	18340.40	1492B-4F-2
18.37	1492	Glycinamide ribotide (GAR)	554661448.41	1492B-4F-2
18.37	1492	Sedoheptulose 1/7-phosphate	1423955.07	1492B-4F-2
18.37	1492	CMP	6632849.40	1492B-4F-2
18.37	1492	UMP	30158.97	1492B-4F-2
18.37	1492	Trehalose/Sucrose/Cellobiose	180431.96	1492B-4F-2
21.82	1492	Succinate/Methylmalonate	17950816.87	1492B-5F-2
21.82	1492	Taurine	2357.30	1492B-5F-2
21.82	1492	Pyroglutamic acid	18957252.79	1492B-5F-2

Table S4-3 Continued.

Depth (mbsf)	Site	Metabolite	Value	IODPCall
21.82	1492	Leucine/Isoleucine	1576384.37	1492B-5F-2
21.82	1492	Salicylate	10014916.61	1492B-5F-2
21.82	1492	Allantoin	49810630.64	1492B-5F-2
21.82	1492	Phenylalanine	903027.04	1492B-5F-2
21.82	1492	Tyrosine	630098.50	1492B-5F-2
21.82	1492	Cystine	1155645.13	1492B-5F-2
21.82	1492	Uridine	14235.81	1492B-5F-2
21.82	1492	Inosine	8019.47	1492B-5F-2
21.82	1492	Glycinamide ribotide (GAR)	551083087.30	1492B-5F-2
21.82	1492	Sedoheptulose 1/7-phosphate	1606563.02	1492B-5F-2
21.82	1492	CMP	8822023.32	1492B-5F-2
21.82	1492	UMP	37492.18	1492B-5F-2
21.82	1492	Trehalose/Sucrose/Cellobiose	454791.80	1492B-5F-2
27.60	1492	Succinate/Methylmalonate	24329924.50	1492B-6F-2
27.60	1492	Taurine	1258.17	1492B-6F-2
27.60	1492	Pyroglutamic acid	19302886.20	1492B-6F-2
27.60	1492	Leucine/Isoleucine	1288454.55	1492B-6F-2
27.60	1492	Salicylate	32314246.82	1492B-6F-2
27.60	1492	Allantoin	66161855.48	1492B-6F-2
27.60	1492	Phenylalanine	1029934.51	1492B-6F-2
27.60	1492	Tyrosine	523107.22	1492B-6F-2
27.60	1492	Cystine	1504820.22	1492B-6F-2
27.60	1492	Uridine	12095.60	1492B-6F-2
27.60	1492	Inosine	172474.18	1492B-6F-2
27.60	1492	Glycinamide ribotide (GAR)	576156083.30	1492B-6F-2
27.60	1492	Sedoheptulose 1/7-phosphate	2733361.27	1492B-6F-2
27.60	1492	CMP	8151248.49	1492B-6F-2
27.60	1492	UMP	52466.94	1492B-6F-2
27.60	1492	Trehalose/Sucrose/Cellobiose	566080.65	1492B-6F-2
32.78	1492	Succinate/Methylmalonate	23394535.90	1492B-7F-1
32.78	1492	Taurine	21978.44	1492B-7F-1
32.78	1492	Pyroglutamic acid	25541189.20	1492B-7F-1
32.78	1492	Leucine/Isoleucine	1594493.79	1492B-7F-1
32.78	1492	Salicylate	33873482.02	1492B-7F-1
32.78	1492	Allantoin	62768795.66	1492B-7F-1
32.78	1492	Phenylalanine	996841.52	1492B-7F-1
32.78	1492	Tyrosine	593779.43	1492B-7F-1
32.78	1492	Cystine	1309287.66	1492B-7F-1
32.78	1492	Uridine	35949.47	1492B-7F-1
32.78	1492	Inosine	25154.71	1492B-7F-1
32.78	1492	Glycinamide ribotide (GAR)	593688787.46	1492B-7F-1
32.78	1492	Sedoheptulose 1/7-phosphate	2534633.44	1492B-7F-1
32.78	1492	CMP	7979922.25	1492B-7F-1
32.78	1492	UMP	37727.43	1492B-7F-1
32.78	1492	Trehalose/Sucrose/Cellobiose	557929.01	1492B-7F-1
35.81	1492	Succinate/Methylmalonate	20611518.86	1492B-9F-2
35.81	1492	Taurine	0.00	1492B-9F-2
35.81	1492	Pyroglutamic acid	26387562.15	1492B-9F-2
35.81	1492	Leucine/Isoleucine	1453869.78	1492B-9F-2
35.81	1492	Salicylate	24432361.42	1492B-9F-2
35.81	1492	Allantoin	54531795.89	1492B-9F-2
35.81	1492	Phenylalanine	942075.79	1492B-9F-2
35.81	1492	Tyrosine	644466.15	1492B-9F-2
35.81	1492	Cystine	1117501.54	1492B-9F-2
35.81	1492	Uridine	17552.22	1492B-9F-2
35.81	1492	Inosine	64712.10	1492B-9F-2
35.81	1492	Glycinamide ribotide (GAR)	534235206.53	1492B-9F-2
35.81	1492	Sedoheptulose 1/7-phosphate	2315109.98	1492B-9F-2
35.81	1492	CMP	6825786.74	1492B-9F-2
35.81	1492	UMP	37772.10	1492B-9F-2
35.81	1492	Trehalose/Sucrose/Cellobiose	416726.71	1492B-9F-2

Table S4-3 Continued.

Depth (mbsf)	Site	Metabolite	Value	IODPCall
40.30	1492	Succinate/Methylmalonate	25234533.43	1492C-11F-2
40.30	1492	Taurine	9181.04	1492C-11F-2
40.30	1492	Pyroglutamic acid	52566541.06	1492C-11F-2
40.30	1492	Leucine/Isoleucine	3613377.47	1492C-11F-2
40.30	1492	Salicylate	33419460.41	1492C-11F-2
40.30	1492	Allantoin	51309605.47	1492C-11F-2
40.30	1492	Phenylalanine	1588012.06	1492C-11F-2
40.30	1492	Tyrosine	1282974.38	1492C-11F-2
40.30	1492	Cystine	873866.92	1492C-11F-2
40.30	1492	Uridine	19361.55	1492C-11F-2
40.30	1492	Inosine	271881.95	1492C-11F-2
40.30	1492	Glycinamide ribotide (GAR)	563011334.49	1492C-11F-2
40.30	1492	Sedoheptulose 1/7-phosphate	2188738.23	1492C-11F-2
40.30	1492	CMP	15519072.82	1492C-11F-2
40.30	1492	UMP	36959.20	1492C-11F-2
40.30	1492	Trehalose/Sucrose/Cellobiose	1205071.80	1492C-11F-2
43.50	1492	Succinate/Methylmalonate	31038150.16	1492C-12F-1
43.50	1492	Taurine	6111.21	1492C-12F-1
43.50	1492	Pyroglutamic acid	32570586.13	1492C-12F-1
43.50	1492	Leucine/Isoleucine	2818006.93	1492C-12F-1
43.50	1492	Salicylate	40224071.51	1492C-12F-1
43.50	1492	Allantoin	70064538.84	1492C-12F-1
43.50	1492	Phenylalanine	1601378.50	1492C-12F-1
43.50	1492	Tyrosine	1427055.67	1492C-12F-1
43.50	1492	Cystine	709450.35	1492C-12F-1
43.50	1492	Uridine	24949.22	1492C-12F-1
43.50	1492	Inosine	24620.80	1492C-12F-1
43.50	1492	Glycinamide ribotide (GAR)	713595578.40	1492C-12F-1
43.50	1492	Sedoheptulose 1/7-phosphate	2651821.17	1492C-12F-1
43.50	1492	CMP	25523074.82	1492C-12F-1
43.50	1492	UMP	106114.52	1492C-12F-1
43.50	1492	Trehalose/Sucrose/Cellobiose	680070.36	1492C-12F-1
54.40	1492	Succinate/Methylmalonate	19754450.48	1492C-14F-2
54.40	1492	Taurine	3759.13	1492C-14F-2
54.40	1492	Pyroglutamic acid	35849840.86	1492C-14F-2
54.40	1492	Leucine/Isoleucine	1977986.13	1492C-14F-2
54.40	1492	Salicylate	21744064.57	1492C-14F-2
54.40	1492	Allantoin	50010346.65	1492C-14F-2
54.40	1492	Phenylalanine	892232.95	1492C-14F-2
54.40	1492	Tyrosine	973462.88	1492C-14F-2
54.40	1492	Cystine	1147252.08	1492C-14F-2
54.40	1492	Uridine	39764.14	1492C-14F-2
54.40	1492	Inosine	12708.81	1492C-14F-2
54.40	1492	Glycinamide ribotide (GAR)	611960708.66	1492C-14F-2
54.40	1492	Sedoheptulose 1/7-phosphate	1694164.91	1492C-14F-2
54.40	1492	CMP	7939485.28	1492C-14F-2
54.40	1492	UMP	52781.26	1492C-14F-2
54.40	1492	Trehalose/Sucrose/Cellobiose	236148.35	1492C-14F-2
68.60	1492	Succinate/Methylmalonate	19738276.48	1492C-15F-1
68.60	1492	Taurine	22671.08	1492C-15F-1
68.60	1492	Pyroglutamic acid	32555324.35	1492C-15F-1
68.60	1492	Leucine/Isoleucine	2407500.65	1492C-15F-1
68.60	1492	Salicylate	22588998.30	1492C-15F-1
68.60	1492	Allantoin	42526166.77	1492C-15F-1
68.60	1492	Phenylalanine	1287037.13	1492C-15F-1
68.60	1492	Tyrosine	1153096.86	1492C-15F-1
68.60	1492	Cystine	1777160.26	1492C-15F-1
68.60	1492	Uridine	15168.08	1492C-15F-1
68.60	1492	Inosine	157947.11	1492C-15F-1
68.60	1492	Glycinamide ribotide (GAR)	575124517.51	1492C-15F-1
68.60	1492	Sedoheptulose 1/7-phosphate	1492504.42	1492C-15F-1

Table S4-3 Continued.

Depth (mbsf)	Site	Metabolite	Value	IODPCall
68.60	1492	CMP	20254780.59	1492C-15F-1
68.60	1492	UMP	35844.59	1492C-15F-1
68.60	1492	Trehalose/Sucrose/Cellobiose	262323.66	1492C-15F-1
77.40	1492	Succinate/Methylmalonate	31259687.71	1492C-17F-2
77.40	1492	Taurine	16147.01	1492C-17F-2
77.40	1492	Pyroglutamic acid	103583999.45	1492C-17F-2
77.40	1492	Leucine/Isoleucine	4766070.33	1492C-17F-2
77.40	1492	Salicylate	48484886.58	1492C-17F-2
77.40	1492	Allantoin	78159669.57	1492C-17F-2
77.40	1492	Phenylalanine	1965172.08	1492C-17F-2
77.40	1492	Tyrosine	1977411.27	1492C-17F-2
77.40	1492	Cystine	1717082.89	1492C-17F-2
77.40	1492	Uridine	81556.10	1492C-17F-2
77.40	1492	Inosine	13086.99	1492C-17F-2
77.40	1492	Glycinamide ribotide (GAR)	923305136.06	1492C-17F-2
77.40	1492	Sedoheptulose 1/7-phosphate	2401224.34	1492C-17F-2
77.40	1492	CMP	11029145.02	1492C-17F-2
77.40	1492	UMP	60891.75	1492C-17F-2
77.40	1492	Trehalose/Sucrose/Cellobiose	1557360.20	1492C-17F-2
1.35	1492	Succinate/Methylmalonate	19756315.76	1492C-1H-1
1.35	1492	Taurine	0.00	1492C-1H-1
1.35	1492	Pyroglutamic acid	19291033.13	1492C-1H-1
1.35	1492	Leucine/Isoleucine	1433120.34	1492C-1H-1
1.35	1492	Salicylate	10994808.34	1492C-1H-1
1.35	1492	Allantoin	47045864.75	1492C-1H-1
1.35	1492	Phenylalanine	916606.94	1492C-1H-1
1.35	1492	Tyrosine	592981.49	1492C-1H-1
1.35	1492	Cystine	1616033.74	1492C-1H-1
1.35	1492	Uridine	12129.78	1492C-1H-1
1.35	1492	Inosine	13883.11	1492C-1H-1
1.35	1492	Glycinamide ribotide (GAR)	626361697.33	1492C-1H-1
1.35	1492	Sedoheptulose 1/7-phosphate	2650313.56	1492C-1H-1
1.35	1492	CMP	4781299.01	1492C-1H-1
1.35	1492	UMP	23849.63	1492C-1H-1
1.35	1492	Trehalose/Sucrose/Cellobiose	146758.72	1492C-1H-1
4.33	1492	Succinate/Methylmalonate	211119015.52	1492C-1H-3
4.33	1492	Taurine	3564901.93	1492C-1H-3
4.33	1492	Pyroglutamic acid	57997777.96	1492C-1H-3
4.33	1492	Leucine/Isoleucine	19500482.32	1492C-1H-3
4.33	1492	Salicylate	13229458.72	1492C-1H-3
4.33	1492	Allantoin	66060166.97	1492C-1H-3
4.33	1492	Phenylalanine	7001090.38	1492C-1H-3
4.33	1492	Tyrosine	5641405.21	1492C-1H-3
4.33	1492	Cystine	2037753.32	1492C-1H-3
4.33	1492	Uridine	7830531.87	1492C-1H-3
4.33	1492	Inosine	13147115.67	1492C-1H-3
4.33	1492	Glycinamide ribotide (GAR)	711602253.24	1492C-1H-3
4.33	1492	Sedoheptulose 1/7-phosphate	5237458.41	1492C-1H-3
4.33	1492	CMP	4875378.86	1492C-1H-3
4.33	1492	UMP	61390697.52	1492C-1H-3
4.33	1492	Trehalose/Sucrose/Cellobiose	3770351.69	1492C-1H-3
81.06	1492	Succinate/Methylmalonate	17191140.32	1492C-20F-1
81.06	1492	Taurine	31860.91	1492C-20F-1
81.06	1492	Pyroglutamic acid	40502042.51	1492C-20F-1
81.06	1492	Leucine/Isoleucine	2609780.45	1492C-20F-1
81.06	1492	Salicylate	21138521.02	1492C-20F-1
81.06	1492	Allantoin	39032597.82	1492C-20F-1
81.06	1492	Phenylalanine	964452.15	1492C-20F-1
81.06	1492	Tyrosine	1203473.14	1492C-20F-1
81.06	1492	Cystine	748141.22	1492C-20F-1
81.06	1492	Uridine	56389.04	1492C-20F-1

Table S4-3 Continued.

Depth (mbsf)	Site	Metabolite	Value	IODPCall
81.06	1492	Inosine	14581.80	1492C-20F-1
81.06	1492	Glycinamide ribotide (GAR)	602898534.32	1492C-20F-1
81.06	1492	Sedoheptulose 1/7-phosphate	952025.73	1492C-20F-1
81.06	1492	CMP	13585747.95	1492C-20F-1
81.06	1492	UMP	51897.02	1492C-20F-1
81.06	1492	Trehalose/Sucrose/Cellobiose	876503.12	1492C-20F-1
90.60	1492	Succinate/Methylmalonate	29497778.05	1492C-22F-1
90.60	1492	Taurine	1908323.60	1492C-22F-1
90.60	1492	Pyroglutamic acid	45453725.01	1492C-22F-1
90.60	1492	Leucine/Isoleucine	26210376.37	1492C-22F-1
90.60	1492	Salicylate	26327124.73	1492C-22F-1
90.60	1492	Allantoin	48823732.11	1492C-22F-1
90.60	1492	Phenylalanine	2789073.58	1492C-22F-1
90.60	1492	Tyrosine	9648682.33	1492C-22F-1
90.60	1492	Cystine	709498.70	1492C-22F-1
90.60	1492	Uridine	1371035.84	1492C-22F-1
90.60	1492	Inosine	577919.06	1492C-22F-1
90.60	1492	Glycinamide ribotide (GAR)	779896821.95	1492C-22F-1
90.60	1492	Sedoheptulose 1/7-phosphate	605106.61	1492C-22F-1
90.60	1492	CMP	25776735.33	1492C-22F-1
90.60	1492	UMP	754035.80	1492C-22F-1
90.60	1492	Trehalose/Sucrose/Cellobiose	414738.69	1492C-22F-1
101.50	1492	Succinate/Methylmalonate	18172945.00	1492C-24F-2
101.50	1492	Taurine	1599.92	1492C-24F-2
101.50	1492	Pyroglutamic acid	22200968.66	1492C-24F-2
101.50	1492	Leucine/Isoleucine	1676439.06	1492C-24F-2
101.50	1492	Salicylate	29078825.66	1492C-24F-2
101.50	1492	Allantoin	43320809.97	1492C-24F-2
101.50	1492	Phenylalanine	841077.80	1492C-24F-2
101.50	1492	Tyrosine	856366.10	1492C-24F-2
101.50	1492	Cystine	960904.43	1492C-24F-2
101.50	1492	Uridine	12154.87	1492C-24F-2
101.50	1492	Inosine	10572.09	1492C-24F-2
101.50	1492	Glycinamide ribotide (GAR)	639601122.63	1492C-24F-2
101.50	1492	Sedoheptulose 1/7-phosphate	730031.84	1492C-24F-2
101.50	1492	CMP	9807557.43	1492C-24F-2
101.50	1492	UMP	51007.71	1492C-24F-2
101.50	1492	Trehalose/Sucrose/Cellobiose	362634.90	1492C-24F-2
8.32	1492	Succinate/Methylmalonate	21891528.91	1492C-3F-1
8.32	1492	Taurine	1702.57	1492C-3F-1
8.32	1492	Pyroglutamic acid	18798486.11	1492C-3F-1
8.32	1492	Leucine/Isoleucine	1647669.40	1492C-3F-1
8.32	1492	Salicylate	10989517.04	1492C-3F-1
8.32	1492	Allantoin	61261351.93	1492C-3F-1
8.32	1492	Phenylalanine	1024455.04	1492C-3F-1
8.32	1492	Tyrosine	762222.70	1492C-3F-1
8.32	1492	Cystine	1352265.12	1492C-3F-1
8.32	1492	Uridine	35065.79	1492C-3F-1
8.32	1492	Inosine	21767.66	1492C-3F-1
8.32	1492	Glycinamide ribotide (GAR)	618848582.48	1492C-3F-1
8.32	1492	Sedoheptulose 1/7-phosphate	1513202.91	1492C-3F-1
8.32	1492	CMP	7070389.70	1492C-3F-1
8.32	1492	UMP	462438.53	1492C-3F-1
8.32	1492	Trehalose/Sucrose/Cellobiose	376937.51	1492C-3F-1
11.68	1492	Succinate/Methylmalonate	28540904.52	1492C-4F-2
11.68	1492	Taurine	7711.01	1492C-4F-2
11.68	1492	Pyroglutamic acid	57904675.82	1492C-4F-2
11.68	1492	Leucine/Isoleucine	3926433.91	1492C-4F-2
11.68	1492	Salicylate	27806390.37	1492C-4F-2
11.68	1492	Allantoin	55904428.88	1492C-4F-2
11.68	1492	Phenylalanine	1698850.67	1492C-4F-2

Table S4-3 Continued.

Depth (mbsf)	Site	Metabolite	Value	IODPCall
11.68	1492	Tyrosine	1953827.70	1492C-4F-2
11.68	1492	Cystine	1404118.94	1492C-4F-2
11.68	1492	Uridine	41850.63	1492C-4F-2
11.68	1492	Inosine	20612.03	1492C-4F-2
11.68	1492	Glycinamide ribotide (GAR)	807360512.97	1492C-4F-2
11.68	1492	Sedoheptulose 1/7-phosphate	1311351.33	1492C-4F-2
11.68	1492	CMP	13559539.72	1492C-4F-2
11.68	1492	UMP	68857.18	1492C-4F-2
11.68	1492	Trehalose/Sucrose/Cellobiose	1058857.69	1492C-4F-2
17.05	1492	Succinate/Methylmalonate	26308345.75	1492C-5F-2
17.05	1492	Taurine	4536.35	1492C-5F-2
17.05	1492	Pyroglutamic acid	43755795.24	1492C-5F-2
17.05	1492	Leucine/Isoleucine	2932637.30	1492C-5F-2
17.05	1492	Salicylate	26948605.93	1492C-5F-2
17.05	1492	Allantoin	54154883.58	1492C-5F-2
17.05	1492	Phenylalanine	1220292.38	1492C-5F-2
17.05	1492	Tyrosine	1689214.21	1492C-5F-2
17.05	1492	Cystine	835998.93	1492C-5F-2
17.05	1492	Uridine	54444.94	1492C-5F-2
17.05	1492	Inosine	20373.34	1492C-5F-2
17.05	1492	Glycinamide ribotide (GAR)	735930322.92	1492C-5F-2
17.05	1492	Sedoheptulose 1/7-phosphate	604004.35	1492C-5F-2
17.05	1492	CMP	14863311.10	1492C-5F-2
17.05	1492	UMP	52328.30	1492C-5F-2
17.05	1492	Trehalose/Sucrose/Cellobiose	705865.81	1492C-5F-2
20.58	1492	Succinate/Methylmalonate	57424738.81	1492C-6F-2
20.58	1492	Taurine	59442953.38	1492C-6F-2
20.58	1492	Pyroglutamic acid	63687023.99	1492C-6F-2
20.58	1492	Leucine/Isoleucine	65639395.54	1492C-6F-2
20.58	1492	Salicylate	70890024.67	1492C-6F-2
20.58	1492	Allantoin	75818354.30	1492C-6F-2
20.58	1492	Phenylalanine	77901544.63	1492C-6F-2
20.58	1492	Tyrosine	86356243.29	1492C-6F-2
20.58	1492	Cystine	96946215.00	1492C-6F-2
20.58	1492	Uridine	110682564.57	1492C-6F-2
20.58	1492	Inosine	129127406.92	1492C-6F-2
20.58	1492	Glycinamide ribotide (GAR)	154950598.21	1492C-6F-2
20.58	1492	Sedoheptulose 1/7-phosphate	3648951.04	1492C-6F-2
20.58	1492	CMP	4604789.02	1492C-6F-2
20.58	1492	UMP	257628.16	1492C-6F-2
20.58	1492	Trehalose/Sucrose/Cellobiose	446758.36	1492C-6F-2
31.05	1492	Succinate/Methylmalonate	24449611.42	1492C-8F-2
31.05	1492	Taurine	5856.81	1492C-8F-2
31.05	1492	Pyroglutamic acid	39089067.13	1492C-8F-2
31.05	1492	Leucine/Isoleucine	2140670.04	1492C-8F-2
31.05	1492	Salicylate	14438332.73	1492C-8F-2
31.05	1492	Allantoin	54864173.81	1492C-8F-2
31.05	1492	Phenylalanine	1540522.13	1492C-8F-2
31.05	1492	Tyrosine	1149176.58	1492C-8F-2
31.05	1492	Cystine	785696.35	1492C-8F-2
31.05	1492	Uridine	34349.76	1492C-8F-2
31.05	1492	Inosine	23402.19	1492C-8F-2
31.05	1492	Glycinamide ribotide (GAR)	751894993.61	1492C-8F-2
31.05	1492	Sedoheptulose 1/7-phosphate	825198.72	1492C-8F-2
31.05	1492	CMP	18237351.01	1492C-8F-2
31.05	1492	UMP	74650.63	1492C-8F-2
31.05	1492	Trehalose/Sucrose/Cellobiose	397210.02	1492C-8F-2
11.66	1493	Succinate/Methylmalonate	136965026.02	1493B-3F-1
11.66	1493	Leucine/Isoleucine	6633216.98	1493B-3F-1
11.66	1493	Allantoin	29071063.25	1493B-3F-1
11.66	1493	sn-Glycerol 3-phosphate	47687408.32	1493B-3F-1

Table S4-3 Continued.

Depth (mbsf)	Site	Metabolite	Value	IODPCall
11.66	1493	2-Isopropylmalate	152882974.56	1493B-3F-1
11.66	1493	Tyrosine	4875266.00	1493B-3F-1
11.66	1493	N-Acetylglutamate	9705137.01	1493B-3F-1
11.66	1493	Cystine	36615393.61	1493B-3F-1
11.66	1493	Uridine	1641724.35	1493B-3F-1
11.66	1493	Inosine	3875859.12	1493B-3F-1
11.66	1493	Glycinamide ribotide (GAR)	732907124.65	1493B-3F-1
11.66	1493	CMP	200336.23	1493B-3F-1
11.66	1493	UMP	24169785.60	1493B-3F-1
11.66	1493	Trehalose/Sucrose/Cellobiose	2363344.70	1493B-3F-1
11.66	1493	AMP/dGMP	50707707.07	1493B-3F-1
11.66	1493	dCDP	10808012.60	1493B-3F-1
11.66	1493	Glutathione disulfide	7741327.31	1493B-3F-1
13.98	1493	Succinate/Methylmalonate	37146699.44	1493B-3F-4
13.98	1493	Leucine/Isoleucine	3073736.76	1493B-3F-4
13.98	1493	Allantoin	29952666.21	1493B-3F-4
13.98	1493	sn-Glycerol 3-phosphate	3899353.00	1493B-3F-4
13.98	1493	2-Isopropylmalate	68278863.70	1493B-3F-4
13.98	1493	Tyrosine	2497534.75	1493B-3F-4
13.98	1493	N-Acetylglutamate	4135744.06	1493B-3F-4
13.98	1493	Cystine	21552615.00	1493B-3F-4
13.98	1493	Uridine	84498.23	1493B-3F-4
13.98	1493	Inosine	46246.42	1493B-3F-4
13.98	1493	Glycinamide ribotide (GAR)	683037867.20	1493B-3F-4
13.98	1493	CMP	2962911.70	1493B-3F-4
13.98	1493	UMP	2976289.73	1493B-3F-4
13.98	1493	Trehalose/Sucrose/Cellobiose	341158.16	1493B-3F-4
13.98	1493	AMP/dGMP	4318983.84	1493B-3F-4
13.98	1493	dCDP	1958309.49	1493B-3F-4
13.98	1493	Glutathione disulfide	1689846.08	1493B-3F-4
22.30	1493	Succinate/Methylmalonate	21924951.59	1493B-5F-2
22.30	1493	Leucine/Isoleucine	764475.81	1493B-5F-2
22.30	1493	Allantoin	43062596.97	1493B-5F-2
22.30	1493	sn-Glycerol 3-phosphate	1845863.74	1493B-5F-2
22.30	1493	2-Isopropylmalate	26435532.05	1493B-5F-2
22.30	1493	Tyrosine	990908.60	1493B-5F-2
22.30	1493	N-Acetylglutamate	1366509.31	1493B-5F-2
22.30	1493	Cystine	13346124.92	1493B-5F-2
22.30	1493	Uridine	24232.01	1493B-5F-2
22.30	1493	Inosine	17211.60	1493B-5F-2
22.30	1493	Glycinamide ribotide (GAR)	741140430.34	1493B-5F-2
22.30	1493	CMP	5132139.78	1493B-5F-2
22.30	1493	UMP	22709.77	1493B-5F-2
22.30	1493	Trehalose/Sucrose/Cellobiose	261532.65	1493B-5F-2
22.30	1493	AMP/dGMP	64095.99	1493B-5F-2
22.30	1493	dCDP	0.00	1493B-5F-2
22.30	1493	Glutathione disulfide	4230.35	1493B-5F-2
26.11	1493	Succinate/Methylmalonate	25488815.40	1493B-6F-2
26.11	1493	Leucine/Isoleucine	946038.24	1493B-6F-2
26.11	1493	Allantoin	48180476.03	1493B-6F-2
26.11	1493	sn-Glycerol 3-phosphate	2036529.31	1493B-6F-2
26.11	1493	2-Isopropylmalate	22238993.42	1493B-6F-2
26.11	1493	Tyrosine	1008514.77	1493B-6F-2
26.11	1493	N-Acetylglutamate	1308591.42	1493B-6F-2
26.11	1493	Cystine	7466006.82	1493B-6F-2
26.11	1493	Uridine	26999.36	1493B-6F-2
26.11	1493	Inosine	32429.85	1493B-6F-2
26.11	1493	Glycinamide ribotide (GAR)	699512241.35	1493B-6F-2
26.11	1493	CMP	761998.68	1493B-6F-2
26.11	1493	UMP	33446.84	1493B-6F-2
26.11	1493	Trehalose/Sucrose/Cellobiose	1261988.86	1493B-6F-2

Table S4-3 Continued.

Depth (mbsf)	Site	Metabolite	Value	IODPCall
26.11	1493	AMP/dGMP	49093.66	1493B-6F-2
26.11	1493	dCDP	0.00	1493B-6F-2
26.11	1493	Glutathione disulfide	5340.16	1493B-6F-2
0.71	1494	Pyroglutamic acid	91695065.46	1494A-1F-1
0.71	1494	Allantoin	27141778.79	1494A-1F-1
0.71	1494	CMP	1288285.46	1494A-1F-1
0.71	1494	Succinate/Methylmalonate	43972364.89	1494A-1F-1
0.71	1494	Tyrosine	2205839.99	1494A-1F-1
0.71	1494	Inosine	241238.17	1494A-1F-1
2.76	1494	Pyroglutamic acid	69686033.97	1494A-1F-3
2.76	1494	Allantoin	53726276.13	1494A-1F-3
2.76	1494	CMP	5799318.82	1494A-1F-3
2.76	1494	Succinate/Methylmalonate	40279468.15	1494A-1F-3
2.76	1494	Tyrosine	1838484.50	1494A-1F-3
2.76	1494	Inosine	158539.10	1494A-1F-3
6.56	1494	Pyroglutamic acid	49370320.84	1494A-2F-2
6.56	1494	Leucine/Isoleucine	3338349.25	1494A-2F-2
6.56	1494	Allantoin	29815000.48	1494A-2F-2
6.56	1494	Glycinamide ribotide (GAR)	558526186.34	1494A-2F-2
6.56	1494	CMP	70207646.70	1494A-2F-2
6.56	1494	Trehalose/Sucrose/Cellobiose	270115.42	1494A-2F-2
6.56	1494	Succinate/Methylmalonate	34675967.19	1494A-2F-2
6.56	1494	Acetylphosphate	37625342.19	1494A-2F-2
6.56	1494	Tyrosine	1457057.04	1494A-2F-2
6.56	1494	Cystine	29439767.76	1494A-2F-2
6.56	1494	Inosine	27523.57	1494A-2F-2
6.56	1494	N-Acetylglucosamine 1/6-phosphate	734943.76	1494A-2F-2
11.83	1494	Pyroglutamic acid	30546355.29	1494A-3F-3
11.83	1494	Leucine/Isoleucine	2233011.65	1494A-3F-3
11.83	1494	Allantoin	53368492.27	1494A-3F-3
11.83	1494	Glycinamide ribotide (GAR)	484135159.05	1494A-3F-3
11.83	1494	CMP	7235206.37	1494A-3F-3
11.83	1494	Trehalose/Sucrose/Cellobiose	476975.86	1494A-3F-3
11.83	1494	Succinate/Methylmalonate	17522077.25	1494A-3F-3
11.83	1494	Acetylphosphate	23898491.76	1494A-3F-3
11.83	1494	Tyrosine	758390.88	1494A-3F-3
11.83	1494	Cystine	8683001.10	1494A-3F-3
11.83	1494	Inosine	9921.61	1494A-3F-3
11.83	1494	N-Acetylglucosamine 1/6-phosphate	589364.45	1494A-3F-3
24.51	1494	Pyroglutamic acid	28768716.66	1494A-6F-2
0.71	1494	Leucine/Isoleucine	4020543.72	1494A-6F-2
24.51	1494	Leucine/Isoleucine	1466971.12	1494A-6F-2
24.51	1494	Allantoin	59994526.89	1494A-6F-2
0.71	1494	Glycinamide ribotide (GAR)	740356431.08	1494A-6F-2
24.51	1494	Glycinamide ribotide (GAR)	321853744.49	1494A-6F-2
24.51	1494	CMP	25607731.22	1494A-6F-2
0.71	1494	Trehalose/Sucrose/Cellobiose	530459.84	1494A-6F-2
24.51	1494	Trehalose/Sucrose/Cellobiose	137018.54	1494A-6F-2
24.51	1494	Succinate/Methylmalonate	16841874.80	1494A-6F-2
0.71	1494	Acetylphosphate	35378431.94	1494A-6F-2
24.51	1494	Acetylphosphate	13029341.42	1494A-6F-2
24.51	1494	Tyrosine	547957.98	1494A-6F-2
0.71	1494	Cystine	41866720.25	1494A-6F-2
24.51	1494	Cystine	1842272.45	1494A-6F-2
24.51	1494	Inosine	159004.50	1494A-6F-2
0.71	1494	N-Acetylglucosamine 1/6-phosphate	1589865.75	1494A-6F-2
24.51	1494	N-Acetylglucosamine 1/6-phosphate	731593.05	1494A-6F-2
30.57	1494	Pyroglutamic acid	35920653.69	1494A-8F-4
2.76	1494	Leucine/Isoleucine	3886348.44	1494A-8F-4
30.57	1494	Leucine/Isoleucine	3383430.02	1494A-8F-4
30.57	1494	Allantoin	36089261.50	1494A-8F-4

Table S4-3 Continued.

Depth (mbsf)	Site	Metabolite	Value	IODPCall
2.76	1494	Glycinamide ribotide (GAR)	###########	1494A-8F-4
30.57	1494	Glycinamide ribotide (GAR)	500108471.28	1494A-8F-4
30.57	1494	CMP	8747788.60	1494A-8F-4
2.76	1494	Trehalose/Sucrose/Cellobiose	1292919.27	1494A-8F-4
30.57	1494	Trehalose/Sucrose/Cellobiose	356136.41	1494A-8F-4
30.57	1494	Succinate/Methylmalonate	37276084.99	1494A-8F-4
2.76	1494	Acetylphosphate	24663571.30	1494A-8F-4
30.57	1494	Acetylphosphate	18689935.16	1494A-8F-4
30.57	1494	Tyrosine	1372230.97	1494A-8F-4
2.76	1494	Cystine	16979083.58	1494A-8F-4
30.57	1494	Cystine	11585839.00	1494A-8F-4
30.57	1494	Inosine	392869.73	1494A-8F-4
2.76	1494	N-Acetylglucosamine 1/6-phosphate	906034.65	1494A-8F-4
30.57	1494	N-Acetylglucosamine 1/6-phosphate	545666.19	1494A-8F-4
7.83	1495	Homocysteine	0.00	1495A-4F-2
7.83	1495	Allantoin	32544752.98	1495A-4F-2
7.83	1495	Cystine	6319406.52	1495A-4F-2
7.83	1495	Glycinamide ribotide (GAR)	378202967.29	1495A-4F-2
7.83	1495	CMP	1562239.54	1495A-4F-2
7.83	1495	Trehalose/Sucrose/Cellobiose	463285.84	1495A-4F-2
7.83	1495	Phenylpropiolic acid	15779859.23	1495A-4F-2
7.83	1495	Sedoheptulose 1/7-phosphate	839543.17	1495A-4F-2
7.83	1495	N-Acetylglucosamine 1/6-phosphate	365741.41	1495A-4F-2
3.00	1495	Homocysteine	543401.28	1495B-2F-2
3.00	1495	Allantoin	35606179.50	1495B-2F-2
3.00	1495	Cystine	3695521.83	1495B-2F-2
3.00	1495	Glycinamide ribotide (GAR)	367624075.96	1495B-2F-2
3.00	1495	CMP	4734879.56	1495B-2F-2
3.00	1495	Trehalose/Sucrose/Cellobiose	82241.72	1495B-2F-2
3.00	1495	Phenylpropiolic acid	17747459.07	1495B-2F-2
3.00	1495	Sedoheptulose 1/7-phosphate	551735.66	1495B-2F-2
3.00	1495	N-Acetylglucosamine 1/6-phosphate	448246.22	1495B-2F-2
7.70	1495	Homocysteine	761018.20	1495B-4F-2
7.70	1495	Allantoin	37095187.17	1495B-4F-2
7.70	1495	Cystine	6667729.43	1495B-4F-2
7.70	1495	Glycinamide ribotide (GAR)	434256993.64	1495B-4F-2
7.70	1495	CMP	383421.86	1495B-4F-2
7.70	1495	Trehalose/Sucrose/Cellobiose	421430.65	1495B-4F-2
7.70	1495	Phenylpropiolic acid	15796897.78	1495B-4F-2
7.70	1495	Sedoheptulose 1/7-phosphate	1011850.35	1495B-4F-2
7.70	1495	N-Acetylglucosamine 1/6-phosphate	425135.71	1495B-4F-2
0.90	1496	Tyrosine	523095.92	1496A-1F-1
0.90	1496	Succinate/Methylmalonate	13492576.51	1496A-1F-1
0.90	1496	Allantoin	20886142.63	1496A-1F-1
0.90	1496	Glycinamide ribotide (GAR)	410735095.56	1496A-1F-1
0.90	1496	Trehalose/Sucrose/Cellobiose	44006.85	1496A-1F-1
0.90	1496	N-Carbamoyl-L-aspartate	1583243.64	1496A-1F-1
0.90	1496	Pyroglutamic acid	19968057.03	1496A-1F-1
0.90	1496	2-hydroxyglutarate	862958.83	1496A-1F-1
0.90	1496	Leucine/Isoleucine	1693060.65	1496A-1F-1
0.90	1496	Homocysteine	1410.78	1496A-1F-1
0.90	1496	Cystine	18997547.54	1496A-1F-1
0.90	1496	CMP	547092.92	1496A-1F-1
0.90	1496	2-Hydroxy-2-methylsuccinate	900119.62	1496A-1F-1
0.90	1496	Uridine	12787.24	1496A-1F-1
0.90	1496	Inosine	12535.52	1496A-1F-1
0.90	1496	UMP	22535.88	1496A-1F-1
0.90	1496	dCDP	0.00	1496A-1F-1
0.90	1496	Guanine	389631.41	1496A-1F-1
2.30	1496	Tyrosine	687474.14	1496A-1F-2
2.30	1496	Succinate/Methylmalonate	8260232.10	1496A-1F-2

Table S4-3 Continued.

Depth (mbsf)	Site	Metabolite	Value	IODPCall
2.30	1496	Allantoin	13638203.05	1496A-1F-2
2.30	1496	Glycinamide ribotide (GAR)	271957496.36	1496A-1F-2
2.30	1496	Trehalose/Sucrose/Cellobiose	39577.15	1496A-1F-2
2.30	1496	N-Carbamoyl-L-aspartate	1081730.88	1496A-1F-2
2.30	1496	Pyroglutamic acid	23680253.24	1496A-1F-2
2.30	1496	2-hydroxyglutarate	855268.51	1496A-1F-2
2.30	1496	Leucine/Isoleucine	2416492.71	1496A-1F-2
2.30	1496	Homocysteine	144408.14	1496A-1F-2
2.30	1496	Cystine	13679697.51	1496A-1F-2
2.30	1496	CMP	4151812.61	1496A-1F-2
2.30	1496	2-Hydroxy-2-methylsuccinate	875945.93	1496A-1F-2
2.30	1496	Uridine	5702.79	1496A-1F-2
2.30	1496	Inosine	9887.03	1496A-1F-2
2.30	1496	UMP	24434.50	1496A-1F-2
2.30	1496	dCDP	1764.07	1496A-1F-2
2.30	1496	Guanine	3613719.31	1496A-1F-2
6.76	1496	Tyrosine	322173.05	1496A-2F-4
6.76	1496	Succinate/Methylmalonate	6188635.82	1496A-2F-4
6.76	1496	Allantoin	13411899.00	1496A-2F-4
6.76	1496	Glycinamide ribotide (GAR)	279715406.85	1496A-2F-4
6.76	1496	Trehalose/Sucrose/Cellobiose	46222.87	1496A-2F-4
6.76	1496	N-Carbamoyl-L-aspartate	1054455.91	1496A-2F-4
6.76	1496	Pyroglutamic acid	17701766.43	1496A-2F-4
6.76	1496	2-hydroxyglutarate	733537.08	1496A-2F-4
6.76	1496	Leucine/Isoleucine	990430.17	1496A-2F-4
6.76	1496	Homocysteine	460285.56	1496A-2F-4
6.76	1496	Cystine	13845868.83	1496A-2F-4
6.76	1496	CMP	3983027.60	1496A-2F-4
6.76	1496	2-Hydroxy-2-methylsuccinate	756550.68	1496A-2F-4
6.76	1496	Uridine	5894.58	1496A-2F-4
6.76	1496	Inosine	11016.97	1496A-2F-4
6.76	1496	UMP	17935.97	1496A-2F-4
6.76	1496	dCDP	0.00	1496A-2F-4
6.76	1496	Guanine	210011.12	1496A-2F-4
9.66	1496	Tyrosine	464188.43	1496A-3F-2
9.66	1496	Succinate/Methylmalonate	11471843.58	1496A-3F-2
9.66	1496	Allantoin	8355339.74	1496A-3F-2
9.66	1496	Glycinamide ribotide (GAR)	200449362.07	1496A-3F-2
9.66	1496	Trehalose/Sucrose/Cellobiose	17243.33	1496A-3F-2
9.66	1496	N-Carbamoyl-L-aspartate	4198918.82	1496A-3F-2
9.66	1496	Pyroglutamic acid	13318739.45	1496A-3F-2
9.66	1496	2-hydroxyglutarate	2816567.43	1496A-3F-2
9.66	1496	Leucine/Isoleucine	1437976.43	1496A-3F-2
9.66	1496	Homocysteine	444695.11	1496A-3F-2
9.66	1496	Cystine	11613128.27	1496A-3F-2
9.66	1496	CMP	3706195.16	1496A-3F-2
9.66	1496	2-Hydroxy-2-methylsuccinate	2840160.00	1496A-3F-2
9.66	1496	Uridine	168865.25	1496A-3F-2
9.66	1496	Inosine	318545.32	1496A-3F-2
9.66	1496	UMP	1168578.96	1496A-3F-2
9.66	1496	dCDP	1487046.12	1496A-3F-2
9.66	1496	Guanine	176977.66	1496A-3F-2
15.15	1496	Tyrosine	778294.74	1496A-4F-2
15.15	1496	Succinate/Methylmalonate	50714507.02	1496A-4F-2
15.15	1496	Allantoin	11745221.70	1496A-4F-2
15.15	1496	Glycinamide ribotide (GAR)	256253193.85	1496A-4F-2
15.15	1496	Trehalose/Sucrose/Cellobiose	233742.33	1496A-4F-2
15.15	1496	N-Carbamoyl-L-aspartate	11916101.73	1496A-4F-2
15.15	1496	Pyroglutamic acid	23597278.44	1496A-4F-2
15.15	1496	2-hydroxyglutarate	17630859.62	1496A-4F-2
15.15	1496	Leucine/Isoleucine	2127074.90	1496A-4F-2

Table S4-3 Continued.

Depth (mbsf)	Site	Metabolite	Value	IODPCall
15.15	1496	Homocysteine	287228.96	1496A-4F-2
15.15	1496	Cystine	12968183.76	1496A-4F-2
15.15	1496	CMP	4446849.72	1496A-4F-2
15.15	1496	2-Hydroxy-2-methylsuccinate	17692024.28	1496A-4F-2
15.15	1496	Uridine	276127.45	1496A-4F-2
15.15	1496	Inosine	989365.95	1496A-4F-2
15.15	1496	UMP	19368137.89	1496A-4F-2
15.15	1496	dCDP	4814396.65	1496A-4F-2
15.15	1496	Guanine	754232.41	1496A-4F-2
19.81	1496	Tyrosine	746603.90	1496A-5F-2
19.81	1496	Succinate/Methylmalonate	9914973.87	1496A-5F-2
19.81	1496	Allantoin	8753568.04	1496A-5F-2
19.81	1496	Glycinamide ribotide (GAR)	201455578.55	1496A-5F-2
19.81	1496	Trehalose/Sucrose/Cellobiose	32650.14	1496A-5F-2
19.81	1496	N-Carbamoyl-L-aspartate	2623440.16	1496A-5F-2
19.81	1496	Pyroglutamic acid	18419848.17	1496A-5F-2
19.81	1496	2-hydroxyglutarate	1409789.48	1496A-5F-2
19.81	1496	Leucine/Isoleucine	2348963.01	1496A-5F-2
19.81	1496	Homocysteine	245465.31	1496A-5F-2
19.81	1496	Cystine	9202490.98	1496A-5F-2
19.81	1496	CMP	4031691.90	1496A-5F-2
19.81	1496	2-Hydroxy-2-methylsuccinate	1435669.08	1496A-5F-2
19.81	1496	Uridine	85943.46	1496A-5F-2
19.81	1496	Inosine	118524.72	1496A-5F-2
19.81	1496	UMP	978865.13	1496A-5F-2
19.81	1496	dCDP	444409.75	1496A-5F-2
19.81	1496	Guanine	116644.99	1496A-5F-2
24.57	1496	Tyrosine	40485.01	1496A-6F-3
24.57	1496	Succinate/Methylmalonate	9931294.16	1496A-6F-3
24.57	1496	Allantoin	11501899.09	1496A-6F-3
24.57	1496	Glycinamide ribotide (GAR)	12271365.87	1496A-6F-3
24.57	1496	Trehalose/Sucrose/Cellobiose	22917.47	1496A-6F-3
24.57	1496	N-Carbamoyl-L-aspartate	215098.28	1496A-6F-3
24.57	1496	Pyroglutamic acid	10209452.84	1496A-6F-3
24.57	1496	2-hydroxyglutarate	268074.77	1496A-6F-3
24.57	1496	Leucine/Isoleucine	10120297.95	1496A-6F-3
24.57	1496	Homocysteine	10759581.39	1496A-6F-3
24.57	1496	Cystine	11929711.80	1496A-6F-3
24.57	1496	CMP	492776.70	1496A-6F-3
24.57	1496	2-Hydroxy-2-methylsuccinate	236868.51	1496A-6F-3
24.57	1496	Uridine	12865.31	1496A-6F-3
24.57	1496	Inosine	15723.52	1496A-6F-3
24.57	1496	UMP	19429.37	1496A-6F-3
24.57	1496	dCDP	0.00	1496A-6F-3
24.57	1496	Guanine	195868.26	1496A-6F-3
29.58	1496	Tyrosine	176037.27	1496A-7F-3
29.58	1496	Succinate/Methylmalonate	7412195.40	1496A-7F-3
29.58	1496	Allantoin	8574734.18	1496A-7F-3
29.58	1496	Glycinamide ribotide (GAR)	192941728.12	1496A-7F-3
29.58	1496	Trehalose/Sucrose/Cellobiose	44608.50	1496A-7F-3
29.58	1496	N-Carbamoyl-L-aspartate	418010.39	1496A-7F-3
29.58	1496	Pyroglutamic acid	10884463.69	1496A-7F-3
29.58	1496	2-hydroxyglutarate	279463.06	1496A-7F-3
29.58	1496	Leucine/Isoleucine	539175.86	1496A-7F-3
29.58	1496	Homocysteine	109300.70	1496A-7F-3
29.58	1496	Cystine	7380157.48	1496A-7F-3
29.58	1496	CMP	1382318.37	1496A-7F-3
29.58	1496	2-Hydroxy-2-methylsuccinate	285565.62	1496A-7F-3
29.58	1496	Uridine	5064.25	1496A-7F-3
29.58	1496	Inosine	2202.94	1496A-7F-3
29.58	1496	UMP	19953.91	1496A-7F-3

Table S4-3 Continued.

Depth (mbsf)	Site	Metabolite	Value	IODPCall
29.58	1496	dCDP	0.00	1496A-7F-3
29.58	1496	Guanine	85246.24	1496A-7F-3
34.67	1496	Tyrosine	259176.44	1496A-8F-3
34.67	1496	Succinate/Methylmalonate	10409142.24	1496A-8F-3
34.67	1496	Allantoin	9625397.93	1496A-8F-3
34.67	1496	Glycinamide ribotide (GAR)	235661171.33	1496A-8F-3
34.67	1496	Trehalose/Sucrose/Cellobiose	0.00	1496A-8F-3
34.67	1496	N-Carbamoyl-L-aspartate	2054634.18	1496A-8F-3
34.67	1496	Pyroglutamic acid	11486698.36	1496A-8F-3
34.67	1496	2-hydroxyglutarate	2174106.09	1496A-8F-3
34.67	1496	Leucine/Isoleucine	831184.13	1496A-8F-3
34.67	1496	Homocysteine	157493.10	1496A-8F-3
34.67	1496	Cystine	11957486.17	1496A-8F-3
34.67	1496	CMP	4077705.36	1496A-8F-3
34.67	1496	2-Hydroxy-2-methylsuccinate	2212545.13	1496A-8F-3
34.67	1496	Uridine	0.00	1496A-8F-3
34.67	1496	Inosine	1334.12	1496A-8F-3
34.67	1496	UMP	19926.25	1496A-8F-3
34.67	1496	dCDP	0.00	1496A-8F-3
34.67	1496	Guanine	69383.23	1496A-8F-3
37.20	1496	Tyrosine	134834.94	1496A-9F-1
37.20	1496	Succinate/Methylmalonate	8002662.61	1496A-9F-1
37.20	1496	Allantoin	115748.52	1496A-9F-1
37.20	1496	Glycinamide ribotide (GAR)	8253757.73	1496A-9F-1
37.20	1496	Trehalose/Sucrose/Cellobiose	161258.68	1496A-9F-1
37.20	1496	N-Carbamoyl-L-aspartate	156433.46	1496A-9F-1
37.20	1496	Pyroglutamic acid	7643583.63	1496A-9F-1
37.20	1496	2-hydroxyglutarate	231391.63	1496A-9F-1
37.20	1496	Leucine/Isoleucine	346529.99	1496A-9F-1
37.20	1496	Homocysteine	101242.79	1496A-9F-1
37.20	1496	Cystine	6659370.97	1496A-9F-1
37.20	1496	CMP	3525.81	1496A-9F-1
37.20	1496	2-Hydroxy-2-methylsuccinate	235001.88	1496A-9F-1
37.20	1496	Uridine	1010.24	1496A-9F-1
37.20	1496	Inosine	5332.47	1496A-9F-1
37.20	1496	UMP	14520.40	1496A-9F-1
37.20	1496	dCDP	2859.64	1496A-9F-1
37.20	1496	Guanine	37646.00	1496A-9F-1
0.61	1496	Allantoin	5787695.10	1496B-1F-1
0.61	1496	Cystine	10083455.97	1496B-1F-1
0.61	1496	Glycinamide ribotide (GAR)	165516267.16	1496B-1F-1
0.61	1496	CMP	651098.09	1496B-1F-1
0.61	1496	Trehalose/Sucrose/Cellobiose	34817.65	1496B-1F-1
2.42	1496	Allantoin	9848036.50	1496B-2F-1
2.42	1496	Cystine	6350026.15	1496B-2F-1
2.42	1496	Glycinamide ribotide (GAR)	218596208.49	1496B-2F-1
2.42	1496	CMP	4012312.54	1496B-2F-1
2.42	1496	Trehalose/Sucrose/Cellobiose	23168.80	1496B-2F-1
8.03	1496	Allantoin	3907466.32	1496B-3F-2
8.03	1496	Cystine	7288999.34	1496B-3F-2
8.03	1496	Glycinamide ribotide (GAR)	108121870.13	1496B-3F-2
8.03	1496	CMP	2778394.44	1496B-3F-2
8.03	1496	Trehalose/Sucrose/Cellobiose	47989.73	1496B-3F-2
10.06	1496	Allantoin	5746651.61	1496B-3F-4
10.06	1496	Cystine	8370434.76	1496B-3F-4
10.06	1496	Glycinamide ribotide (GAR)	158613899.29	1496B-3F-4
10.06	1496	CMP	3644920.43	1496B-3F-4
10.06	1496	Trehalose/Sucrose/Cellobiose	3470.44	1496B-3F-4
12.67	1496	Allantoin	4000332.39	1496B-4F-2
12.67	1496	Cystine	7534757.08	1496B-4F-2
12.67	1496	Glycinamide ribotide (GAR)	117736311.26	1496B-4F-2

Table S4-3 Continued.

Depth (mbsf)	Site	Metabolite	Value	IODPCall
12.67	1496	CMP	3772421.13	1496B-4F-2
12.67	1496	Trehalose/Sucrose/Cellobiose	11932.73	1496B-4F-2
18.07	1496	Allantoin	6750784.68	1496B-5F-2
18.07	1496	Cystine	7419268.97	1496B-5F-2
18.07	1496	Glycinamide ribotide (GAR)	176870900.87	1496B-5F-2
18.07	1496	CMP	2825547.79	1496B-5F-2
18.07	1496	Trehalose/Sucrose/Cellobiose	163251.97	1496B-5F-2
21.87	1496	Allantoin	32086746.97	1496B-6F-1
21.87	1496	Cystine	38812864.43	1496B-6F-1
21.87	1496	Glycinamide ribotide (GAR)	49157868.19	1496B-6F-1
21.87	1496	CMP	1528960.29	1496B-6F-1
21.87	1496	Trehalose/Sucrose/Cellobiose	18719.74	1496B-6F-1
26.32	1496	Allantoin	8850864.00	1496B-7F-1
26.32	1496	Cystine	9744652.55	1496B-7F-1
26.32	1496	Glycinamide ribotide (GAR)	236045195.23	1496B-7F-1
26.32	1496	CMP	2895654.88	1496B-7F-1
26.32	1496	Trehalose/Sucrose/Cellobiose	78516.22	1496B-7F-1
2.06	1497	Allantoin	8808016.04	1497A-2F-1
2.06	1497	Glycinamide ribotide (GAR)	119179657.59	1497A-2F-1
2.06	1497	Sedoheptulose 1/7-phosphate	254767.85	1497A-2F-1
2.06	1497	N-Acetylglucosamine 1/6-phosphate	302863.63	1497A-2F-1
2.06	1497	CMP	539656.02	1497A-2F-1
2.06	1497	Trehalose/Sucrose/Cellobiose	77169.87	1497A-2F-1
4.56	1497	Allantoin	10185953.10	1497A-2F-3
4.56	1497	Glycinamide ribotide (GAR)	107602606.33	1497A-2F-3
4.56	1497	Sedoheptulose 1/7-phosphate	279236.03	1497A-2F-3
4.56	1497	N-Acetylglucosamine 1/6-phosphate	376296.39	1497A-2F-3
4.56	1497	CMP	2076702.27	1497A-2F-3
4.56	1497	Trehalose/Sucrose/Cellobiose	57087.06	1497A-2F-3
5.40	1497	Allantoin	10621877.61	1497A-4F-2
5.40	1497	Glycinamide ribotide (GAR)	143704959.26	1497A-4F-2
5.40	1497	Sedoheptulose 1/7-phosphate	164294.01	1497A-4F-2
5.40	1497	N-Acetylglucosamine 1/6-phosphate	585718.45	1497A-4F-2
5.40	1497	CMP	5375737.86	1497A-4F-2
5.40	1497	Trehalose/Sucrose/Cellobiose	49681.77	1497A-4F-2
14.65	1497	Allantoin	5960654.41	1497A-5F-2
14.65	1497	Glycinamide ribotide (GAR)	75652102.03	1497A-5F-2
14.65	1497	Sedoheptulose 1/7-phosphate	318842.08	1497A-5F-2
14.65	1497	N-Acetylglucosamine 1/6-phosphate	297482.81	1497A-5F-2
14.65	1497	CMP	355994.38	1497A-5F-2
14.65	1497	Trehalose/Sucrose/Cellobiose	71078.57	1497A-5F-2
19.50	1497	Allantoin	94782.45	1497A-6F-2
19.50	1497	Glycinamide ribotide (GAR)	7988057.00	1497A-6F-2
19.50	1497	Sedoheptulose 1/7-phosphate	659651.45	1497A-6F-2
19.50	1497	N-Acetylglucosamine 1/6-phosphate	141721.15	1497A-6F-2
19.50	1497	CMP	138253.24	1497A-6F-2
19.50	1497	Trehalose/Sucrose/Cellobiose	207456.11	1497A-6F-2
1.15	1497	Allantoin	9304529.41	1497B-1F-1
1.15	1497	Cystine	2550254.84	1497B-1F-1
1.15	1497	Glycinamide ribotide (GAR)	162106660.39	1497B-1F-1
1.15	1497	CMP	11841813.59	1497B-1F-1
1.15	1497	Trehalose/Sucrose/Cellobiose	20644.16	1497B-1F-1
3.10	1497	Allantoin	5618384.95	1497B-1F-3
3.10	1497	Cystine	1703060.98	1497B-1F-3
3.10	1497	Glycinamide ribotide (GAR)	98354631.09	1497B-1F-3
3.10	1497	CMP	2603042.72	1497B-1F-3
3.10	1497	Trehalose/Sucrose/Cellobiose	25352.97	1497B-1F-3
11.05	1497	Allantoin	10866314.84	1497B-3F-2
11.05	1497	Cystine	1283995.52	1497B-3F-2
11.05	1497	Glycinamide ribotide (GAR)	129460565.06	1497B-3F-2
11.05	1497	CMP	1233528.52	1497B-3F-2

Table S4-3 Continued.

Depth (mbsf)	Site	Metabolite	Value	IODPCall
11.05	1497	Trehalose/Sucrose/Cellobiose	27210.68	1497B-3F-2
15.65	1497	Allantoin	286251.80	1497B-5F-2
15.65	1497	Cystine	3023321.52	1497B-5F-2
15.65	1497	Glycinamide ribotide (GAR)	20754740.79	1497B-5F-2
15.65	1497	CMP	150528.02	1497B-5F-2
15.65	1497	Trehalose/Sucrose/Cellobiose	37162.15	1497B-5F-2
20.41	1497	Allantoin	2236887.72	1497B-6F-2
20.41	1497	Cystine	1441134.78	1497B-6F-2
20.41	1497	Glycinamide ribotide (GAR)	57546153.26	1497B-6F-2
20.41	1497	CMP	1133475.55	1497B-6F-2
20.41	1497	Trehalose/Sucrose/Cellobiose	184371.63	1497B-6F-2
0.00	na	Allantoin	795621.80	Drill Fluid 1
0.00	na	Cystine	1066062.53	Drill Fluid 1
0.00	na	Glucosamine phosphate	340625.39	Drill Fluid 1
0.00	na	Glycinamide ribotide (GAR)	28924363.33	Drill Fluid 1
0.00	na	Trehalose/Sucrose/Cellobiose	5680.07	Drill Fluid 1
0.00	na	Allantoin	786071.43	Drill Fluid 2
0.00	na	Cystine	1129053.83	Drill Fluid 2
0.00	na	Glucosamine phosphate	342518.53	Drill Fluid 2
0.00	na	Glycinamide ribotide (GAR)	29394503.33	Drill Fluid 2
0.00	na	Trehalose/Sucrose/Cellobiose	2916.21	Drill Fluid 2

CHAPTER 5

CONCLUSIONS, LIMITATIONS, AND FUTURE DIRECTIONS

Conclusions

In this dissertation, I explored the role of uncultivated microbes in marine sediments through a combination of next generation sequencing techniques and geochemical and small organic molecule analyses. Through this exploration, several key findings have emerged.

Key findings

1) Downcore analysis of marine sediments at the White Oak River estuary support that the ostensible obligate methanotroph ANME-1 archaea is potentially capable of both methane oxidation and methane production and also pointed to the sulfate reducer *Desulfatiglans* spp. as a likely syntroph of ANME-1 during methane oxidation.
2) Long-term incubations of White Oak River estuary sediments demonstrated that putative methanotroph ANME-3 only increased in abundance during the time that methane was produced and after sulfate was depleted, suggesting that it is capable of methane production. Moreover, it could not be primed to oxidize methane when added to sulfate reducing incubations.
3) Long-term incubations of White Oak River estuary sediments indicate that the majority of observed microbes, including clades of sulfate reducers, do not increase or decrease abruptly in response to the major redox shift from sulfate reduction to methanogenesis
4) We successfully isolated single cell genomes from mud volcanoes associated with the Mariana Forearc, these are the first genomes isolated from these sites as well as in a marine environment in excess of pH 12.
5) We successfully created downcore metabolite profiles of small organic metabolites from these mud volcanoes, which indicated that each site had a unique make up.

Despite evidence that the non-monophyletic group named ANME's were found in abundance in marine sediments considered to be methanogenic and contain the genes necessary for methane production, this group has been considered to only be methanotrophic (41, 44). We hypothesized that depending on the geochemical conditions it could be thermodynamically possible to switch the direction of the methane production pathway, which is strongly dependent on the concentration of molecular hydrogen controlled by their sulfate reducing bacterial partner (18). This was supported in Chapter 2, in which we provided evidence that ANME-1 increased in abundance in both the zone of methane oxidation and methane production in a downcore of White Oak River estuary sediments. Our conclusion is further supported by geochemical models

(16, 37), other ANME-1 enrichments (35, 101), the reversibility of the methanogenic biochemical pathway (176), and dominance of ANME-1 in common marine sediments in geographically widespread areas (44, 78, 176).

However, using sediments from the same source in long-term incubations in Chapter 3, ANME-1 was not found to be present, rather ANME-3 was dominant. ANME-3 could not be induced to increase in abundance during the period of sulfate reduction with added methane present. Instead, ANME-3 increased in abundance after sulfate was depleted and concurrent to methane production, indicating that it was responsible for the produced methane. Though our data suggests that some OTUs from ANME I and III are likely methanogens and several OTU's of ANME-1 are potentially capable of switching between the production and destruction of methane, the hypothesis of molecular hydrogen dictating the direction is not supported and the exact mechanism remains unknown.

In Chapter 4, we provided thirty partially complete single cell genomes from mud volcanoes associated with the Mariana Forearc. These add to a growing body of evidence attempting to characterize microbial communities at springs effected by serpentinization sourced fluids (131, 133, 135, 148, 149, 177). The evidence provided here supports the work of Suzuki et al, which focused on serpentinization sourced springs in California. This work showed distinct microbes at each spring. In contrast, the work presented here focused on serpentinization sourced mud volcanoes, which is driven by source depth of the fluid from the subducting slab. This trend in source depth was further supported by unique composition and abundance of small organic metabolites from each site. The theory that "Everything is everywhere, but the environment selects", put forth by Bass Becking in the 1930's, suggests that the extreme conditions such as alkalinity, elevated hydrogen, reduced chemicals, and limitations on bioavailable inorganic carbon have the potential to uncover novel survival mechanisms and unique microbial populations at the Mariana convergent margin; of which, the work contained in Chapter 4 only scratched the surface. Geological processes such as serpentinization are as old as the Earth and provide sources of energy and nutrients for microbes at the ocean floor that could have fueled life before the energy of the sun was harnessed through photosynthesis (53, 55, 68); therefore, much is to be gained from further examination of these sites.

Limitations

Despite evidence that OTUs from ANME 1 and 3 are potential methanogens, they have hitherto remained unculturable, possibly in part due to their slow rate of growth and need for a sulfate reducing partner. Without this isolation, ascertaining the true mechanism of growth will be difficult, as the genomic and transcriptomic data from mixed communities cannot provide the same level of certainty. The long durations required of the incubations described here, upwards of 900 days, also make replaceability difficult and impactable. The apparent heterogeneity of ANME populations in the sediments taken from the White Oak River estuary was unforeseen. After the domination of ANME-1 in Chapter II it was expected that they would also dominate the incubations in Chapter 3. This was not the case, and in fact, an entirely unrelated population of ANME-3 took its place.

Although microbes at other locations have adapted to alkaline pHs, the conditions seen in Chapter IV at the Mariana Forearc may be too extreme for all but the more moderate conditions near the seafloor itself to allow microbial life to persist (38, 58, 63). These conditions compounded with low biomass make nucleic acid extraction difficult; however, we are confident that with the right optimization and extraction techniques this can be mitigated (178, 179). Another possibility is that microbes found here are only transient members of the surrounding marine and pelagic sediment environment and have little influence on the surrounding geochemistry before being slowly selected against by elevated pH and porewater geochemistry. This possibility, though unfortunate, could lead to the conclusion that serpentinization sourced mud volcanoes are too hostile for life and therefore not a likely analog for an early Earth. Additionally, any microbes found here are likely novel since these seamounts have never been sampled in this way (58). Though taxonomic relatedness to microbes with known metabolisms gives an indication of a recovered cell's metabolic potential, to better determine the putative metabolisms possible and available to each cell and community as a whole, further genomic analysis is necessary (i.e., metagenomic or metatranscriptomic).

Due to the labile nature of metabolites, it is unlikely that we will get a large set of unaltered metabolites, as observed in pure cultures (180). Single cell sorting in marine sediments is difficult and the acquisition and subsequent sequencing expensive. SAGs typically yield far fewer assembled genomes than can be generated from shotgun metagenomic sequencing. This is made up for in the quality of a genome, which can be attributed to a single individual as opposed to an amalgam of many DNA fragments that bin together based on chosen criteria such as 97%

similarity. It is possible that there is no relationship between the metabolites and tested geochemistry. These are geologically active sites that are highly reducing, which could lead to many abiotic reactions that produce the small organic molecules measured. Hydrocarbons and amino acids have been shown to be produced abiotically under conditions similar to serpentinization (56). In addition, the cell lysis protocol used to obtain SAGs used an alkaline buffer; if cells are adapted to alkaline environments, this lysis could fail.

Future Directions

ANME's and methane cycling microbes as a whole are a small fraction of the microbial community in marine sediments but are ecologically important due to their role in the creation and ultimate destruction of a potent greenhouse gas, making them worthy of further study. The prevalence of metabolically reversible ANME-1 on Earth suggests that this level of extreme metabolic flexibility may be a general feature of organisms specialized to survive in ultra-low energy environments. This could be used as a guide in the search for habitable places on Earth and extraterrestrial environments. Furthermore, the role of the vast majority of microbial clades in marine sediments remain uncultured and likely will remain so, in part, due to their slow rate of growth. In previous work, we proposed a tool for estimating turnover using Fractional Read Abundance times Cells (FRAxC), which combines next generation sequencing of the 16S rRNA gene with total cell counts in a crude attempt to enumerate individuals in a microbial population over the course of a sampling regime. Using this tool, it was possible to estimate turnover rates of an OTU or ASV in a heterogenous sample set of slow growing microbes. This is useful for marine sediments, as turnover time in an incubation of methanogens was estimated at between 7 and 12 days, which would render culturing problematic (18).

Several serpentinization sourced springs have been studied in the past few years, mostly terrestrial. However, the Mariana Forearc has a unique geological and chemical composition due to the high flow rate, fluid composition, association with a submarine seamount, and isolation from terrestrial inputs. These mud volcanoes may potentially serve as an analog for an early Earth, since the geological processes that provide reduced chemicals and nutrients to microbes in these marine sediments, as a stable feature associated with plate tectonics, are commonly separated from direct influences of photosynthetically-derived biomass [3, 9]. It is also theorized that the same serpentinization reactions occurring at this site could be occurring on Enceladus, a moon of Saturn, resulting in liquid water rich in molecular hydrogen, an important source of

energy for microbial life [10, 11]. Thus, by examining how microbes are adapted to this extreme environment on Earth, we will gain insights into exobiology and the origins of life on our own planet. Single cell genomics is a new and potentially revolutionary tool in microbiology and has never been applied to serpentinization sourced marine sediment. It is possible to assemble a pangenome of a microbial taxon from shotgun metagenomic amplification. These genomes, however, are an amalgam of all the DNA that bins using certain 97% similarity criteria and are often subject to chimeric sequences. Additionally, pathway reconstruction is unclear. By amplifying the genome of a single sorted microbial cell, the metabolic potential of that cell can be conclusively pinned to that cell and is not subject to the limitations of metagenomic techniques.

REFERENCES

1. Edwards KJ, Becker K, Colwell F. 2012. The Deep, Dark Energy Biosphere: Intraterrestrial Life on Earth. Annu Rev Earth Planet Sci 40:551–568.
2. Kallmeyer J, Pockalny R, Adhikari RR, Smith DC, D'Hondt S. 2012. Global distribution of microbial abundance and biomass in subseafloor sediment. Proc Natl Acad Sci 109:16213–16216.
3. Rappé MS, Giovannoni SJ. 2003. The uncultured microbial majority. Annu Rev Microbiol 57:369–94.
4. Edwards KJ, Becker K, Colwell F. 2012. The deep, dark energy biosphere: Intraterrestrial life on earth. Annu Rev Earth Planet Sci 40:551–568.
5. Offre P, Spang A, Schleper C. 2013. Archaea in biogeochemical cycles. Annu Rev Microbiol 67:437–57.
6. Orcutt BN, Sylvan JB, Knab NJ, Edwards KJ. 2011. Microbial ecology of the dark ocean above, at, and below the seafloor. Microbiol Mol Biol Rev 75:361–422.
7. Froelich PN, Klinkhammer GP, Bender ML, Luedtke NA, Heath GR, Cullen D, Dauphin P, Hammond D, Hartman B, Maynard V. 1979. Early oxidation of organic matter in pelagic sediments of the eastern equatorial Atlantic: suboxic diagenesis. Geochim Cosmochim Acta.
8. Schrenk MO, Brazelton WJ, Lang SQ. 2013. Serpentinization, Carbon, and Deep Life. Rev Mineral Geochemistry 75:575–606.
9. Lehmann J, Kleber M. 2015. The contentious nature of soil organic matter. Nature 528:60–68.
10. Reeburgh WS. 2007. Oceanic Methane Biogeochemistry. Chem Rev 486–513.
11. D'Hondt S, Jørgensen BB, Miller DJ, Batzke A, Blake R, Cragg BA, Cypionka H, Dickens GR, Ferdelman T, Hinrichs K-U, Holm NG, Mitterer R, Spivack A, Wang G, Bekins B, Engelen B, Ford K, Gettemy G, Rutherford SD, Sass H, Skilbeck CG, Aiello IW, Guèrin G, House CH, Inagaki F, Meister P, Naehr T, Niitsuma S, Parkes RJ, Schippers A, Smith DC, Teske A, Wiegel J, Padilla CN, Acosta JLS. 2004. Distributions of microbial activities in deep subseafloor sediments. Science 306:2216–2221.
12. Parkes RJ, Cragg B, Roussel E, Webster G, Weightman A, Sass H. 2014. A review of prokaryotic populations and processes in sub-seafloor sediments, including biosphere:geosphere interactions. Mar Geol 352:409–425.
13. Parkes RJ, Webster G, Cragg BA, Weightman AJ, Newberry CJ, Ferdelman TG, Kallmeyer J, Jørgensen BB, Aiello IW, Fry JC. 2005. Deep sub-seafloor prokaryotes stimulated at interfaces over geological time. Nature 436:390–394.
14. Martens C., Albert DB, Alperin MJ. 1998. Biogeochemical processes controlling methane in gassy coastal sediments—Part 1. A model coupling organic matter flux to gas production, oxidation and transport. Cont Shelf Res 18:1741–1770.
15. Jorgensen BB, Kasten S. 2006. Sulfar Cycling and Methane OxidationMarine Geochemistry. Springer, Berlin; Heidelberg.
16. Hoehler TM, Alperin MJ, Albert DB, Martens CS. 1998. Thermodynamic control on hydrogen concentrations in anoxic sediments. Geochim Cosmochim Acta 62:1745–1756.
17. Bethke CM, Ding D, Jin Q, Sanford RA. 2008. Origin of microbiological zoning in groundwater flows. Geology 36:739–742.
18. Kevorkian R, Bird JT, Shumaker A, Lloyd KG. 2018. Estimating population turnover rates by relative quantification methods reveals microbial dynamics in marine sediment. Appl Environ Microbiol 84:1–16.
19. Thauer RK, Kaster A-K, Seedorf H, Buckel W, Hedderich R. 2008. Methanogenic archaea: ecologically relevant differences in energy conservation. Nat Rev Microbiol

6:579–591.
20. Liu Y, Whitman WB. 2008. Metabolic, phylogenetic, and ecological diversity of the methanogenic archaea, p. 171–189. *In* Annals of the New York Academy of Sciences.
21. Egger M, Riedinger N, Mogollón JM, Jørgensen BB. 2018. Global diffusive fluxes of methane in marine sediments. Nat Geosci 11:421–425.
22. Muyzer G, Stams AJM. 2008. The ecology and biotechnology of sulphate-reducing bacteria. Nat Rev Microbiol 6:441–454.
23. Poulsen M, Schwab C, Jensen BB, Engberg RM, Spang A, Canibe N, Højberg O, Milinovich G, Fragner L, Schleper C, Weckwerth W, Lund P, Schramm A, Urich T. 2013. Methylotrophic methanogenic Thermoplasmata implicated in reduced methane emissions from bovine rumen. Nat Commun 4:1428.
24. Narihiro T, Sekiguchi Y. 2011. Oligonucleotide primers, probes and molecular methods for the environmental monitoring of methanogenic archaea. Microb Biotechnol 4:585–602.
25. Boetius A, Ravenschlag K, Schubert CJ, Rickert D, Widdel F, Gieseke A, Amann R, Jørgensen BB, Witte U, Pfannkuche O. 2000. A marine microbial consortium apparently mediating anaerobic oxidation of methane. Nature 407:623–626.
26. Laso-Peréz R, Wegener G, Knittel K, Widdel F. 2016. Thermophilic archaea activate butane via alkyl-CoM formation. Nature 1–36.
27. Evans PN, Parks DH, Chadwick GL, Robbins SJ, Orphan VJ, Golding SD, Tyson GW. 2015. Methane metabolism in the archaeal phylum Bathyarchaeota revealed by genome-centric metagenomics. Science (80-) 350:434–438.
28. Saunois M. 2016. The global methane budget 2000–2012. Earth Syst Sci Data 8:697–751.
29. Beal EJ, House CH, Orphan VJ. 2009. Manganese- and iron-dependent marine methane oxidation. Science (80-) 325:184–187.
30. Scheller S, Goenrich M, Boecher R, Thauer RK, Jaun B. 2010. The key nickel enzyme of methanogenesis catalyses the anaerobic oxidation of methane. Nature 465:606–608.
31. Lang SQ, Früh-Green GL, Bernasconi SM, Lilley MD, Proskurowski G, Méhay S, Butterfield DA. 2012. Microbial utilization of abiogenic carbon and hydrogen in a serpentinite-hosted system. Geochim Cosmochim Acta 92:82–99.
32. Skennerton CT, Chourey K, Iyer R, Hettich RL, Tyson GW, Orphan VJ. 2017. Methane-fueled syntrophy through extracellular electron transfer : uncovering the genomic traits conserved within diverse bacterial partners of anaerobic methanotrophic archaea. MBio 8:1–14.
33. Wegener G, Krukenberg V, Ruff SE, Kellermann MY, Knittel K. 2016. Metabolic capabilities of microorganisms involved in and associated with the anaerobic oxidation of methane. Front Microbiol 7:1–16.
34. Vigneron A, Cruaud P, Pignet P, Caprais J-C, Cambon-Bonavita M-A, Godfroy A, Toffin L. 2013. Archaeal and anaerobic methane oxidizer communities in the Sonora Margin cold seeps, Guaymas Basin (Gulf of California). ISME J 1–14.
35. Wegener G, Krukenberg V, Riedel D, Tegetmeyer HE, Boetius A. 2015. Intercellular wiring enables electron transfer between methanotrophic archaea and bacteria. Nature 526:587–590.
36. Knittel K, Boetius A. 2009. Anaerobic oxidation of methane: progress with an unknown process. Annu Rev Microbiol 63:311–34.
37. Hoehler TM, Alperin MJ, Albert DB, Martens CS. 1994. Field and laboratory studies of methane oxidation in an anoxic marine sediment: Evidence for a methanogen-sulfate reducer consortium. Global Biogeochem Cycles 8:451–463.

38. Madigan MT, M. MJ, Bender KS, Buckley DH, Allan SD. 2015. Brock Biology of Microorganisms.Fourteenth. Pearson, Boston.
39. Hoehler TM, Bebout BM, Des Marais DJ. 2001. The role of microbial mats in the production of reduced gases on the early Earth. Nature 412:324–327.
40. Garrity GM. 2012. Bergey's Manual of Systematic Bacteriology: Volume One: The Archaea and the Deeply Branching and Phototrophic Bacteria. Springer Science & Business Media.
41. Meyerdierks A, Kube M, Kostadinov I, Teeling H, Glöckner FO, Reinhardt R, Amann R. 2010. Metagenome and mRNA expression analyses of anaerobic methanotrophic archaea of the ANME-1 group. Environ Microbiol 12:422–439.
42. Hallam SJ, Putnam N, Preston CM, Detter JC, Rokhsar D, Richardson PM, DeLong EF. 2004. Reverse methanogenesis: testing the hypothesis with environmental genomics. Science.
43. Beulig F, Roy H, McGlynn SE, Jorgensen BB. 2018. Cryptic CH4 cycling in the sulfate–methane transition of marine sediments apparently mediated by ANME-1 archaea. ISME J.
44. Lloyd KG, Alperin MJ, Teske A. 2011. Environmental evidence for net methane production and oxidation in putative ANaerobic MEthanotrophic (ANME) archaea. Environ Microbiol 13:2548–2564.
45. Lazar CS, Baker BJ, Seitz KW, Teske AP. 2017. Genomic reconstruction of multiple lineages of uncultured benthic archaea suggests distinct biogeochemical roles and ecological niches. ISME J 11:1118–1129.
46. Kelley CA, Martens CS, Ussler W. 1995. Methane dynamics across a tidally flooded riverbank margin. Limnol Oceanogr 40:1112–1129.
47. Baker BJ, Lazar CS, Teske AP, Dick GJ. 2015. Genomic resolution of linkages in carbon, nitrogen, and sulfur cycling among widespread estuary sediment bacteria. Microbiome 3:14.
48. Kelley CA, Martens CS, Chanton JP. 1990. Variations in sedimentary rates in the carbon remineralization Variations White Oak River estuary North Carolina. Limnology 35:372–383.
49. Berner RA. 1980. Early diagenesis: A theoretical approachNo. 1. Princeton University Press.
50. Fryer P, Wheat CG, Mottl MJ. 1999. Mariana blueschist mud volcanism: Implications for conditions within the subduction zone. Geology 27:103–106.
51. Mottl MJ, Komor SC, Fryer P, Moyer CL. 2003. Deep-slab fluids fuel extremophilic Archaea on a Mariana forearc serpentinite mud volcano: Ocean Drilling Program Leg 195. Geochemistry, Geophys Geosystems 4:1–14.
52. Mottl MJ, Wheat CG, Fryer P, Gharib J, Martin JB. 2004. Chemistry of springs across the Mariana forearc shows progressive devolatilization of the subducting plate. Geochim Cosmochim Acta 68:4915–4933.
53. Russell MJ, Hall a. J, Martin W. 2010. Serpentinization as a source of energy at the origin of life. Geobiology 8:355–371.
54. Fryer P, Wheat CG, Williams T, Scientists E 366. 2017. International Ocean Discovery Program Expedition 366 Preliminary Report.
55. Sleep NH, Meibom A, Fridriksson T, Coleman RG, Bird DK. 2004. H2-rich fluids from serpentinization: geochemical and biotic implications. Proc Natl Acad Sci 101:12818–12823.
56. McCollom TM. 2013. Laboratory Simulations of Abiotic Hydrocarbon Formation in

Earth's Deep Subsurface. Rev Mineral Geochemistry 75:467–494.
57. Martin W, Baross J, Kelley D, Russell MJ. 2008. Hydrothermal vents and the origin of life. Nat Rev Microbiol 6:805–814.
58. Curtis AC, Wheat CG, Fryer P, Moyer CL. 2013. Mariana forearc serpentinite mud volcanoes harbor novel communities of extremophilic archaea. Geomicrobiol J 30:430–441.
59. Kelley DS, Karson J a, Fru GL, Yoerger DR, Shank TM, Butterfield D a, Hayes JM, Schrenk MO, Olson EJ, Proskurowski G, Jakuba M, Bradley A, Larson B, Ludwig K, Glickson D, Buckman K, Bradley AS, Brazelton WJ, Roe K, Bernasconi SM, Elend MJ, Lilley MD, Baross J a, Summons RE, Sylva SP. 2005. A serpentinite-hosted ecosystem: the lost city hydrothermal field. Science (80-) 307:1428–1434.
60. Kelley DS, Karson JA, Blackman DK, Früh-Green GL, Butterfield DA, Lilley MD, Olson EJ, Schrenk MO, Roe KK, Lebon GT, Rivizzigno P. 2001. An off-axis hydrothermal vent field near the mid-atlantic ridge at 30° n. Nature 412:145–149.
61. D'Hondt S, Rutherford S. 2002. Metabolic activity of subsurface life in deep sea sediments. Science (80-) 295:2067–2070.
62. Brazelton WJ, Schrenk MO, Kelley DS, Baross JA. 2006. Methane- and sulfur-metabolizing microbial communities dominate the lost city hydrothermal field ecosystem. Appl Environ Microbiol 72:6257–6270.
63. Kelley DS, Karson J a, Fru GL, Yoerger DR, Shank TM, Butterfield D a, Hayes JM, Schrenk MO, Olson EJ, Proskurowski G, Jakuba M, Bradley A, Larson B, Ludwig K, Glickson D, Buckman K, Bradley AS, Brazelton WJ, Roe K, Bernasconi SM, Elend MJ, Lilley MD, Baross J a, Summons RE, Sylva SP. 2005. A Serpentinite-Hosted Ecosystem: The Lost City Hydrothermal Field. Science (80-) 307:1428–1434.
64. Horikoshi K. 1999. Alkaliphiles: some applications of their products for biotechnology. Microbiol Mol Biol Rev 63:735–750.
65. Mulkidjanian AY, Dibrov P, Galperin MY. 2008. The past and present of sodium energetics: May the sodium-motive force be with you. Biochim Biophys Acta - Bioenerg 1777:985–992.
66. Baross JA, Hoffman SE. 1985. Submarine hydrothermal vents and associated gradient environments as sites for the origin and evolution of life. Orig Life Evol Biosph 15:327–345.
67. Lang SQ, Früh-Green GL, Bernasconi SM, Brazelton WJ, Schrenk MO, McGonigle JM. 2018. Deeply-sourced formate fuels sulfate reducers but not methanogens at Lost City hydrothermal field. Sci Rep 8:755.
68. Chapelle FH, O'Neill K, Bradley PM, Methé BA, Ciufo SA, Knobel LL, Lovley DR. 2002. A hydrogen-based subsurface microbial community dominated by methanogens. Nature 415:312–315.
69. Matson DL, Castillo JC, Lunine J, Johnson T V. 2007. Enceladus' plume: Compositional evidence for a hot interior. Icarus 187:569–573.
70. Kubo K, Lloyd KG, F Biddle J, Amann R, Teske A, Knittel K. 2012. Archaea of the Miscellaneous Crenarchaeotal Group are abundant, diverse and widespread in marine sediments. ISME J 6:1949–1965.
71. Cassandre SL, Baker BJ, Seitz K, Hyde AS, Dick GJ, Hinrichs K-U, Teske AP. 2015. Genomic evidence for distinct carbon substrate preferences and ecological niches of Bathyarchaeota in estuarine sediments. Environ Microbiol.
72. Seitz KW, Lazar CS, Hinrichs K-U, Teske AP, Baker BJ. 2016. Genomic reconstruction of a novel, deeply branched sediment archaeal phylum with pathways for acetogenesis and

sulfur reduction. ISME J 1–10.
73. Meador TB, Bowles M, Lazar CS, Zhu C, Teske A, Hinrichs K. 2015. The archaeal lipidome in estuarine sediment dominated by members of the Miscellaneous Crenarchaeotal Group. Environ Microbiol 17:2441–2458.
74. Baker BJ, Saw JH, Lind AE, Lazar CS, Hinrichs KU, Teske AP, Ettema TJG. 2016. Genomic inference of the metabolism of cosmopolitan subsurface Archaea, Hadesarchaea. Nat Microbiol 1:1–7.
75. Mori K, Iino T, Suzuki KI, Yamaguchi K, Kamagata Y. 2012. Aceticlastic and NaCl-requiring methanogen "Methanosaeta pelagica" sp. Nov., isolated from marine tidal flat sediment. Appl Environ Microbiol 78:3416–3423.
76. Podar M, Abulencia CB, Walcher M, Hutchison D, Zengler K, Garcia JA, Holland T, Cotton D, Hauser L, Keller M. 2007. Targeted access to the genomes of low-abundance organisms in complex microbial communities. Appl Environ Microbiol 73:3205–3214.
77. Campbell BJ, Kirchman DL. 2012. Bacterial diversity, community structure and potential growth rates along an estuarine salinity gradient. ISME J 7:210–220.
78. Underwood S, Lapham L, Teske A, Lloyd KG. 2016. Microbial community structure and methane-cycling activity of subsurface sediments at Mississippi Canyon 118 before the Deepwater Horizon disaster. Deep Res Part II Top Stud Oceanogr 129:148–156.
79. Lloyd KG, Steen AD, Ladau J, Yin J, Crosby L. 2018. Phylogenetically novel uncultured microbial cells dominate Earth microbiomes. mSystems 3:e00055-18.
80. Valentine DL, Reeburgh WS, Blanton DC. 2000. A culture apparatus for maintaining H2 at sub-nanomolar concentrations. J Microbiol Methods.
81. Nauhaus K, Albrecht M, Elvert M, Boetius A, Widdel F. 2007. In vitro cell growth of marine archaeal-bacterial consortia during anaerobic oxidation of methane with sulfate. Environ Microbiol 9:187–196.
82. Suzuki MT, Giovannoni SJ. 1996. Bias caused by template annealing in the amplification of mixtures of 16S rRNA genes by PCR. Appl Environ Microbiol 62:2–8.
83. Mumy KL, Findlay RH. 2004. Convenient determination of DNA extraction efficiency using an external DNA recovery standard and quantitative-competitive PCR. J Microbiol Methods 57:259–268.
84. Holmkvist L, Ferdelman TG, Jørgensen BB. 2011. A cryptic sulfur cycle driven by iron in the methane zone of marine sediment (Aarhus Bay, Denmark). Geochim Cosmochim Acta 75:3581–3599.
85. Whiticar MJ. 1999. Carbon and hydrogen isotope systematics of bacterial formation and oxidation of methane. Chem Geol 161:291–314.
86. Orphan VJ, House CH, Hinrichs K, McKeegan KD, Delong EF. 2001. Methane-Consuming Archaea Revealed by Directly Coupled Isotopic and Phylogenetic Analysis studies that combine phylogenetic surveys of. Science (80-) 293:484–488.
87. Alperin MJ, Reeburgh WS, Whiticar MJ. 1988. Carbon and hydrogen isotope fractionation resulting from anaerobic methane oxidation. Global Biogeochem Cycles 2:279–288.
88. Holler T, Wegener G, Knittel K, Boetius A, Brunner B, Kuypers MMM, Widdel F. 2009. Substantial 13 C/ 12 C and D/H fractionation during anaerobic oxidation of methane by marine consortia enriched in vitro. Environ Microbiol Rep 1:370–376.
89. Miroshnichenko ML, Kolganova T V., Spring S, Chernyh N, Bonch-Osmolovskaya EA. 2010. Caldithrix palaeochoryensis sp. nov., a thermophilic, anaerobic, chemo-organotrophic bacterium from a geothermally heated sediment, and emended description of the genus Caldithrix. Int J Syst Evol Microbiol 60:2120–2123.

90. Polz MF, Cavanaugh CM. 1998. Bias in Template-to-Product Ratios in Multitemplate PCR. Society 64:3724–3730.
91. He Y, Li M, Perumal V, Feng X, Fang J, Xie J, Sievert SM, Wang F. 2016. Genomic and enzymatic evidence for acetogenesis among multiple lineages of the archaeal phylum Bathyarchaeota widespread in marine sediments. Nat Microbiol 35:1–9.
92. Nobu MK, Narihiro T, Kuroda K, Ran M, Liu W-T. 2016. Chasing the elusive Euryarchaeota class WSA2: genomes reveal a uniquely fastidious methyl-reducing methanogen. ISME J 2:1–10.
93. Stokke R, Roalkvam I, Lanzen A, Haflidason H, Steen IH. 2012. Integrated metagenomic and metaproteomic analyses of an ANME-1-dominated community in marine cold seep sediments. Environ Microbiol 14:1333–1346.
94. McGlynn SE, Chadwick GL, Kempes CP, Orphan VJ. 2015. Single cell activity reveals direct electron transfer in methanotrophic consortia. Nature 526:531–535.
95. Lotka AJ. 1910. Contribution to the Theory of Periodic Reactions. J Phys Chem 14:271–274.
96. Beulig F, Røy H, Glombitza C, Jørgensen BB. 2018. Control on rate and pathway of anaerobic organic carbon degradation in the seabed. Proc Natl Acad Sci 115:367–372.
97. Finkel SE. 2006. Long-term survival during stationary phase: evolution and the GASP phenotype. Nat Rev Microbiol 4:113–20.
98. Holler T, Widdel F, Knittel K, Amann R, Kellermann MY, Hinrichs K-U, Teske A, Boetius A, Wegener G. 2011. Thermophilic anaerobic oxidation of methane by marine microbial consortia. ISME J.
99. Reeve JN. 1997. Growth- and Substrate-Dependent Transcription of the Formate Dehydrogenase (fdhCAB) Operon in Methanobacterium thermoformicicum Z-245. Microbiology 179:899–908.
100. Kato S, Kosaka T, Watanabe K. 2008. Comparative transcriptome analysis of responses of Methanothermobacter thermautotrophicus to different environmental stimuli. Environ Microbiol 10:893–905.
101. Yoshinaga MY, Holler T, Goldhammer T, Wegener G, Pohlman JW, Brunner B, Kuypers MMM, Hinrichs K, Elvert M. 2014. Carbon isotope equilibration during sulphate-limited anaerobic oxidation of methane. Nat Geosci.
102. Meyerdierks A, Kube M, Lombardot T, Knittel K, Bauer M, Glöckner FO, Reinhardt R, Amann R. 2005. Insights into the genomes of archaea mediating the anaerobic oxidation of methane. Environ Microbiol 7:1937–1951.
103. Wang F-P, Zhang Y, Chen Y, He Y, Qi J, Hinrichs K-U, Zhang X-X, Xiao X, Boon N. 2014. Methanotrophic archaea possessing diverging methane-oxidizing and electron-transporting pathways. ISME J 8:1069–1078.
104. Gennis RB. 1987. The cytochromes of Escherichia coli. FEMS Microbiol Rev 46:387–399.
105. Mukhopadhyay B, Johnson EF, Wolfe RS. 2000. A novel pH2 control on the expression of flagella in the hyperthermophilic strictly hydrogenotrophic methanarchaeaon Methanococcus jannaschii. Proc Natl Acad Sci 97:11522–7.
106. Caporaso JG, Lauber CL, Walters WA, Berg-Lyons D, Huntley J, Fierer N, Owens SM, Betley J, Fraser L, Bauer M, Gormley N, Gilbert JA, Smith G, Knight R. 2012. Ultra-high-throughput microbial community analysis on the Illumina HiSeq and MiSeq platforms. ISME J 6:1621–1624.
107. Pruesse E, Quast C, Knittel K, Fuchs BM, Ludwig W, Peplies J, Glöckner FO. 2007. SILVA: A comprehensive online resource for quality checked and aligned ribosomal RNA

sequence data compatible with ARB. Nucleic Acids Res 35:7188–7196.
108. Benninger L, Martens CS. 1978. Sources and Fates of Sedimentary Organic Matter in the White Oak and Neuse River Estuaries. Water Resour Res Inst Univ North Carolina.
109. Huber JA, Welch DB, Morrison HG, Huse SM, Neal PR, Butterfield DA, Sogin ML. 2007. Microbial population structures in the deep marine biosphere. Science 318:97–100.
110. Sogin ML, Morrison HG, Huber JA, Welch DM, Huse SM, Neal PR, Arrieta JM, Herndl GJ. 2011. Microbial Diversity in the Deep Sea and the Underexplored "Rare Biosphere." Proc Natl Acad Sci 103:12115–12120.
111. Bertram S, Blumenberg M, Michaelis W, Siegert M, Krüger M, Seifert R. 2013. Methanogenic capabilities of ANME-archaea deduced from 13C-labelling approaches. Environ Microbiol.
112. Alperin MJ, Blair NE, Albert DB, Hoehler TM, Martens CS. 1992. Factors that control the stable carbon isotopic composition of methane produced in an anoxic marine sediment. Global Biogeochem Cycles 6:271–291.
113. Hoehler TM, Albert DB, Alperin MJ, Martens CS. 1999. Acetogenesis from CO2 in an anoxic marine sediment. Limnol Oceanogr 44:662–667.
114. Smith KS, Ingram-Smith C. 2007. Methanosaeta, the forgotten methanogen? Trends Microbiol 15:150–155.
115. Imachi H, Sekiguchi Y, Ohashi A, Kamagata Y, Sakai S, Hanada S, Harada H. 2008. Methanolinea tarda gen. nov., sp. nov., a methane-producing archaeon isolated from a methanogenic digester sludge. Int J Syst Evol Microbiol 58:294–301.
116. Mikucki JA, Liu Y, Delwiche M, Colwell FS, Boone DR. 2003. Isolation of a methanogen from deep marine sediments that contain methane hydrates, and description of Methanoculleus submarinus sp. nov. Appl Environ Microbiol.
117. Parkes RJ, Cragg BA, Banning N, Brock F, Webster G, Fry JC, Hornibrook E, Pancost RD, Kelly S, Knab N, Jørgensen BB, Rinna J, Weightman AJ. 2007. Biogeochemistry and biodiversity of methane cycling in subsurface marine sediments (Skagerrak, Denmark). Environ Microbiol 9:1146–1161.
118. Knittel K, Lösekann T, Boetius A, Kort R, Amann R. 2005. Diversity and distribution of methanotrophic archaea at cold seeps. Appl Environ Microbiol 71:467–479.
119. Zhou J, He Q, Hemme CL, Mukhopadhyay A, Hillesland K, Zhou A, He Z, Van Nostrand JD, Hazen TC, Stahl DA, Wall JD, Arkin AP. 2011. How sulphate-reducing microorganisms cope with stress: lessons from systems biology. Nat Rev Microbiol 9:452–466.
120. Mills HJ, Hunter E, Humphrys M, Kerkhof L, McGuinness L, Huettel M, Kostka JE. 2008. Characterization of nitrifying, denitrifying, and overall bacterial communities in permeable marine sediments of the northeastern Gulf of Mexico. Appl Environ Microbiol 74:4440–4453.
121. McMurdie PJ, Holmes S. 2013. Phyloseq: An R Package for Reproducible Interactive Analysis and Graphics of Microbiome Census Data. PLoS One 8.
122. Bolger AM, Lohse M, Usadel B. 2014. Trimmomatic: A flexible trimmer for Illumina sequence data. Bioinformatics 30:2114–2120.
123. Langmead B, Salzberg SL. 2012. Fast gapped-read alignment with Bowtie 2. Nat Methods 9:357–359.
124. Eren AM, Esen ÖC, Quince C, Vineis JH, Morrison HG, Sogin ML, Delmont TO. 2015. Anvi'o: an advanced analysis and visualization platform for 'omics data. PeerJ 3:e1319.
125. Li H, Wysoker A, Fennell T, Marth G, Abecasis G, Ruan J, Durbin R, Homer N, Handsaker B, Subgroup 1000 Genome Project Data Processing. 2009. The Sequence

Alignment/Map format and SAMtools. Bioinformatics 25:2078–2079.
126. Hyatt D, Chen G-L, Locascio PF, Land ML, Larimer FW, Hauser LJ. 2010. Prodigal: prokaryotic gene recognition and translation initiation site identification. BMC Bioinformatics 11:119.
127. Kanehisa M, Sato Y, Morishima K. 2016. BlastKOALA and GhostKOALA: KEGG Tools for Functional Characterization of Genome and Metagenome Sequences. J Mol Biol 428:726–731.
128. Team RC. 1993. R: A language and environment for statistical computing. R Foundation for Statistical Computing, Vienna Austria.
129. Hoehler TM. 2007. An Energy Balance Concept for Habitability. Astrobiology 6:573–578.
130. Twing KI, Brazelton WJ, Kubo MDY, Hyer AJ, Cardace D, Hoehler T, McCollom TM, Schrenk MO. 2017. Serpentinization-influenced groundwater harbors extremely low diversity microbial communities adapted to high pH. Front Microbiol 8:308.
131. Suzuki S, Kuenen JG, Schipper K, Van Der Velde S, Ishii S, Wu A, Sorokin DY, Tenney A, Meng X, Morrill PL, Kamagata Y, Muyzer G, Nealson KH. 2014. Physiological and genomic features of highly alkaliphilic hydrogen-utilizing Betaproteobacteria from a continental serpentinizing site. Nat Commun 5.
132. Meyer-Dombard DR, Woycheese KM, Yargicoglu EN, Cardace D, Shock EL, Gulecal-Pektas Y, Temel M. 2015. High pH microbial ecosystems in a newly discovered, ephemeral, serpentinizing fluid seep at Yanarta (Chimera), Turkey. Front Microbiol 6:1–13.
133. Suzuki S, Ishii S, Wu A, Cheung A, Tenney A, Wanger G, Kuenen JG, Nealson KH. 2013. Microbial diversity in The Cedars, an ultrabasic, ultrareducing, and low salinity serpentinizing ecosystem. Proc Natl Acad Sci 110:15336–15341.
134. Merino N, Aronson HS, Bojanova DP, Feyhl-Buska J, Wong ML, Zhang S, Giovannelli D. 2019. Living at the Extremes: Extremophiles and the Limits of Life in a Planetary Context. Front Microbiol 10.
135. Tiago I, Veríssimo A. 2013. Microbial and functional diversity of a subterrestrial high pH groundwater associated to serpentinization. Environ Microbiol 15:1687–1706.
136. Ijiri A, Inagaki F, Kubo Y, Adhikari RR, Hattori S. 2018. Deep-biosphere methane production stimulated by geofluids in the Nankai accretionary complex. Sci Adv 4:1–16.
137. Brazelton WJ, Morrill PL, Szponar N, Schrenk MO. 2013. Bacterial communities associated with subsurface geochemical processes in continental serpentinite springs. Appl Environ Microbiol 79:3906–3916.
138. Hulme SM, Wheat CG, Fryer P, Mottl MJ. 2010. Pore water chemistry of the Mariana serpentinite mud volcanoes: A window to the seismogenic zone. Geochemistry, Geophys Geosystems 11.
139. Paulot F, Jacob DJ, Johnson MT, Bell TG, Baker AR, Keene WC, Lima ID, Doney SC. 2015. Global oceanic emission of ammonia: Constraints from seawater and atmospheric observations. Global Biogeochem Cycles 29:217–221.
140. Parks DH, Imelfort M, Skennerton CT, Hugenholtz P, Tyson GW. 2015. CheckM: assessing the quality of microbial genomes recovered from isolates, single cells, and metagenomes. Genome Res 25:1043–55.
141. Stepanauskas R, Fergusson EA, Brown J, Poulton NJ, Tupper B, Labonté JM, Becraft ED, Brown JM, Pachiadaki MG, Povilaitis T, Thompson BP, Mascena CJ, Bellows WK, Lubys A. 2017. Improved genome recovery and integrated cell-size analyses of individual uncultured microbial cells and viral particles. Nat Commun 8.

142. Arkin AP, Stevens RL, Cottingham RW, Maslov S, Henry CS, Dehal P, Ware D, Perez F, Harris NL, Canon S, Sneddon MW, Henderson ML, Riehl WJ, Gunter D, Murphy-Olson D, Chan S, Kamimura RT, Brettin TS, Meyer F, Chivian D, Weston DJ, Glass EM, Davison BH, Kumari S, Allen BH, Baumohl J, Best AA, Bowen B, Brenner SE, Bun CC, Chandonia J-M, Chia J-M, Colasanti R, Conrad N, Davis JJ, DeJongh M, Devoid S, Dietrich E, Drake MM, Dubchak I, Edirisinghe JN, Fang G, Faria JP, Frybarger PM, Gerlach W, Gerstein M, Gurtowski J, Haun HL, He F, Jain R, Joachimiak MP, Keegan KP, Kondo S, Kumar V, Land ML, Mills M, Novichkov P, Oh T, Olsen GJ, Olson B, Parrello B, Pasternak S, Pearson E, Poon SS, Price G, Ramakrishnan S, Ranjan P, Ronald PC, Schatz MC, Seaver SMD, Shukla M, Sutormin RA, Syed MH, Thomason J, Tintle NL, Wang D, Xia F, Yoo H, Yoo S. 2016. The DOE Systems Biology Knowledgebase (KBase). bioRxiv 1–21.
143. Eickenbusch P, Takai K, Sissmann O, Suzuki S, Menzies C, Sakai S, Sansjofre P, Tasumi E, Bernasconi SM, Glombitza C, Morono Y, Jorgensen BB, Lever MA. 2019. Origin of short-chain organic acids in serpentinite mud volcanoes of the Mariana Convergent Margin. Front Microbiol.
144. Kyryakov P, Beach A, Richard VR, Burstein MT, Leonov A, Levy S, Titorenko VI. 2012. Caloric restriction extends yeast chronological lifespan by altering a pattern of age-related changes in trehalose concentration. Front Physiol 3:1–11.
145. Sekiguchi Y, Muramatsu M, Imachi H, Narihiro T, Ohashi A, Harada H, Hanada S, Kamagata Y. 2008. Thermodesulfovibrio aggregans sp. nov. and Thermodesulfovibrio thiophilus sp. nov., anaerobic,thermophilic, sulfate-reducing bacteria isolated from thermophilic methanogenic sludge, and emended description of the genus Thermodesulfovibrio. Int J Syst Evol Microbiol 58:2541–2548.
146. Momper L, Aronson HS, Amend JP. 2018. Genomic description of "Candidatus abyssubacteria," a novel subsurface lineage within the candidate phylum hydrogenedentes. Front Microbiol 9:1–11.
147. Frank J, Lücker S, Vossen RHAM, Jetten MSM, Hall RJ, Op Den Camp HJM, Anvar SY. 2018. Resolving the complete genome of Kuenenia stuttgartiensis from a membrane bioreactor enrichment using Single-Molecule Real-Time sequencing /631/208/212/748 /631/326/41/2530 /631/326/41/2142 /631/326/171/1878 article. Sci Rep 8:1–10.
148. Plümper O, King HE, Geisler T, Liu Y, Pabst S, Savov IP, Rost D, Zack T. 2017. Subduction zone forearc serpentinites as incubators for deep microbial life. Proc Natl Acad Sci 114:4324–4329.
149. Brazelton WJ, Ludwig KA, Sogin ML, Andreishcheva EN, Kelley DS, Shen C-C, Edwards RL, Baross JA. 2010. Archaea and bacteria with surprising microdiversity show shifts in dominance over 1,000-year time scales in hydrothermal chimneys. Proc Natl Acad Sci 107:1612–1617.
150. Orcutt BN, Sylvan JB, Rogers DR, Delaney J, Lee RW, Girguis PR. 2015. Carbon fixation by basalt-hosted microbial communities. Front Microbiol 6:1–14.
151. Postberg F, Khawaja N, Abel B, Choblet G, Glein CR, Gudipati MS, Henderson BL, Hsu H, Kempf S, Klenner F, Moragas-klostermeyer G, Magee B, Nölle L, Perry M, Reviol R, Schmidt J, Srama R, Stolz F, Tobie G, Trieloff M, Waite JH. 2018. Macromolecular organic compounds from the depths of Enceladus. Nature 558.
152. Sorokin DY, Berben T, Melton ED, Overmars L, Vavourakis CD, Muyzer G. 2014. Microbial diversity and biogeochemical cycling in soda lakes. Extremophiles 18:791–809.
153. Vavourakis CD, Ghai R, Rodriguez-Valera F, Sorokin DY, Tringe SG, Hugenholtz P, Muyzer G. 2016. Metagenomic insights into the uncultured diversity and physiology of

microbes in four hypersaline soda lake brines. Front Microbiol 7:1–18.
154. Abraham W, Rohde M. 2014. The Prokaryotes. The Prokaryotes 545–577.
155. Staley J, Konopka A. 1985. Measurement of In Situ Activities of Nonphotosynthetic Microorganisms in Aquatic and Terrestrial Habitats. Annu Rev Microbiol 39:321–346.
156. Harwani D. 2014. The Great Plate Count Anomaly and the Unculturable Bacteria. Int J Sci Res 2:350–351.
157. Brazelton WJ, Nelson B, Schrenk MO. 2012. Metagenomic evidence for H2 oxidation and H2 production by serpentinite-hosted subsurface microbial communities. Front Microbiol 2:1–16.
158. McCollom TM, Seewald JS. 2006. Carbon isotope composition of organic compounds produced by abiotic synthesis under hydrothermal conditions. Earth Planet Sci Lett 243:74–84.
159. Lu W, Clasquin M, Melamund E, Amador-Noguez D, Caudy A, Rabinowitz JD. 2010. Metabolomic analysis via reversed-phase ion-pairing liquid chromatography coupled to a stand-alone Orbitrap mass spectrometer - Supporting information. Anal Chem 82:3212–3221.
160. Glombitza C, Pedersen J, Røy H, Jørgensen BB. 2014. Direct analysis of volatile fatty acids in marine sediment porewater by two-dimensional ion chromatography-mass spectrometry. Limnol Oceanogr Methods 12:455–468.
161. Rinke C, Lee J, Nath N, Goudeau D, Thompson B, Poulton N, Dmitrieff E, Malmstrom R, Stepanauskas R, Woyke T. 2014. Obtaining genomes from uncultivated environmental microorganisms using FACS-based single-cell genomics. Nat Protoc 9:1038–1048.
162. Blainey PC. 2013. The future is now: single-cell genomics of bacteria and archaea. FEMS Microbiol Rev 37:407–427.
163. Stepanauskas R. 2012. Single cell genomics: An individual look at microbes. Curr Opin Microbiol 15:613–620.
164. Kozich JJ, Westcott SL, Baxter NT, Highlander SK, Schloss PD. 2013. Development of a dual-index sequencing strategy and curation pipeline for analyzing amplicon sequence data on the miseq illumina sequencing platform. Appl Environ Microbiol 79:5112–5120.
165. Bankevich A, Nurk S, Antipov D, Gurevich AA, Dvorkin M, Kulikov AS, Lesin VM, Nikolenko SI, Pham S, Prjibelski AD, Pyshkin A V., Sirotkin A V., Vyahhi N, Tesler G, Alekseyev M a., Pevzner P a. 2012. SPAdes: A New Genome Assembly Algorithm and Its Applications to Single-Cell Sequencing. J Comput Biol 19:455–477.
166. Seemann T. 2014. Prokka: Rapid prokaryotic genome annotation. Bioinformatics 30:2068–2069.
167. Teske A, Hinrichs K, Edgcomb V, Gomez DV, Kysela D, Sylva SP, Mitchell L, Jannasch HW, Gomez ADV, Sogin ML. 2002. Microbial Diversity of Hydrothermal Sediments in the Guaymas Basin : Evidence for Anaerobic Methanotrophic Communities Microbial Diversity of Hydrothermal Sediments in the Guaymas Basin : Evidence for Anaerobic Methanotrophic Communities †. Appl Environ Microbiol 68:1994–2007.
168. Altschul SF, Gish W, Miller W, Myers EW, Lipman DJ. 1990. Basic local alignment search tool. J Mol Biol 215:403–410.
169. Melamud E, Vastag L, Rabinowitz JD. 2010. Metabolomic analysis and visualization engine for LC-MS data. Anal Chem 82:9818–9826.
170. Wickham H. 2009. ggplot2: elegant graphics for data analysis. Springer, New York.
171. Letunic I, Bork P. 2019. Interactive Tree Of Life (iTOL) v4: recent updates and new developments. Nucleic Acids Res 2–5.
172. Lê S, Josse J, Husson F. 2008. FactoMinerR: An R Package for Multivariate Analysis. J

Stat Softw 25.
173. Jari Oksanen, F. Guillaume Blanchet, Michael Friendly, Roeland Kindt, Pierre Legendre D, McGlinn, Peter R. Minchin, R. B. O'Hara, Gavin L. Simpson, Peter Solymos MHH, Stevens ES and HW. 2018. vegan: Community Ecology Package. R package version 2.5-3.
174. Dray S, Dufour A. 2007. The ade4 Package: Implementing the Duality Diagram for Ecologists. J Stat Softw 22:1–20.
175. Shannon P, Markiel A, Ozier O, Baliga N s., Wang JT, Ramage D, Amin N, Schwikoski B, Ideker T. 2003. Cytoscape: A Software Environment for Integrated Models of Biomolecular Interaction Networks. Genome Res 13:426.
176. Beulig F, Røy H, McGlynn SE, Jørgensen BB. 2019. Cryptic CH4 cycling in the sulfate–methane transition of marine sediments apparently mediated by ANME-1 archaea. ISME J 13:250–262.
177. Woycheese KM, Meyer-Dombard DR, Cardace D, Argayosa AM, Arcilla CA. 2015. Out of the dark: Transitional subsurface-to-surface microbial diversity in a terrestrial serpentinizing seep (Manleluag, Pangasinan, the Philippines). Front Microbiol 6:1–12.
178. Lever M a., Torti A, Eickenbusch P, Michaud AB, Å antl-Temkiv T, JÃ¸rgensen BB. 2015. A modular method for the extraction of DNA and RNA, and the separation of DNA pools from diverse environmental sample types. Front Microbiol 6.
179. Mills HJ, Reese BK, Shepard AK, Riedinger N, Dowd SE, Morono Y, Inagaki F. 2012. Characterization of Metabolically Active Bacterial Populations in Subseafloor Nankai Trough Sediments above, within, and below the Sulfate–Methane Transition Zone. Front Microbiol 3:1–12.
180. Brauer MJ, Yuan J, Bennett BD, Lu W, Kimball E, Botstein D, Rabinowitz JD. 2006. Conservation of the metabolomic response to starvation across two divergent microbes. Proc Natl Acad Sci 103:19302–19307.

VITA

Richard Thomas Kevorkian was born in Roanoke, Virginia on March 24, 1990 to parents George and JoAnn Kevorkian. One of five children, he would graduate from William Byrd High School in 2008. Following graduation, Richard moved to Blacksburg, VA where he attended Virginia Polytechnic Institute and State University. In May of 2012 Richard would graduate with a Bachelor of Science in Biology. He next moved south to Knoxville, Tennessee where he began studying in the field of biogeochemistry under the leadership of Dr. Karen Lloyd in order to pursue a Master of Science degree in Microbiology at the University of Tennessee which he completed in 2015 before continuing his PhD work. Following his graduation at Tennessee he will be pursuing a career as a homemaker alongside Alexandra Emmons in Fort Collins, CO.